ABSTRACT

Title of Dissertation: ***A numerical investigation of variability in particulate organic matter transport and fate, phytoplankton and primary production, and denitrification in a partially mixed estuary.***

Hao Wang, Doctor of Philosophy, 2020

Dissertation directed by: Professor Raleigh Hood, University of Marine Estuarine Environmental Sciences, University of Maryland Center for Environmental Science

In Chesapeake Bay substantial quantities of organic matter are produced during the spring bloom, which contributes to severe chronic bottom oxygen depletion during the summertime. However, the details of this transport in the estuarine system under realistic forcing is still unclear. In this Research, a three-dimensional model was used to investigate the production, transport, and fate of organic matter in Chesapeake Bay. Analysis of a control volume in the deep channel revealed that the sinking flux of fast-sinking particulate organic nitrogen (PON) into the deep channel is comparable to the horizontal advective transport. The model analysis also revealed a pronounced east to west transport of PON during the springtime and a tendency to export mass from the eastern shore to the deep channel and from the deep channel to the western shore of the Chesapeake Bay, and also a convergence of mass transport on the

western shore. This transport is consistent with the lateral estuarine circulation in Chesapeake Bay that arises due to the asymmetry of the flood-neap tidal cycle. In addition, the model revealed that seasonal variations in wind alter the magnitude and distribution of organic matter flux in the along channel and cross channel direction, with northerly winds during the springtime favoring more northward organic matter transport and more organic matter accumulation in the deep channel, however, the lateral net flux direction remains the same.

In Chesapeake Bay, phytoplankton biomass typically peaks in spring whereas primary production peaks in summer. For this to happen, phytoplankton growth rates must be low in spring and high in summer and very likely there must be low grazing losses in spring and high grazing losses in summer as well. In this research, a three dimensional coupled physical-biological model is used to explore how these seasonal patterns in phytoplankton and primary production arise during the year from 2000 to 2005. It is shown that with the seasonal variation of maximum carbon to chlorophyll ratio, temperature control on phytoplankton growth, and temperature-dependent zooplankton grazing effects, my model can capture the spring peak in phytoplankton biomass and the summer peak in the primary production, agreeing well with the observations. The model simulates high phytoplankton growth rates in the summer, with the maximum growth rates occurring in late summer. The model also reveals that nutrient supply shifts from river-derived nitrate in the springtime to organic matter- derived ammonium during summer. The simulation results also reveal that a substantial fraction of the ammonium that supports the high summer production is derived from allochthonous transport rather than autochthonous ammonium

production. The transport process provides as large as 50% ammonium needed for uptake during summertime in the mesohaline Chesapeake Bay. My research also confirms the importance of nutrient recycling in supporting high summer production in Chesapeake Bay.

Denitrification is an essential process in the marine nitrogen cycle because it removes bioavailable nitrogen from the aquatic system. Current understanding of denitrification variability in Chesapeake Bay is severely constrained by the sparse observations that provide insufficient coverage in both space and time. In this research, denitrification variability is examined in the Chesapeake Bay using a three dimensional coupled physical-biogeochemical model based on the Regional Ocean Modelling System (ROMS). Model simulations indicate that denitrification occurs not only in the sediment but also in the water column at significant, though somewhat lower rates. Model results indicated that the water column accounts for around 7.5% of the total denitrification amount that occurred in the system during the 2001 and 2002 period of this study. This conflicts with the historical assumption that water column denitrification in Chesapeake Bay is negligible. The model also reveals the spatial patterns in denitrification with more denitrification occurring in the upper to middle bay due to higher availability of organic matter in these areas compared to the lower bay. In terms of temporal variability, denitrification peaks in the sediment in spring while in the water column it peaks in the summer. The reason for this difference in the timing is related to the availability of oxygen: In the spring oxygen levels in the water column are too high to allow denitrification so it happens only in the sediment where low oxygen levels persist all year around. In summer low oxygen

and depletion of nitrate below the pycnocline completely shuts down denitrification in the sediment in the mesohaline and polyhaline region of the by. However, water column denitrification continues at the interface between oxygenated waters near the surface and oxygen-depleted waters below where coupled nitrification-denitrification happens. The model also reveals that denitrification removes significant quantities of biologically available nitrogen, meaning that without this process, more summertime primary production would occur in the form of more surface chlorophyll, increasing as much as 10ug/L in the middle bay region, which would, in turn, lead to more oxygen depletion.

NUMERICAL INVESTIGATION ON PARTICULATE ORGANIC MATTER TRANSPORT AND FATE, GROSS PRIMARY PRODUCTION AND DENITRIFICATION IN A PARTIALLY MIXED ESTUARY

by

Hao Wang

Dissertation submitted to the Faculty of the Graduate School of the
University of Maryland, College Park, in partial fulfillment
of the requirements for the degree of
Doctor of Philosophy
2020

Advisory Committee:
Dr. Raleigh Hood, Chair
Dr. Jian Shen
Dr. Larry Sanford
Dr. Jeffrey Cornwell
Dr. Wen Long
Dean's Representative: Dr. Karen Prestegaard

Dedication

Dedicate to Houhua Wang and Jinling Wu, my loving and selfless parents.

Acknowledgements

I cannot express my gratitude enough to my advisor, Raleigh Hood, for his academic guidance and financial support throughout my Ph.D. study in Horn Point Laboratory, University of Maryland Center for Environmental Science. Trained as a physical oceanographer, I struggled a lot in understanding the complicated estuarine ecosystem and scientific question development. Raleigh guided me through that hard time period with patience and significant effort. I am also very fortunate to have a committee that includes Wen Long, Jian Shen, Larry Sanford and Jeffrey Cornwell. Wen Long has an amazingly high level of expertise in computational fluid dynamics and helped me substantially in understanding the ROMS model code and shell. Without Wen's help I would not have succeeded with the ROMS modeling work. I also want to express my thanks to Dr. Jian Shen for sharing his expertise in water quality modeling and for always providing excellent insights and ideas. I also want to express many thanks to Dr. Larry Sanford, for generously sharing his expertise in coastal physical oceanography and estuarine sediment transport. Talking with Larry helped me better understand estuarine circulation mechanisms and dynamics. I also want to thank Jeff Cornwell for his guidance related to the third chapter on denitrification and for sharing his life's work and deep understanding derived from measuring denitrification in Chesapeake Bay and many other systems. I also want to express thanks for the COMT project which funded much of my research and the PI Dr. Marjorie A.M. Friedrichs for leading that effort. Through the COMT project I

also gained access to Dr. Malcom Scully, who I would like to thank helping me many times over the course of my studies. I also want express may thanks for Dr. Jinhua Wang from Nanjing Hydraulic Research Institute, who is also an expert in hydrodynamic modeling, for his technical assistance during his visit in UMCES-HPL. I also give my thanks to Professor Yang Xiao in Hohai University for his encouragement during his visit to UMCES-HPL. I would also like to thank the faculty in the UMCES-MEES program who helped me along the way including, in particular, Professor Mike Roman, Professor Ming Li, Professor Jian Zhao, Professor Meng Xia, Professor Victoria Coles, Professor Michel Kemp, Professor Jeremy Testa, Professor Walter Boynton, and Professor Peter Goodwin, all of whom supported and helped to guide my graduate life making it a wonderful experience. Besides that, I want to thank the students who organized the Ian Morris Scholar visits, in which top scientists visited HPL and engaged with students. I gained substantially from discussions with Dr. Mark Stacey from UC Berkeley in 2016 and Dr. Katja Fennel from Dalhousie University in 2018.

Last but not least, I want to thank my entire family. I am grateful for my parents, who were under a lot of pressure themselves during my Ph.D. studies, as they have been a persistent source of love and encouragement. I now wish them to remain happy and healthy.

Table of Contents

List of Tables

List of Figures

Chapter 1: Introduction and Overview

Motivation

Particulate organic nitrogen transport

Estuaries are semi-enclosed water bodies and transition zones that connect freshwater to marine environments with strong salinity gradients Geyer and MacCready (2014) and they are often negatively influenced by human activity (Howarth et al. 2011). Over the past several decades, estuaries worldwide (Rabalais et al. 2009) have suffered from anthropogenic eutrophication stemming from agricultural fertilization (Zhang 2017) and disposal of urban and industrial waste waters (Smil 2000) with elevated nitrogen levels (Deegan et al. 2012). The resulting increases in primary production can lead to the generation of particulate organic matter (POM) and elevated biological oxygen demand. Eutrophication is one of the leading risks to estuarine ecosystem integrity (Paerl and Scott 2010) and jeopardizes these ecosystems through, in particular, depletion of bottom water oxygen (Breitburg et al. 2018; Diaz and Rosenberg 2008; Testa et al. 2018b).

The eutrophication-fueled POM that drives depletion of oxygen may be subjected to diverse transport pathways in natural highly stratified (Ralston et al. 2010), partially mixed (Scully and Geyer 2012) and well-mixed (Wei et al. 2017) estuarine systems before it arrives at the bottom. Estuaries with complex bathymetry (Scully 2016; Scully and Friedrichs 2007) can have heterogeneous residence times and circulation patterns due to the interaction of river discharge, tidal asymmetry (Zhang et al. 2018) and wind forcing (Li and Li 2011; Li and Li 2012). This variability will result in

retention, settling and remineralization of POM in some areas and mixing, transport and dispersal of POM on others. Understanding POM transport, transformation and fate in estuaries is clearly important for understanding then negative impacts of eutrophication.

Chesapeake Bay is the largest estuary in the US and one of the most productive estuaries on the east coast of North America. Eutrophication of Chesapeake Bay began with land clearing in the 18th century (Boesch et al. 2001) that resulted in increased nutrient loading. Today the Bay suffers from excessive primary production resulting in chronic bottom oxygen depletion during the summer (Cowan and Boynton 1996). Many studies have been conducted that focus on the onset and development of oxygen depletion in Chesapeake Bay (Kemp et al. 2005; Murphy et al. 2011; Testa and Kemp 2014). In contrast, relatively few studies have been conducted that focus on the complicated physical and biological processes that control the transport and fate of the POM in the estuary that drives the oxygen depletion. There are the direct sources of POM input from the overlying water column via sinking that drive the deep-water oxygen depletion (Li et al. 2016; Zhou et al. 2014). In addition, there are indirect sources from the shallow flanks of the estuary and the lower Bay via advection, but the relative importance of these have not been extensively studied.

In the second chapter of my thesis, a three-dimensional hydrodynamic and nitrogen-based biogeochemical model was employed to study the particulate organic nitrogen (PON) transport, transformation and fate in Chesapeake Bay. My objectives were to identify the spatial and temporal variability in the autochthonous and allochthonous

processes that deliver PON (which includes phytoplankton and organic detritus) to the deep channel of the Bay. In achieving these objectives, I hope to discern the physical and biological factors that lead to the accumulation of PON in the thalweg of the Bay that fuels summertime bottom dissolved oxygen depletion (Testa and Kemp 2014).

Gross Primary Production and biomass

The process that transforms dissolved inorganic carbon, nitrogen, phosphorus to organic form is called primary production. Primary production forms the base of estuarine food web and so is a key driver of higher trophic level productivity (Blanchard et al. 2012; Cloern and Jassby 2010). Factors governing phytoplankton dynamics in coastal and estuarine systems include water temperature, light availability, salinity, stratification and nutrient availability (Cloern 1996). The strong nutrient, light, and salinity gradients (Gle et al. 2008; Kocum et al. 2002; Lohrenz et al. 1999) along with the three-dimensional estuarine circulation (Geyer and MacCready 2014) give rise to complex variations in primary production in both time and space. There is a growing need to fully comprehend the factors that control primary production, especially in highly eutrophic urbanized estuaries (Kemp et al. 2009) where improving water quality and water security have emerged as important issues (Strokal et al. 2015).

In Chesapeake Bay, the largest estuary in North America, excessive nutrient inputs from major tributaries like the Susquehanna River and Potomac Rivers (Zhou et al. 2014) stimulates excessive phytoplankton growth, which contributes to high biological oxygen demand and the development of large recurring hypoxic and

anoxic conditions (Kemp et al. 2005). Yet the current understanding of the factors that control the spatial and temporal variability in primary production and biological oxygen demand in Chesapeake Bay is still rudimentary in many respects. There has been only a handful of in situ studies of primary production variability in the Chesapeake Bay (Adolf et al. 2006; Harding et al. 2002; Kemp et al. 1997). These studies have revealed that phytoplankton biomass (chlorophyll) and phytoplankton primary production are not tightly linked to one another, with chlorophyll often peaking in spring and primary production usually peaking in summer (Malone et al. 1988). However, the data that have been used to characterize these patterns are relatively sparse and there is tremendous seasonal and interannual variability in the chlorophyll and production patterns. Although ocean color-based measurements of chlorophyll concentration and estimates of primary production provide the potential to help fill the observational gaps, they may not be able to capture the observed disconnect between chlorophyll and primary production, nor can they reveal the underlying mechanisms (Son et al. 2014). Suffice it to say, there is insufficient observational data available to adequately characterize the seasonal and interannual chlorophyll and primary production variability in Chesapeake Bay, much less determine the factors that control it.

The seasonal variability of phytoplankton biomass and growth rate in coastal and estuarine systems varies substantially (Cloern and Jassby 2010). For example, in the northern Gulf of Mexico, the peak growth rate happens in the late spring and beginning of summer coincident with the biomass peak (Fennel et al. 2011). Nonetheless, several-fold seasonal variations in the phytoplankton growth rate are

also presented in the intermediate part in Gulf of Mexico from the model (Fennel et al. 2011). This is in contrast to the aforementioned decoupling of the phytoplankton biomass and production rate peaks in Chesapeake Bay (Malone et al. 1988) which is also indicative of large seasonal variations in phytoplankton growth rate. Qin and Shen (2017) established a three-dimensional water quality model and introduced a variable growth coefficient that allows the model to simulate observed phytoplankton biomass variations in the James River. Although this parameter is not exactly the same as growth rate, it is interesting to note that at least 2 to 3 fold seasonal variations in this parameter must be imposed from spring to summer to get the model to correctly simulate the seasonal variability in phytoplankton biomass (Qin and Shen 2017). In a related study, Liu and de Swart (2018) established a two dimensional idealized dynamic phytoplankton production model that can simulate the vertical distribution of phytoplankton, and also the spatial distribution of growth rate in spring under different stratification conditions in the Columbia River, but they did not simulate the growth rate variation across the season. Cerco and Noel (2004) established a process-based biogeochemical model that can generally capture the seasonal variability of primary production in Chesapeake Bay as revealed by observations from the 1990s. However, upon close inspection in some years there are large discrepancies between the modeled and observed primary production, and the phytoplankton biomass variability is not shown. None of the previous biogeochemical modeling work conducted in Chesapeake Bay (Cerco and Noel 2004; Feng et al. 2015; Shen et al. 2019; Testa et al. 2014; Xu and Hood 2006) has successfully simulated the observed seasonal transition of both primary production (which

generally peaks in summer) and accumulation of biomass (which generally peaks in spring), nor have any of these studies examined how phytoplankton growth rate must vary seasonally to make this happen, or what the environmental factors are that control this growth rate variability. From Adolf et al. (2006) observations, it can be estimated that the summertime phytoplankton growth rate should be about 3-5 times larger than the growth rate in springtime in order to capture the observed seasonal changes in phytoplankton biomass and primary production.

Although satellite-based primary production results (Son et al. 2014) obtained in recent years provide more large-scale coverage and resolution, the physical, biogeochemical and physiological mechanisms behind the observed patterns are difficult to discern. This difficulty is exacerbated by the fact that satellites tell you very little about what is going on under the surface of the water. However, a processed based physical-biogeochemical model including growth, aggregation and mortality can cover a large spatial scale and multiple years' and potentially provide direct insights into the factors that control the seasonal patterns in phytoplankton biomass and primary production in Chesapeake Bay if the model can be parameterized to capture these patterns.

Denitrification

Low-efficiency agricultural utilization of nitrogen in fertilizer (Mueller et al. 2017; Zhang 2017) combined with auto and industrial emissions of NOx, septic system release of both organic and inorganic nitrogen and release of nitrogen in municipal wastewater treatment effluent result in significant nitrogen loading worldwide, considerably impacting the global nitrogen cycle (Bouwman et al. 2009).

Conventional denitrification, from the sequential reduction of nitrate to nitrite, then to nitric oxide and nitrous oxide and finally becoming dinitrogen gas (Zumft 1997) has long been considered as the primary sink process in the nitrogen cycle that can help to mitigate the effects of excessive fixed nitrogen loading (Cowan and Boynton 1996) in aquatic ecosystems that suffer from eutrophication (Christensen et al. 1987; Seitzinger and Giblin 1996). Given the magnitude of the ecological and economic problems that are caused by eutrophication (Bonaglia et al. 2014; Dodds et al. 2009; Kemp et al. 2005; Smith 2003), it is essential to understand the nitrogen cycle in aquatic ecosystems, and especially nitrogen removal processes like denitrification for its application in nutrient management. At the global scale both shelf sediments (Seitzinger et al. 2006) and open ocean oxygen minimum zones which include the Arabian Sea (Bulow et al. 2010; Ward et al. 2009), the eastern tropical South Pacific (Chang et al. 2010; Lam et al. 2009) and eastern tropical North Pacific (Horak et al. 2016) are well-studied hot spots for nitrogen loss via denitrification. In contrast, the relative importance of sediment and water column denitrification in estuaries has not been extensively studied (Kemp et al. 1990).

Chesapeake Bay, which is the largest estuary in United States, suffers from eutrophication due to excessive nitrogen loading as in other coastal waters (Kemp et al. 2005; Kemp et al. 2009). During the summertime, the chronic oxygen depletion in bottom water (Testa and Kemp 2014; Testa et al. 2018a; Testa et al. 2018b) promotes denitrification that transforms nitrate to nitrogen gas (Cornwell et al. 1999; Cowan and Boynton 1996; Kana et al. 2006), which is then released to the atmosphere. Therefore, understanding the spatial and temporal variability of denitrification in

Chesapeake Bay is of great importance for understanding the Chesapeake Bay nitrogen cycle, budget, and also for nutrient management efforts. An example of the importance of denitrification can be seen in measurements of bottom water NO_3^- in the main stem mesohaline Bay (e.g., CB3.3C) every year when values drop from 10-30 µmol/L in early summer to zero in less than one month. This happens after bottom water oxygen levels are depleted forcing facultative heterotrophic bacteria to switch to using NO_3^- as an alternative elector acceptor (Zumft 1997). This loss of nitrogen via generation of dinitrogen gas represents a substantial term in the Chesapeake Bay nitrogen cycle, yet the number of measurements that have been collected to characterize denitrification rates in the Bay are surprisingly sparse and, remarkably, they are restricted almost entirely to the benthos (Boynton et al. 1995). There are no reported measurements of water column denitrification in Chesapeake Bay. This is in contrast to the open ocean where water column denitrification rates have been routinely measuring for many years (Fuchsman et al. 2017; Fuchsman et al. 2019). Since a large volume of the bay becomes anoxic during summer there must be significant amounts of water column denitrification as observed in the open ocean, yet this was ignored in the nitrogen budget that was estimated by Boynton et al. (1995). Using a global model, DeVries et al. (2012) estimated that about 28% of the oceanic nitrogen loss occurs in the ocean water column oxygen minimum zones. In contrast, the relative importance of water column versus benthic denitrification in Chesapeake Bay is still unknown.

In addition to denitrification, there is another pathway of nitrogen loss in marine systems through anaerobic ammonium oxidation (ANAMMOX) (Bulow et al. 2010;

Dalsgaard et al. 2003; Dalsgaard and Thamdrup 2002; Lam et al. 2009; Thamdrup and Dalsgaard 2002). As with denitrification, there are also a very limited number of reported rates of dinitrogen gas production due to the ANAMMOX process in Chesapeake Bay (Babbin et al. 2016; Babbin and Ward 2013; Rich et al. 2008). Babbin and Ward (2013) suggested that the stoichiometry of organic matter, rather than the total amount of organic matter, regulates the relative contributions of ANAMMOX and denitrification to overall nitrogen loss in Chesapeake Bay. Rich et al. (2008) found that the percent of N_2 production due to ANAMMOX ranged from 0 to 22% in Chesapeake Bay, with the highest percentages occurring in the freshwater portion of the main stem of the upper bay. Due to the controversy and uncertainty surrounding the role of ANNAMOX in driving nitrogen loss in marine systems, combined with the difficulty of representing ANNAMOX in marine biogeochemical models, I only consider heterotrophic denitrification in this research.

Modeling technology provides a powerful tool to help us quantify the nitrogen cycle and denitrification variability over a wide range of space and time scales (Bianucci et al. 2012; Fennel et al. 2009; Fennel et al. 2006; Testa et al. 2013). Feng et al. (2015) used a coupled physical-biogeochemical model to determine five-year average nitrogen budget for the entire Chesapeake Bay without presenting a spatial and temporal variability in detail and the relative contribution between the water column and sediment.

Dissertation Structure

In my dissertation, it is structed as follows: In Chapter 1, I conducted numerical investigations of particulate organic nitrogen production, transport and fate in a

partially mixed estuary, Chesapeake Bay, using a validated model that focused on having the best possible model skill for chlorophyll; In Chapter 2, I used the same model, but with the tuning and validation focused on a balance between the best chlorophyll skill and gross primary production skill at the seasonal time scale, to investigate the lag peak between the phytoplankton biomass accumulation in the spring and peak gross primary production in the summer, as well as the mechanisms controlling these patterns; In Chapter 3, I used the same model, but with model skill balance between the chlorophyll, nitrogen, oxygen and denitrification, to conduct research on temporal and spatial variability of denitrification, and its possible effect on the nitrogen cycle in Chesapeake Bay. Through all this research, I hope to understand how physical and biogeochemical processes control the observed biogeochemical variability in Chesapeake Bay.

References

Adolf, J.E., C.L. Yeager, W.D. Miller, M.E. Mallonee, and L.W. Harding. 2006. Environmental forcing of phytoplankton floral composition, biomass, and primary productivity in Chesapeake Bay, USA. *Estuarine Coastal and Shelf Science* 67: 108-122. doi: 10.1016/j.ecss.2005.11.030

Babbin, A.R., A. Jayakumar, and B.B. Ward. 2016. Organic Matter Loading Modifies the Microbial Community Responsible for Nitrogen Loss in Estuarine Sediments. *Microbial Ecology* 71: 555-565. doi: 10.1007/s00248-015-0693-5

Babbin, A.R., and B.B. Ward. 2013. Controls on Nitrogen Loss Processes in Chesapeake Bay Sediments. *Environmental Science & Technology* 47: 4189-4196. doi: 10.1021/es304842r

Bianucci, L., K. Fennel, and K.L. Denman. 2012. Role of sediment denitrification in water column oxygen dynamics: comparison of the North American East and West Coasts. *Biogeosciences* 9: 2673-2682. doi: 10.5194/bg-9-2673-2012

Blanchard, J.L., S. Jennings, R. Holmes, J. Harle, G. Merino, J.I. Allen, J. Holt, N.K. Dulvy, and M. Barange. 2012. Potential consequences of climate change for primary production and fish production in large marine ecosystems.

Philosophical Transactions of the Royal Society B-Biological Sciences 367: 2979-2989. doi: 10.1098/rstb.2012.0231

Boesch, D., E. Burreson, W. Dennison, E. Houde, M. Kemp, V. Kennedy, R. Newell, K. Paynter, R. Orth, and R. Ulanowicz. 2001. Factors in the Decline of Coastal Ecosystems. *Science* 293: 1589. doi: 10.1126/science.293.5535.1589c

Bonaglia, S., F.J.A. Nascimento, M. Bartoli, I. Klawonn, and V. Bruchert. 2014. Meiofauna increases bacterial denitrification in marine sediments. *Nature Communications* 5. doi: 10.1038/ncomms6133

Bouwman, A.F., A.H.W. Beusen, and G. Billen. 2009. Human alteration of the global nitrogen and phosphorus soil balances for the period 1970-2050. *Global Biogeochemical Cycles* 23. doi: 10.1029/2009GB003576

Boynton, W., J. Garber, R. Summers, and W. Kemp. 1995. Inputs, transformations, and transport of nitrogen and phosphorus in Chesapeake Bay and selected tributaries. *Estuaries and Coasts* 18: 285-314. doi: 10.2307/1352640

Breitburg, D., L.A. Levin, A. Oschlies, M. Grégoire, F.P. Chavez, D.J. Conley, V. Garçon, D. Gilbert, D. Gutiérrez, K. Isensee, G.S. Jacinto, K.E. Limburg, I. Montes, S.W.A. Naqvi, G.C. Pitcher, N.N. Rabalais, M.R. Roman, K.A. Rose, B.A. Seibel, M. Telszewski, M. Yasuhara, and J. Zhang. 2018. Declining oxygen in the global ocean and coastal waters. *Science* 359. doi: 10.1126/science.aam7240

Bulow, S.E., J.J. Rich, H.S. Naik, A.K. Pratihary, and B.B. Ward. 2010. Denitrification exceeds anammox as a nitrogen loss pathway in the Arabian Sea oxygen minimum zone. *Deep-Sea Research Part I-Oceanographic Research Papers* 57: 384-393. doi: 10.1016/j.dsr.2009.10.014

Cerco, C.F., and M.R. Noel. 2004. Process-based primary production modeling in Chesapeake Bay. *Marine Ecology Progress Series* 282: 45-58. doi: 10.3354/meps282045

Chang, B.X., A.H. Devol, and S.R. Emerson. 2010. Denitrification and the nitrogen gas excess in the eastern tropical South Pacific oxygen deficient zone. *Deep-Sea Research Part I-Oceanographic Research Papers* 57: 1092-1101. doi: 10.1016/j.dsr.2010.05.009

Christensen, J.P., J.W. Murray, A.H. Devol, and L.A. Codispoti. 1987. Denitrification in continental shelf sediments has major impact on the oceanic nitrogen budget. *Global Biogeochemical Cycles* 1: 97-116. doi: 10.1029/GB001i002p00097

Cloern, J.E. 1996. Phytoplankton bloom dynamics in coastal ecosystems: A review with some general lessons from sustained investigation of San Francisco Bay, California. *Reviews of Geophysics* 34: 127-168. doi: 10.1029/96rg00986

Cloern, J.E., and A.D. Jassby. 2010. Patterns and Scales of Phytoplankton Variability in Estuarine-Coastal Ecosystems. *Estuaries and Coasts* 33: 230-241. doi: 10.1007/s12237-009-9195-3

Cornwell, J.C., W.M. Kemp, and T.M. Kana. 1999. Denitrification in coastal ecosystems: methods, environmental controls, and ecosystem level controls, a review. *Aquatic Ecology* 33: 41-54. doi: 10.1023/A:1009921414151

Cowan, J.L.W., and W.R. Boynton. 1996. Sediment-water oxygen and nutrient exchanges along the longitudinal axis of Chesapeake Bay: Seasonal patterns,

controlling factors and ecological significance. *Estuaries* 19: 562-580. doi: 10.2307/1352518

Dalsgaard, T., D.E. Canfield, J. Petersen, B. Thamdrup, and J. Acuna-Gonzalez. 2003. N-2 production by the anammox reaction in the anoxic water column of Golfo Dulce, Costa Rica. *Nature* 422: 606-608. doi: 10.1038/nature01526

Dalsgaard, T., and B. Thamdrup. 2002. Factors controlling anaerobic ammonium oxidation with nitrite in marine sediments. *Applied and Environmental Microbiology* 68: 3802-3808. doi: 10.1128/aem.68.8.3802-3808.2002

Deegan, L.A., D.S. Johnson, R.S. Warren, B.J. Peterson, J.W. Fleeger, S. Fagherazzi, and W.M. Wollheim. 2012. Coastal eutrophication as a driver of salt marsh loss. *Nature* 490: 388. doi: 10.1038/nature11533

DeVries, T., C. Deutsch, F. Primeau, B. Chang, and A. Devol. 2012. Global rates of water-column denitrification derived from nitrogen gas measurements. *Nature Geoscience* 5: 547-550. doi: 10.1038/ngeo1515

Diaz, R.J., and R. Rosenberg. 2008. Spreading dead zones and consequences for marine ecosystems. *Science* 321: 926-929. doi: 10.1126/science.1156401

Dodds, W.K., W.W. Bouska, J.L. Eitzmann, T.J. Pilger, K.L. Pitts, A.J. Riley, J.T. Schloesser, and D.J. Thornbrugh. 2009. Eutrophication of US Freshwaters: Analysis of Potential Economic Damages. *Environmental Science & Technology* 43: 12-19. doi: 10.1021/es801217q

Feng, Y., M.A.M. Friedrichs, J. Wilkin, H.Q. Tian, Q.C. Yang, E.E. Hofmann, J.D. Wiggert, and R.R. Hood. 2015. Chesapeake Bay nitrogen fluxes derived from a land-estuarine ocean biogeochemical modeling system: Model description, evaluation, and nitrogen budgets. *Journal of Geophysical Research-Biogeosciences* 120: 1666-1695. doi: 10.1002/2015jg002931

Fennel, K., D. Brady, D. Di Toro, R.W. Fulweiler, W.S. Gardner, A. Giblin, M.J. McCarthy, A. Rao, S. Seitzinger, M. Thouvenot-Korppoo, and C. Tobias. 2009. Modeling denitrification in aquatic sediments. *Biogeochemistry* 93: 159-178. doi: 10.1007/s10533-008-9270-z

Fennel, K., R. Hetland, Y. Feng, and S. DiMarco. 2011. A coupled physical-biological model of the Northern Gulf of Mexico shelf: model description, validation and analysis of phytoplankton variability. *Biogeosciences* 8: 1881-1899. doi: 10.5194/bg-8-1881-2011

Fennel, K., J. Wilkin, J. Levin, J. Moisan, J. O'Reilly, and D. Haidvogel. 2006. Nitrogen cycling in the Middle Atlantic Bight: Results from a three-dimensional model and implications for the North Atlantic nitrogen budget. *Global Biogeochemical Cycles* 20. doi: 10.1029/2005GB002456

Fuchsman, C.A., A.H. Devol, J.K. Saunders, C. McKay, and G. Rocap. 2017. Niche Partitioning of the N Cycling Microbial Community of an Offshore Oxygen Deficient Zone. *Frontiers in Microbiology* 8: 18. doi: 10.3389/fmicb.2017.02384

Fuchsman, C.A., B. Paul, J.T. Staley, E.V. Yakushev, and J.W. Murray. 2019. Detection of Transient Denitrification During a High Organic Matter Event in the Black Sea. *Global Biogeochemical Cycles* 33: 143-162. doi: 10.1029/2018gb006032

Geyer, W.R., and P. MacCready. 2014. The Estuarine Circulation. *Annual Review of Fluid Mechanics* 46: 175-197. doi: 10.1146/annurev-fluid-010313-141302

Gle, C., Y. Del Amo, B. Sautour, P. Laborde, and P. Chardy. 2008. Variability of nutrients and phytoplankton primary production in a shallow macrotidal coastal ecosystem (Arcachon Bay, France). *Estuarine Coastal and Shelf Science* 76: 642-656. doi: 10.1016/j.ecss.2007.07.043

Harding, L.W., M.E. Mallonee, and E.S. Perry. 2002. Toward a Predictive Understanding of Primary Productivity in a Temperate, Partially Stratified Estuary. *Estuarine, Coastal and Shelf Science* 55: 437-463. doi: 10.1006/ecss.2001.0917

Horak, R.E.A., W. Ruef, B.B. Ward, and A.H. Devol. 2016. Expansion of denitrification and anoxia in the eastern tropical North Pacific from 1972 to 2012. *Geophysical Research Letters* 43: 5252-5260. doi: 10.1002/2016gl068871

Howarth, R., F. Chan, D.J. Conley, J. Garnier, S.C. Doney, R. Marino, and G. Billen. 2011. Coupled biogeochemical cycles: eutrophication and hypoxia in temperate estuaries and coastal marine ecosystems. *Frontiers in Ecology and the Environment* 9: 18-26. doi: 10.1890/100008

Kana, T.M., J.C. Cornwell, and L.J. Zhong. 2006. Determination of denitrification in the Chesapeake Bay from measurements of N-2 accumulation in bottom water. *Estuaries and Coasts* 29: 222-231. doi: 10.1007/bf02781991

Kemp, W.M., W.R. Boynton, J.E. Adolf, D.F. Boesch, W.C. Boicourt, G. Brush, J.C. Cornwell, T.R. Fisher, P.M. Glibert, J.D. Hagy, L.W. Harding, E.D. Houde, D.G. Kimmel, W.D. Miller, R.I.E. Newell, M.R. Roman, E.M. Smith, and J.C. Stevenson. 2005. Eutrophication of Chesapeake Bay: historical trends and ecological interactions. *Marine Ecology Progress Series* 303: 1-29. doi: 10.3354/Meps303001

Kemp, W.M., P. Sampou, J. Caffrey, M. Mayer, K. Henriksen, and W.R. Boynton. 1990. Ammonium recycling versus denitrification in Chesapeake Bay sediments. *Limnology and Oceanography* 35: 1545-1563. doi: 10.4319/lo.1990.35.7.1545

Kemp, W.M., E.M. Smith, M. Marvin-DiPasquale, and W.R. Boynton. 1997. Organic carbon balance and net ecosystem metabolism in Chesapeake Bay. *Marine Ecology Progress Series* 150: 229-248. doi: 10.3354/meps150229

Kemp, W.M., J.M. Testa, D.J. Conley, D. Gilbert, and J.D. Hagy. 2009. Temporal responses of coastal hypoxia to nutrient loading and physical controls. *Biogeosciences* 6: 2985-3008. doi: 10.5194/bg-6-2985-2009

Kocum, E., G.J.C. Underwood, and D.B. Nedwell. 2002. Simultaneous measurement of phytoplanktonic primary production, nutrient and light availability along a turbid, eutrophic UK east coast estuary (the Colne Estuary). *Marine Ecology Progress Series* 231: 1-12. doi: 10.3354/meps231001

Lam, P., G. Lavik, M.M. Jensen, J. van de Vossenberg, M. Schmid, D. Woebken, G. Dimitri, R. Amann, M.S.M. Jetten, and M.M.M. Kuypers. 2009. Revising the nitrogen cycle in the Peruvian oxygen minimum zone. *Proceedings of the National Academy of Sciences of the United States of America* 106: 4752-4757. doi: 10.1073/pnas.0812444106

Li, M., Y.J. Lee, J.M. Testa, Y. Li, W.F. Ni, W.M. Kemp, and D.M. Di Toro. 2016. What drives interannual variability of hypoxia in Chesapeake Bay: Climate forcing versus nutrient loading? *Geophysical Research Letters* 43: 2127-2134. doi: 10.1002/2015gl067334

Li, Y., and M. Li. 2011. Effects of winds on stratification and circulation in a partially mixed estuary. *Journal of Geophysical Research-Oceans* 116. doi: 10.1029/2010jc006893

Li, Y., and M. Li. 2012. Wind-driven lateral circulation in a stratified estuary and its effects on the along-channel flow. *Journal of Geophysical Research-Oceans* 117. doi: 10.1029/2011jc007829

Liu, B., and H.E. de Swart. 2018. Quantifying the Effect of Salinity Stratification on Phytoplankton Density Patterns in Estuaries. *Estuaries and Coasts* 41: 453-470. doi: 10.1007/s12237-017-0276-4

Lohrenz, S.E., G.L. Fahnenstiel, D.G. Redalje, G.A. Lang, M.J. Dagg, T.E. Whitledge, and Q. Dortch. 1999. Nutrients, irradiance, and mixing as factors regulating primary production in coastal waters impacted by the Mississippi River plume. *Continental Shelf Research* 19: 1113-1141. doi: 10.1016/s0278-4343(99)00012-6

Malone, T., L. Crocker, S. Pike, and B. Wendler. 1988. Influences of river flow on the dynamics of phytoplankton production in a partially stratified estuary. *Marine Ecology Progress Series*: 235-249. doi: 10.3354/meps048235

Mueller, N.D., L. Lassaletta, B.C. Runck, G. Billen, J. Garnier, and J.S. Gerber. 2017. Declining spatial efficiency of global cropland nitrogen allocation. *Global Biogeochemical Cycles* 31: 245-257. doi: 10.1002/2016GB005515

Murphy, R.R., W.M. Kemp, and W.P. Ball. 2011. Long-Term Trends in Chesapeake Bay Seasonal Hypoxia, Stratification, and Nutrient Loading. *Estuaries and Coasts* 34: 1293-1309. doi: 10.1007/s12237-011-9413-7

Paerl, H.W., and J.T. Scott. 2010. Throwing Fuel on the Fire: Synergistic Effects of Excessive Nitrogen Inputs and Global Warming on Harmful Algal Blooms. *Environmental Science & Technology* 44: 7756-7758. doi: 10.1021/es102665e

Qin, Q., and J. Shen. 2017. The contribution of local and transport processes to phytoplankton biomass variability over different timescales in the Upper James River, Virginia. *Estuarine Coastal and Shelf Science* 196: 123-133. doi: 10.1016/j.ecss.2017.06.037

Rabalais, N.N., R.E. Turner, R.J. Diaz, and D. Justic. 2009. Global change and eutrophication of coastal waters. *Ices Journal of Marine Science* 66: 1528-1537. doi: 10.1093/icesjms/fsp047

Ralston, D.K., W.R. Geyer, J.A. Lerczak, and M. Scully. 2010. Turbulent mixing in a strongly forced salt wedge estuary. *Journal of Geophysical Research* 115. doi: 10.1029/2009jc006061

Rich, J.J., O.R. Dale, B. Song, and B.B. Ward. 2008. Anaerobic ammonium oxidation (Anammox) in Chesapeake Bay sediments. *Microbial Ecology* 55: 311-320. doi: 10.1007/s00248-007-9277-3

Scully, M.E. 2016. Mixing of dissolved oxygen in Chesapeake Bay driven by the interaction between wind-driven circulation and estuarine bathymetry. *Journal of Geophysical Research-Oceans* 121: 5639-5654. doi: 10.1002/2016jc011924

Scully, M.E., and C.T. Friedrichs. 2007. The importance of tidal and lateral asymmetries in stratification to residual circulation in partially mixed estuaries. *Journal of Physical Oceanography* 37: 1496-1511. doi: 10.1175/jpo3071.1

Scully, M.E., and W.R. Geyer. 2012. The role of advection, straining, and mixing on the tidal variability of estuarine stratification. *Journal of Physical Oceanography* 42: 855-868. doi: 10.1175/jpo-d-10-05010.1

Seitzinger, S., J.A. Harrison, J.K. Bohlke, A.F. Bouwman, R. Lowrance, B. Peterson, C. Tobias, and G. Van Drecht. 2006. Denitrification across landscapes and waterscapes: A synthesis. *Ecological Applications* 16: 2064-2090. doi: 10.1890/1051-0761(2006)016[2064:dalawa]2.0.co;2

Seitzinger, S.P., and A.E. Giblin. 1996. Estimating denitrification in North Atlantic continental shelf sediments. *Biogeochemistry* 35: 235-260. doi: 10.1007/BF02179829

Shen, C.Q., J.M. Testa, M. Li, W.J. Cai, G.G. Waldbusser, W.F. Ni, W.M. Kemp, J. Cornwell, B.S. Chen, J. Brodeur, and J.Z. Su. 2019. Controls on Carbonate System Dynamics in a Coastal Plain Estuary: A Modeling Study. *Journal of Geophysical Research-Biogeosciences* 124: 61-78. doi: 10.1029/2018jg004802

Smil, V. 2000. Phosphorus in the environment: Natural flows and human interferences. *Annual Review of Energy and the Environment* 25: 53-88. doi: 10.1146/annurev.energy.25.1.53

Smith, V.H. 2003. Eutrophication of freshwater and coastal marine ecosystems - A global problem. *Environmental Science and Pollution Research* 10: 126-139. doi: 10.1065/espr2002.12.142

Son, S., M. Wang, and L.W. Harding. 2014. Satellite-measured net primary production in the Chesapeake Bay. *Remote Sensing of Environment* 144: 109-119. doi: 10.1016/j.rse.2014.01.018

Strokal, M., C. Kroeze, L.L. Li, S.J. Luan, H.Z. Wang, S.S. Yang, and Y.S. Zhang. 2015. Increasing dissolved nitrogen and phosphorus export by the Pearl River (Zhujiang): a modeling approach at the sub-basin scale to assess effective nutrient management. *Biogeochemistry* 125: 221-242. doi: 10.1007/s10533-015-0124-1

Testa, J.M., D.C. Brady, D.M. Di Toro, W.R. Boynton, J.C. Cornwell, and W.M. Kemp. 2013. Sediment flux modeling: Simulating nitrogen, phosphorus, and silica cycles. *Estuarine, Coastal and Shelf Science* 131: 245-263. doi: 10.1016/j.ecss.2013.06.014

Testa, J.M., and W.M. Kemp. 2014. Spatial and temporal patterns in winter-spring oxygen depletion in Chesapeake Bay bottom waters. *Estuaries and Coasts* 37: 1432-1448. doi: 10.1007/s12237-014-9775-8

Testa, J.M., W.M. Kemp, and W.R. Boynton. 2018a. Season-specific trends and linkages of nitrogen and oxygen cycles in Chesapeake Bay. *Limnology and Oceanography* 63: 2045-2064. doi: 10.1002/lno.10823

Testa, J.M., Y. Li, Y.J. Lee, M. Li, D.C. Brady, D.M. Di Toro, W.M. Kemp, and J.J. Fitzpatrick. 2014. Quantifying the effects of nutrient loading on dissolved O2 cycling and hypoxia in Chesapeake Bay using a coupled hydrodynamic–

biogeochemical model. *Journal of Marine Systems* 139: 139-158. doi: 10.1016/j.jmarsys.2014.05.018

Testa, J.M., R.R. Murphy, D.C. Brady, and W.M. Kemp. 2018b. Nutrient- and Climate-Induced Shifts in the Phenology of Linked Biogeochemical Cycles in a Temperate Estuary. *Frontiers in Marine Science* 5. doi: 10.3389/fmars.2018.00114

Thamdrup, B., and T. Dalsgaard. 2002. Production of N-2 through anaerobic ammonium oxidation coupled to nitrate reduction in marine sediments. *Applied and Environmental Microbiology* 68: 1312-1318. doi: 10.1128/aem.68.3.1312-1318.2002

Ward, B.B., A.H. Devol, J.J. Rich, B.X. Chang, S.E. Bulow, H. Naik, A. Pratihary, and A. Jayakumar. 2009. Denitrification as the dominant nitrogen loss process in the Arabian Sea. *Nature* 461: 78-U77. doi: 10.1038/nature08276

Wei, X., M. Kumar, and H.M. Schuttelaars. 2017. Three-Dimensional Salt Dynamics in Well-Mixed Estuaries: Influence of Estuarine Convergence, Coriolis, and Bathymetry. *Journal of Physical Oceanography* 47: 1843-1871. doi: 10.1175/JPO-D-16-0247.1

Xu, J., and R.R. Hood. 2006. Modeling biogeochemical cycles in Chesapeake Bay with a coupled physical–biological model. *Estuarine, Coastal and Shelf Science* 69: 19-46. doi: 10.1016/j.ecss.2006.03.021

Zhang, W., Y. Cao, Y.L. Zhu, J.H. Zheng, X.M. Ji, Y.W. Xu, Y. Wu, and A.J.F. Hoitink. 2018. Unravelling the causes of tidal asymmetry in deltas. *Journal of Hydrology* 564: 588-604. doi: 10.1016/j.jhydrol.2018.07.023

Zhang, X. 2017. Biogeochemistry: A plan for efficient use of nitrogen fertilizers. *Nature* 543: 322-323. doi: 10.1038/543322a

Zhou, Y., D. Scavia, and A.M. Michalak. 2014. Nutrient loading and meteorological conditions explain interannual variability of hypoxia in the Chesapeake Bay. *Limnology and Oceanography* 59: 373-384. doi: 10.4319/lo.2014.59.2.0373

Zumft, W.G. 1997. Cell biology and molecular basis of denitrification. *Microbiology and Molecular Biology Reviews* 61: 533-+. doi: 10.1128/.61.4.533-616.1997

Chapter 2: Transport and Fate of Particulate Organic Nitrogen in Chesapeake Bay: A numerical study

Abstract

In Chesapeake Bay substantial quantities of organic matter are produced during the spring bloom, which contributes to severe chronic bottom oxygen depletion during the summertime. However, the details of this transport in the estuarine system under realistic forcing is still unclear. In this Research, a three-dimensional model was used to investigate the production, transport, and fate of organic matter in Chesapeake Bay. Analysis of a control volume in the deep channel revealed that the sinking flux of fast-sinking particulate organic nitrogen (PON) into the deep channel is comparable to the horizontal advective transport. The model analysis also revealed a pronounced east to west transport of PON during the springtime and a tendency to export mass from the eastern shore to the deep channel and from the deep channel to the western shore of the Chesapeake Bay, and also a convergence of mass transport on the western shore. This transport is consistent with the lateral estuarine circulation in Chesapeake Bay that arises due to the asymmetry of the flood-neap tidal cycle. In addition, the model revealed that seasonal variations in wind alter the magnitude and distribution of organic matter flux in the along channel and cross channel direction, with northerly winds during the springtime favoring more northward organic matter transport and more organic matter accumulation in the deep channel, however, the lateral net flux direction remains the same.

Introduction

Estuaries are semi-enclosed water bodies and transition zones that connect freshwater to marine environments with strong salinity gradients (Geyer and MacCready 2014) and they are often negatively influenced by human activity (Howarth et al. 2011). Estuaries worldwide (Rabalais et al. 2009) have suffered over the past several decades from eutrophication caused agricultural fertilization (Zhang 2017) and dumping of nitrogen-enriched industrial and urban waste waters (Deegan et al. 2012; Smil 2000). The resulting increases in primary production can lead to the generation of particulate organic matter (POM) and elevated biological oxygen demand. Eutrophication is one of the leading risks to estuarine ecosystem integrity (Paerl and Scott 2010) and jeopardizes these ecosystems through, in particular, depletion of bottom water oxygen (Breitburg et al. 2018; Diaz and Rosenberg 2008; Testa et al. 2018).

The eutrophication-fueled POM that drives depletion of oxygen may be subjected to diverse transport pathways in natural highly stratified (Ralston et al. 2010), partially mixed (Scully and Geyer 2012) and well-mixed (Wei et al. 2017) estuarine systems before it arrives at the bottom. Estuaries with complex bathymetry (Scully 2016b; Scully and Friedrichs 2007) can have heterogeneous residence times (Du and Shen 2016) and circulation patterns due to the interaction of river discharge, tidal asymmetry (Zhang et al. 2018) and wind forcing (Li and Li 2011; Li and Li 2012). This variability will result in retention, settling and remineralization of POM in some areas and mixing, transport and dispersal of POM on others. Understanding POM

transport, transformation and fate in estuaries is clearly important for understanding the negative impacts of eutrophication.

Chesapeake Bay is the largest estuary in the US and one of the most productive estuaries on the east coast of North America (Figure 2.1a,b). Eutrophication of Chesapeake Bay began with land clearing in the 18th century (Boesch et al. 2001) that resulted in increased nutrient loading. Today the Bay suffers from excessive primary production resulting in chronic bottom oxygen depletion during the summer (Cowan and Boynton 1996). Many studies have been conducted that focus on the onset and development of oxygen depletion in Chesapeake Bay (Kemp et al. 2005; Murphy et al. 2011; Testa and Kemp 2014). In contrast, relatively few studies have been conducted that focus on the complicated physical and biological processes that control the transport and fate of the POM in the estuary that drives the oxygen depletion. Accumulating evidence suggests that there is a connection between bottom water accumulation of organic matter during springtime and the summertime hypoxia (Testa and Kemp 2012; Testa et al. 2018). There are direct sources of POM input from the overlying water column via sinking that drive the deep-water oxygen depletion (Testa and Kemp 2014). In addition, there are indirect sources from the shallow flanks of the estuary (Kemp et al. 1997) and the lower Bay via gravitational circulation, but the relative importance of these have not been extensively studied.

In this research, a three-dimensional hydrodynamic and nitrogen-based biogeochemical model was employed to study the particulate organic nitrogen (PON) transport, transformation and fate in Chesapeake Bay (Figure 2.1c,d). My objectives were to identify the spatial and temporal variability in the autochthonous and

allochthonous processes that deliver PON (which includes phytoplankton, zooplankton and organic detritus) to the deep channel of the Bay. In achieving these objectives, I hope to discern the physical and biological factors that lead to the accumulation of PON in the thalweg of the Bay (Figure 2.1e) that fuels summertime bottom dissolved oxygen depletion (Testa and Kemp 2014).

This paper is structured as follows. In Section 2, I provide a description of the numerical models that were used in the study along with a description of the PON volume transport flux methods and an assessment of model skill. In Section 3, I examine the results of a 6-year simulation of Chesapeake Bay. These results illustrate the transport patterns and the fate of PON in different organic forms in the Bay and their seasonal and spatial and variability. In Section 4, I discuss the physical and biological mechanisms that cause the observed transport patterns in the context of previous investigations and provide suggestions for future work. Lastly, the primary findings are briefly summarized in section 5.

Methods

The physical Model

The physical component of the coupled model is based on the Regional Ocean Modeling System (ROMS) version 3.6 (Shchepetkin and McWilliams 2005), and the model domain and horizontal grid follow the Chesapeake Bay community implementation of ROMS (ChesROMS) (Xu et al. 2012). The physical component is identical to that described in previous research (Scully 2013; Scully 2016a). The domain spans the region from 77.2°W to 75.0°W and from 36°N to 40°N, covering the main stem and primary tributaries of Chesapeake Bay, as well as part of the mid-

Atlantic Bight (Figure 2.1c). The horizontal grid spacing varies with the highest resolution (430 m) in the northern Bay near the Chesapeake and Delaware Canal, lowest resolution (12 km) in the southern end of the mid-Atlantic Bight, and average grid spacing within the Chesapeake Bay of 1.7 km. The model has 20 terrain-following vertical layers with a higher resolution near the surface and bottom boundaries. The bottom topography is also smoothed to avoid pressure gradient errors caused by steep bathymetry (Scully 2013). ChesROMS is forced by open ocean tides and non-tidal water levels, river discharge, winds, and heat exchange across the air-sea interface. Water level forcing at the oceanic boundary includes nine tidal harmonic constituents and the observed non-tidal water level based on an interpolation between observed values at Duck, NC and Wachepreque, VA. Chapman's condition for surface elevation and Flather's condition for barotropic velocity is applied to the barotropic component at the open ocean boundary, while for the baroclinic component a radiation condition is used for velocity and a radiation condition with nudging is used for temperature and salinity. Climatological temperature and salinity from the World Ocean Atlas 2001was used for nudging at the open ocean boundary. Atmospheric forcing quantities, including 3-hourly winds, net shortwave and downward longwave radiations, air temperature, relative humidity, and pressure, are obtained from the National Center for Environmental Prediction (NCEP) North American Regional Reanalysis (NARR) model products.

The Biogeochemical Model

The biogeochemical model is based on an NPZD-type, nitrogen-based ecosystem model (Fennel et al. 2006), which comes bundled with the ROMS source code. The

model (Figure 2.1d) has been modified as described in Wiggert et al. (2017) and it is very similar to the model described in Feng et al. (2015). Here I focus on the components of the model that differ from Wiggert et al. (2017). The detailed model equations and parameters are provided and described in Table 0-1 and Table 0-2 in the Appendices.

The biogeochemical model contains ten state variables: phytoplankton, chlorophyll, zooplankton, ammonium, nitrate, dissolved organic nitrogen, inorganic suspended sediment, small detritus, large detritus and oxygen. With the exception of chlorophyll, oxygen and ISS, all of the state variables are in nitrogen units (Figure 2.1d). The dissolved oxygen (DO) component of the biogeochemical model includes representation of air–sea exchange, oxygen produced during photosynthesis, and oxygen demand associated with: 1) nitrification; 2) zooplankton metabolic costs; and 3) remineralization of particulate and dissolved organic matter within the water column and the benthos. The DO configuration allows the remineralization processes to transition from oxic to anoxic states in both the water column and the sediments. The original Feng et al. (2015) biogeochemical model assumes aerobic respiration in the water column and a fixed fraction (14%) of anoxic remineralization in the sediments. However, during the summertime in Chesapeake Bay the sub-pycnocline water column transitions to hypoxic and fully anoxic conditions in the mesohaline deep channel and, as a result, the sediments also transition to fully anoxic conditions (Kemp et al. 2005; Kemp et al. 2009). Thus, during the summer in the mesohaline deep channel, organic matter is remineralized anaerobically in both the sub-pycnocline waters and in the sediments with nitrate acting as the alternative electron

acceptor. In order to account for the impacts of changing water column oxygen concentrations my model has been modified as described in Wiggert et al. (2017) to allow the ratio of anaerobic to aerobic remineralization to change in response to changes in the oxygen concentrations in the overlying water column extending all the way to a fully anoxic overlying water column with the bottom sediment transitioning to fully anaerobic remineralization. As this transition takes place the stoichiometry of sediment remineralization switches from coupled nitrification-denitrification (which does not require NO_3^- from the overlying water column) to denitrification (which does require nitrate from the overlying water column).

The dissolved organic nitrogen (DON) pool is of a similar magnitude to the inorganic nitrogen pool in Chesapeake Bay (Boynton et al. 1995) and it has a pronounced effect on the nitrogen budget in the estuary (Bradley et al. 2010). Therefore, a single DON state variable was added to the model as described in Wiggert et al. (2017). The sources of DON are from the river, algal exudation and mortality, and zooplankton excretion. This DON is remineralized both aerobically and anaerobically like particulate organic nitrogen throughout the year.

The light attenuation model is the same as that which is described in Xu et al. (2005). Following Xu and Hood (2006) the sinking speed for phytoplankton varies as a function of season with a high sinking speed in winter and spring to represent the dominance of large diatoms that sink rapidly, while during summertime, the sinking speed is reduced to represent the dominance of small flagellates and dinoflagellates that sink slowly (Marshall and Nesius 1996). The maximum carbon to chlorophyll is also assumed to increase during summertime following Cerco and Noel (2004), which

impacts the models calculated chlorophyll concentrations. For the model results I defined PON to be the sum of phytoplankton, zooplankton, small detritus, and large detritus together for validation. For the PON budget analysis, the zooplankton was ignored because it contributes very little to bottom PON flux during springtime. For the river boundary nutrient forcing, I used measured values form the Chesapeake Bay Program upstream station located as close as possible to the river boundary (Brown et al. 2013) in the model domain (for NH_4^+, NO_3^-, chlorophyll, oxygen and DON) rather than using watershed model outputs as in Feng et al. (2015). A general carbon to chlorophyll ration value 50 and Redfield is applied to get the riverside phytoplankton value. Riverside zooplankton was set 1/10 of phytoplankton. Half of TSS was set to be OSS and rest was ISS. For total detritus, we get that though OSS (phytoplankton +zooplankton). Then 1/3 of the OSS was set to be small detritus and 2/3 was set to be large detritus (Xu and Hood 2006).

Volumetric transport flux calculation

ROMS provides a basic volume transport diagnostic program to investigate different physical processes such as horizontal advection, vertical advection and diffusion in the momentum and tracer transport governing equations, and this program has been widely used by other investigators (Pan et al. 2014; Scully 2010b; Wang et al. 2013). However, the original diagnostic program does not provide information about the tracer volume transport direction. For this study it was critical to know where the volume flux comes from and where it goes in order to examine, for example, the east-west asymmetry in Chesapeake Bay volume transport. For this research I modified the ROMS volume transport code so that it can calculate volume and tracer transport

and direction on each side of a control volume and integrate the transport over time to generate a budget. Three narrow control volumes were selected to better understand the PON flux transport and transformation in the deep channel of Chesapeake Bay and its exchange with the flank regions. A_1-A_1 was positioned in the deep channel along the mainstem of Chesapeake Bay, A_2-A_2 was positioned parallel to the deep channel on the western shore, and A_3-A_3 was positioned parallel to the deep channel on the eastern shore (Figure 2.2a). These volumes were one grid cell wide and six layers thick extending upward from the bottom as shown in Figure 2.2b.

Model scenarios: Base run and experimental scenarios

In order to investigate the impacts of variations in wind and river forcing on PON transport a sensitivity analysis was carried out with different wind and river input forcing. The details of these different runs are presented in Table 2-1.

Results

Model validation

My model produced similar, and in some respects better, skill in simulating chlorophyll, PON, nitrate, ammonium, and dissolved oxygen, compared to previous Chesapeake Bay modeling studies (Feng et al. 2015; Irby et al. 2016; Li et al. 2009; Testa et al. 2014), as presented in Figure 2.3 to Figure 2.7.

Target diagrams (Hofmann et al. 2008; Jolliff et al. 2009) are presented in Figure 2.3. The model captures the mean values of the measurement data. The normalized bias is less than 0.5 for most of the chlorophyll stations (Figure 2.3 a) and less than 0.25 for oxygen (Figure 2.3b), NH_4^+ (Figure 2.3c) and NO_3^- (Figure 2.3 d) results. The model

tends to overestimate the mean chlorophyll and oxygen values in the northern bay stations while it underestimates them in the southern bay. For NO_3^-, the model slightly overpredicted the mean values in the southern bay and it underestimated the mean values in the northern bay. The model also overpredicted the variability of in chlorophyll, oxygen, NH_4^+ and NO_3^-. The model reproduced the oxygen variability more accurately than the other biogeochemical state variables.

The Taylor diagrams (Taylor 2001) provide a similar assessment of the model skill (Figure 2.4). The oxygen displayed the highest correlation coefficient. The model skill was better in the northern bay region for NH_4^+ and NO_3^- compared to the southern bay region. For nitrate, the model was closer to the mean in the northern bay region with relatively high correlation coefficients (Figure 2.4d).

The spatial distribution of the model skill (Willmott 1981) depicted in Figure 2.5, shows that the overall skill values decrease from oxygen to NO_3^-/ NH_4^+ to chlorophyll, which is typical for coupled physical-biogeochemical model simulations (Feng et al. 2015; Irby et al. 2016). For chlorophyll, the highest skill is in the CB4.4 region with values > 0.6 with only slightly lower skill values in the upper and lower bay (Figure 2.5a). Oxygen shows highest skill at ~0.9 throughout the bay (Figure 2.5b). An overall decreasing trend in the model skill was observed for NH_4^+ from 0.75 at the CB3.3C to near 0.6 at the bay mouth station CB6.4. The model simulation skill for NO_3^- is relatively high in the upper bay achieving ~0.8 at station CB3.3C and then decreasing southward. The southern bay stations from CB5.4 to CB7.1 had relatively low simulation skill between 0.5 to 0.6, except station CB6.4.

Not only does the model capture both seasonal variability of the chlorophyll, but also the spatial variability in the along channel direction as well as local vertical distributions. Note that high bottom chlorophyll was observed in spring in the CBP data, as well as in my model, for example at stations CB3.3C and CB4.2C during the year 2005 (Figure 2.6) with skill of 0.7 and 0.63, respectively. This phenomenon of bottom accumulation of chlorophyll in the spring, which was also noted and simulated by Xu and Hood (2006), has not been addressed in other Chesapeake Bay biogeochemical modeling studies (for example, Da et al. 2018; Feng et al. 2015). High chlorophyll concentrations develop during the spring in Chesapeake Bay due to blooms of large diatoms. These diatoms subsequently sink to the bottom resulting in the "inverted chlorophyll profiles" noted by Xu and Hood (2006). The model also captures the seasonal, as well as interannual variability of bottom PON in the system with pronounced interannually variability (Figure 2.7). High bottom PON levels (more than 50 μmol Nitrogen/L) were observed and simulated during springtime many years at the mesohaline stations CB4.1C, CB4.2C and CB4.3C. These high values largely disappear during summertime. Wet years, like 2003 also produced more PON in the bottom compared to dry years like 2002. Given these results I consider that this model generally captured both the temporal and spatial variability in the nitrogen cycle in Chesapeake Bay.

Deep channel particulate organic matter budget from base run A1

The primary motivation for this research is to better understand where the POM/PON comes from that gives rise to the oxygen depletion in the deep channel of Chesapeake Bay during summer. Toward this end, it is possible to separate the autochthonous

(physical) and allochthonous (biological) processes that control PON variability through the model budget analysis. Figure 2.8 depicts monthly averaged PON transport due to advection and sinking over the entire deep channel control volume A_1-A_1 during the model periods 2000 to 2005. Substantial variability was observed in the monthly averaged biological and physical transports. In all, autochthonous (physical) and allochthonous (biogeochemical) sinking (sink in Figure 2.8) contributions of PON to the deep channel were approximately the same magnitude (Figure 2.8). The peak values occurred in mid-spring (April), they sharply decreased in the summer and they increased again in the fall. The magnitudes of both autochthonous and allochthonous transport processes were related to PON concentration, i.e., the transports were highest in the spring and fall when the PON concentrations were highest and they were lowest in summer when the PON concentrations were lowest. For the physical processes, the cross channel (east-west, xadv in Figure 2.8) transport is positive, i.e., it adds PON to the deep channel, while the along channel (north-south, yadv in Figure 2.8) transport acts as a sink term for the deep channel PON budget. The net horizontal advection (hadv in Figure 2.8) contributes to PON accumulation in the deep channel with the largest contribution due to lateral processes, i.e., PON lateral transport (xadv in Figure 2.8). In contrast, the vertical advection is a sink term, i.e., it moves PON upward and out of the deep channel. The horizontal and vertical advection processes are approximately the same magnitude and display similar seasonal variability (Figure 2.8). Vertical diffusion is also a sink term but it is very small compared to the other terms (vdiff in Figure 2.8).

For the biological processes, sinking always contributed to PON accumulation in the deep channel and the contributions were highest in the spring and lowest during summer (Figure 2.9), reflecting the seasonal changes in PON concentration. Figure 2.9 shows the contribution of PON in the form of phytoplankton, small detritus and large detritus to the deep channel. The contribution due to sinking was always larger than the losses due to mortality, coagulation and grazing for phytoplankton and large and small detritus (self-sinking in Figure 2.9a,b,c). Coagulation was the major loss term for the phytoplankton budget, and it is a source term for large detritus, consistent with the biogeochemical transformations between different forms of PON in the model. The coagulation was especially large during March and April when the chlorophyll concentrations were largest. The remineralization processes all act as a sink transforming PON to DIN for both large and small detritus (Figure 2.9a,b,c). There is less remineralization of large detritus during summertime because there is less large detritus. During summertime the detritus pool is dominated by small detritus or small size organic matter particles. In my model, small detritus remineralization occurs from May to November (Figure 2.9c).

Considerable PON accumulation in the deep channel of Chesapeake Bay is due to sinking from above, as observed in the open ocean (Fernandez-Urruzola et al. 2016). The downward sinking process transports organic matter from euphotic zone to aphotic zone. The largest downward sinking flux of PON to the lower water column happens during spring in association with the spring bloom, which highlights the importance of high concentrations of large, rapid-sinking PON in spring. In Chesapeake Bay these large rapid-sinking particles are due to diatom blooms that

happen in the spring when the grazing pressure is low. As a result, much of the diatom biomass escapes grazing and sinks to the bottom where it accumulates in the deep channel. In the summertime, the downward PON flux is close to zero due to the low PON concentrations and low sinking speeds. These low concentrations are due to predation and remineralization during summer. In Chesapeake Bay the phytoplankton community in summer is dominated by small flagellates and dinoflagellates that sink slowly and are subject to high predation pressure (Adolf et al. 2006; Marshall and Nesius 1996). As a result, very little of this biomass escapes grazing and sinks to the bottom.

It is important to emphasize that the circulation dynamics of the Bay are relatively stable over daily to monthly timescales, while, in contrast, POM and phytoplankton concentrations exhibit considerable variability over these time scales due to variations in primary production. As a result, the variability in both the sinking flux and advective transport flux magnitude is driven primarily by variations in the PON concentrations that are high in spring and fall and low in summer.

Two additional control volumes that run parallel to the deep channel (sections A_2-A_2 and A_3-A_3 depicted in Figure 2.2a) were analyzed to quantify the PON fluxes on the flanks of the deep channel A1-A1. For example, the blue color represents the volume flux (Figure 2.10a) along the left side of A1-A1 the interface, while the red color represents the volume flux along the right side of A_1-A_1. Positive values represent fluxes in the eastward direction while negative value represent fluxes in the westward direction.

These sections revealed that there is a PON flux accumulation in the deep channel A_1-A_1 (Figure 2.10a) with more flux (red color) coming into the A_1-A_1 control volume from the right side and less flux (blue color) coming out from the left side (blue color), resulting an accumulation. Throughout the season, left flux (blue color) for the A_2-A_2 (Figure 2.10b) transect is always positive, representing PON transport toward the east. In contrast, the right flux (red color) was negative (moving toward the west) in the spring, and then reversed during summer (positive, toward the east/thalweg), which indicates a local convergence along the flank in the spring. That is, along A_2-A_2 during spring there is export of organic matter from the western shore toward the deep channel, and there is also export of some organic matter toward the western shore from the deep channel in the bottom water. In contrast, during summer the transport along A_2-A_2 is toward the east/thalweg. For A_3-A_3, the general pattern is exporting to the deep channel (from east to west in Figure 2.10) throughout the year. These results reveal substantial exchange between the flank and the deep channel as suggested by Scully et al. (2009) with the most significant PON flux occurring in the springtime.

Sensitivity Experiments

Model run B1 (with no wind forcing) was conducted and compared with the reference run A1 (with wind forcing). This comparison revealed that winds play an important role in altering the PON mass distribution in the bay, especially during March and April when, more bottom PON was found in the mid- and northern bay (red color, Figure 2.11), and less bottom PON was found in the lower bay (blue color, Figure 2.11). This shift in the PON distribution is consistent with the role of wind influence

on the estuarine circulation: predominantly northerly winds during the winter and spring tend to enhance the estuarine circulation and thus induce more bottom PON transport northward. Lateral flux results without wind are presented in Figure 2.12a. This figure shows that the peak flux in 2005 in April dropped to 6×10^6 mole nitrogen /day, more than 40% lower than the six years averaged April value presented in Figure 2.10a, but the net flux direction remained the same. That is, although the magnitude changed, the net PON flux along A_1-A_1 was still westward with accumulation in the deep channel and export of PON to western shore. Without wind the transport along A_2-A_2 is altered but still convergent during the spring and eastward throughout much of the year. Without wind the transport along A_3-A_3 remains largely unchanged, i.e., the transport is westward with more flux out of the left side and less flux out of the right side (red color and blue color, respectively, in Figure 2.12c. Northerly winds prevail during the spring time (Figure 2.12d). Without the wind effects, the PON spatial distribution is altered substantially, but the lateral flux patterns remain largely unchanged.

A comparison of model runs A1 and B2 (N-S wind shut down) also elucidated the role of N-S wind in shifting the PON laterally. Differences in the bottom PON concentrations between these runs (Figure 2.13) shows that there is significant enhancement of bottom PON concentrations during spring (particularly in March) in the run with N-S wind (base run A1) compared to the run without N-S wind (sensitivity run B2).

Lee et al. (2013) point out that relatively larger amounts of organic matter are transported into the deep channel in 2003 compared 2000. Similar results were

observed in the model when the when 2003 wind forcing was replaced by the wind forcing from 2000 (sensitivity run C1). This change resulted in more organic matter accumulation in the middle region of deep channel of the bay during April (Figure 2.14). However, it should be noted that, although the wind is important and Susquehanna River discharge is similar between 2000 and 2003 (Lee et al. 2013), river discharge in the Potomac River differs between these two years. The bottom PON decreased noticeably when 2003 Potomac river discharge was replaced by that in 2000 (Figure 2.15, run C2). Thus, the lateral river forcing also effects PON transport and distribution especially in the southern bay region (Du and Shen 2017). Model results also show the importance of using different sinking speeds for phytoplankton. Model run C3, which uses a low sinking speed for phytoplankton as in Feng et al. (2015) and Fennel et al. (2006) while maintaining the high sinking speed for large detritus, alters the spatial PON distribution and thalweg lateral volume flux significantly (Figure 2.16 and Table 2-2). The peak of the flux was shifted from April (base run) to February (slow phytoplankton sinking speed). I speculate that this is due to decreased denitrification that removes les nitrogen out of the system. While more organic matter was produced during the spring bloom during March and April, bottom concentrations are not as high as the run A1.

These model experiments reveal that different factors like wind direction, river flow and sinking speed have a significant impact on PON distributions and fluxes, i.e., the PON distributions and fluxes changed substantially among these experiments, and the timing of the flux peaks also shifted. However, the general PON flux patterns in all of these experiments are similar: the deep channel is accepting more PON from

eastern flank than its exporting to the western flank, resulting a net accumulation in the deep channel (Table 2-2). In addition, vertical advection results a net loss of PON from the deep channel in all these experiments.

Discussion

Mechanism for organic matter transport laterally in Chesapeake Bay

The volume transport results, including phytoplankton, and small and large detritus, revealed, in general, that PON near the bottom of the Chesapeake Bay on the eastern side of the deep channel will move westward towards the deep channel, and that PON accumulated in deep channel will move westward towards the western shore. This result of westward bottom PON transport is consistent with earlier research in Chesapeake Bay by Malone et al. (1986) who concluded that the accumulation of biomass in the western shore was primarily physically driven. These transport patterns in Chesapeake Bay are consistent with the lateral circulation pattern reported in the partially mixed Hudson River estuary (Scully et al. 2009). They result from the asymmetry in the strength in the lateral flow through the interaction between the baroclinic pressure gradient and the lateral Ekman transport in the bottom boundary layer. During the flood tides the lateral Ekman transport is consistent with the baroclinic pressure gradient while during the ebb tide it opposes it, making a net lateral residual flow that is clockwise looking up estuary (Scully et al. 2009). For Chesapeake Bay, freshwater input from large western shore tributaries dilutes the western side of the bay, enhancing the bottom flow towards the western shore. This was further demonstrated through the model run B1 without winds effects where the

change in the PON lateral transport pattern was consistent with this estuarine circulation theory (Figure 2.12b). In addition, the transport of PON from the western shore downslope to the deep channel and the convergence with the westward upslope flux from the deep channel in the main run during spring has been observed in other research (Chen and Sanford 2009; Olabarrieta et al. 2018). The convergence of PON flux during spring on the western shore flank revealed in the A_2-A_2 budget analysis is due to freshwater laying on top of saltwater on the western shore flank, which is, in turn, due to the Coriolis forcing that pushes freshwater westward which then creates and eastward for barotropic pressure gradient (higher water level in western side). At the same time, deep channel high density water is pushed westward, as previously described. The conceptual diagram for lateral transport of flux is displayed in Figure 2.17.

Wind also played an important role in shifting the bottom PON transport and distribution bay wide from the previous run comparisons. Frequent wind from the north would favor more bottom PON transport northward along the bottom, resulting in elevated bottom PON concentrations in the upper bay and reduced PON concentrations in the lower bay. This wind's role in shifting PON fluxes and distributions during springtime is consistent with wind effects on estuarine circulation (Xie and Li 2018; Xie et al. 2017). Du and Shen (2016) concluded that there is significant variation in the horizontal distribution of residence time, which it is consistent with my finding that the magnitude of transport changed significantly when the winds were altered.

Importance of organic matter downward flux

The vertical fluxes of particulate organic matter play a crucial role in the distribution of nutrients throughout the oceans (Fernandez-Urruzola et al. 2016) as well as in Chesapeake Bay (Hagy et al. 2005). When the sinking rate of phytoplankton is relatively small phytoplankton are transported primarily by mixing and advection and they do not accumulate near the bottom (results not shown here). It is crucial to have elevated sinking rates in the winter and spring in order to reproduce the chlorophyll accumulation that is observed near the bottom in spring (Xu and Hood 2006). Whether or not it is crucial to have these elevated phytoplankton sinking rates for realistic simulation of the Chesapeake Bay nitrogen cycle is an open question. It is possible to choose a large sinking speed for detritus and still achieve organic matter accumulation in the deep channel and therefore drawdown of bottom water oxygen concentrations as in Feng et al. (2015), i.e., applying a large sinking speed for large detritus while using a small sinking speed for phytoplankton. Suffice it to say, there is considerable uncertainty in how to set sinking rates in Chesapeake Bay biogeochemical models. As mentioned in Smetacek (1985), the enhancement of sinking through the formation of large flocs (Shen et al. 2018a; Shen et al. 2018b) can lead to settling rates as high as 10 to100 m d^{-1}, sufficient to deposit an entire diatom bloom to Chesapeake Bay sediments within one day (Hagy et al. 2005). Therefore, with the present bi-weekly or monthly measurements conducted by CBP it is possible that these measurements fail to capture this potentially rapid and important process (Hagy et al. 2005). Increasing the CBP sampling frequency in the mainstem Bay from February to May would help constrain sinking speeds in models.

The budget analysis revealed that the sinking transport (cyan in Figure 2.8) was balanced by vertical advection (purple in Figure 2.8). The monthly averaged vertical velocity at 16m depth reveals that in the middle-upper Bay, the flow tends to be upward (Figure 2.18a,b,c,d), thus, balancing the sinking process, while in the lower bay the flow and the sinking fluxes are both downward, commensurate with the bottom PON concentration north-south gradually decreasing (Figure 2.18e to l), resulting a loss term for the vertical advection process on PON budget.

Implication for hypoxia issue in Chesapeake Bay

Extensive investigations have been undertaken to better understand the mechanisms that control the oxygen depletion in Chesapeake Bay during summer (for example, Scully 2010a; Wang et al. 2015; Zhou et al. 2014). The modeling conducted in this study revealed that the large pool of PON that is deposited in the deep channel in the spring is largely remineralized by summer. The mechanism for deposition to the deep channel is through combination of POM sinking and lateral circulation. That is, our model results showed that the lateral circulation contributes to POM accumulation in the deep channel while the classic two-layer gravitational circulation and vertical advection processes move POM out of the deep channel. Other research has pointed out the potential importance of this lateral process for transporting PON from flank to the adjacent deep channel (Kemp et al. 1997; Shen et al. 2019; Testa et al. 2014) but without quantifying the PON transport and its seasonal variation. Our model has been used to quantify this phenomenon.

It should also be pointed out that during the summertime, although the flux is significantly lower, the lateral circulation is still exporting PON to the deep channel

(Figure 2.12b,c). This fact could help to explain the finding that spring bloom-generated organic matter is insufficient to maintain water column biological oxygen demand through the entire summer (Testa and Kemp 2014). This lateral process of shifting PON from the flanks to the deep channel may provide the organic matter supply that continues to drive oxygen consumption in the deep channel region during summertime. These results suggest that the classic Chesapeake Bay paradigm, that organic matter produced by the spring bloom and subsequently deposited on the bottom drives oxygen depletion in the summer (Kemp et al. 1992; Malone et al. 1988), might need to be extended to consider the role of lateral PON transport.

Conclusion

The coupled physical-biogeochemical model presented in this research was shown to have reasonably good skill in reproducing the spatial and temporal variability of PON and other biogeochemical constituents in Chesapeake Bay similar to previous modeling research (Feng et al. 2015; Testa et al. 2014). Given this skill the model was considered valid to examine PON production, transport, and transformation in Chesapeake Bay. From my analysis I conclude, in general, that in Chesapeake Bay bottom PON moves from eastern flank of the bay to the thalweg and that the thalweg also exports PON to the western shore. I also observed that PON moves from western shore towards the thalweg during spring, resulting in a PON convergence and accumulation on the western flank of the deep channel.

Wind forcing also plays an important role in shifting the spatial distribution of the PON during springtime when substantial organic matter is produced. The northerly wind during springtime pushes bottom PON northward while the southwesterly wind

drives bottom PON transport towards the west. Although the wind modulates the PON volume transport magnitudes and changes the transport direction in some seasons, it does not fundamentally alter the dominant lateral circulation pattern, i.e., the general westward flow near the bottom due to the ebb-flood asymmetry lateral flow, as well as the observed convergence on the western shore flank of the deep channel during spring due to the freshwater inputs from the western shore tributaries.

Further, I conclude that the sinking of particulate matter is an important process that transports PON to the deep channel with the organic matter sinking contributing the same magnitude of PON fluxes as the lateral processes. This conclusion also highlights the fact that the sinking speeds of phytoplankton and detritus are important parameters for modeling PON flux that are poorly constrained. Moreover, the monthly-weekly measurement of chlorophyll and other biogeochemical variable is, potentially, not frequent enough to capture rapid downward chlorophyll and detritus flux events as suggested by other investigations during springtime (Hagy et al. 2005).

Finally, although the lateral PON flux to the deep channel of the bay during summertime is small compare with the flux during spring, these lateral processes still move PON from the eastern and western shore flanks toward the deep channel. This lateral transport potentially provides an important supply of organic matter that fuels continued oxygen consumption in the deep channel during summer. This suggests that lateral POM transport processes and, more generally, the three-dimensional PON

transport must be considered for understanding where the organic matter comes from that results oxygen depletion in the deep channel of Chesapeake Bay.

Acknowledgements

I thank Jerry Wiggert for sharing an earlier version of the biogeochemical model code. I thank Dr. Rivs, Dr. Bever and Dr. Ralston for sharing scripts for data processing. The CBP data used for model forcing and validation were downloaded from the Chesapeake Bay Program monitoring database website (https://www.chesapeakebay.net/what/data). This research was supported by the NOAA COMT project via the IOOS Office, awards NA10NOS0120063 and NA11NOS0120141. The first author was also supported by the China Scholarship Council (201206710006) and University of Maryland Center for Environmental Science Teaching Assistantships. This paper is University of Maryland Center for Environmental Science contribution no. XXXX.

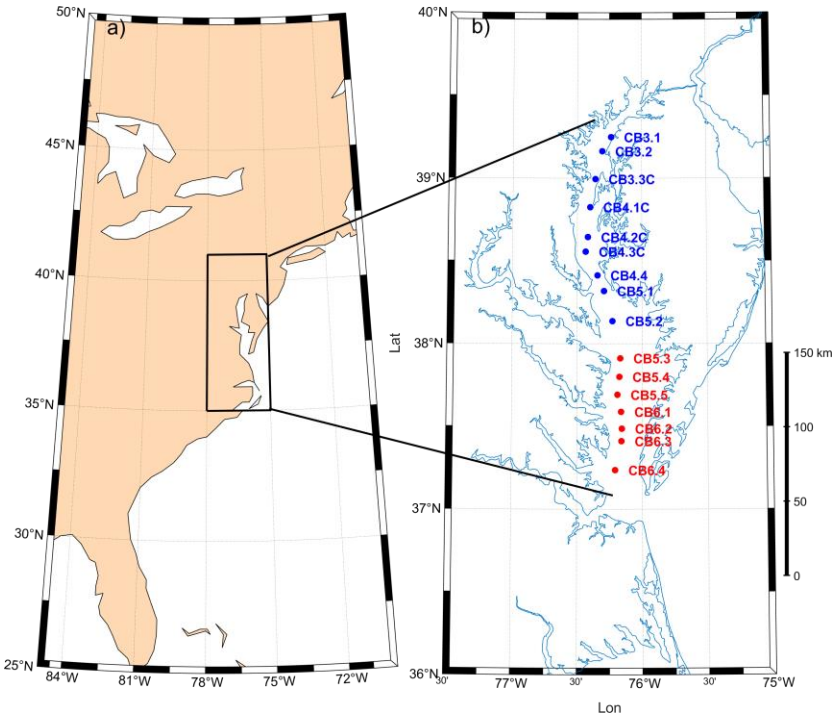

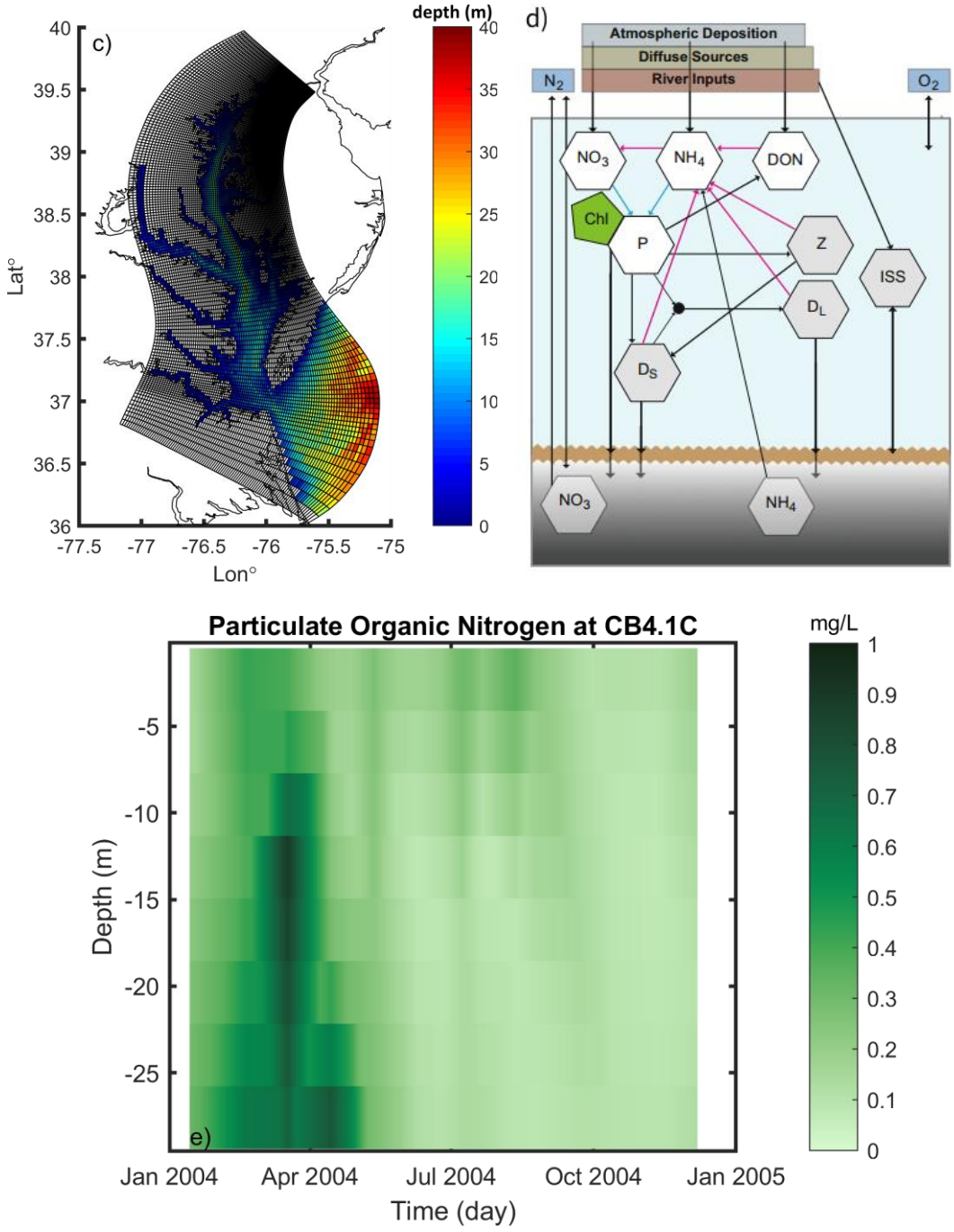

Figure 2.1: a) and b) Research domain, the points represent the CBP monitoring station locations used in this study; c) ChesROMS horizontal grid structure; d) Biogeochemical model schematic; e) CBP data PON concentration as function of depth from January 2004 through January 2005 at station CB4.1C.

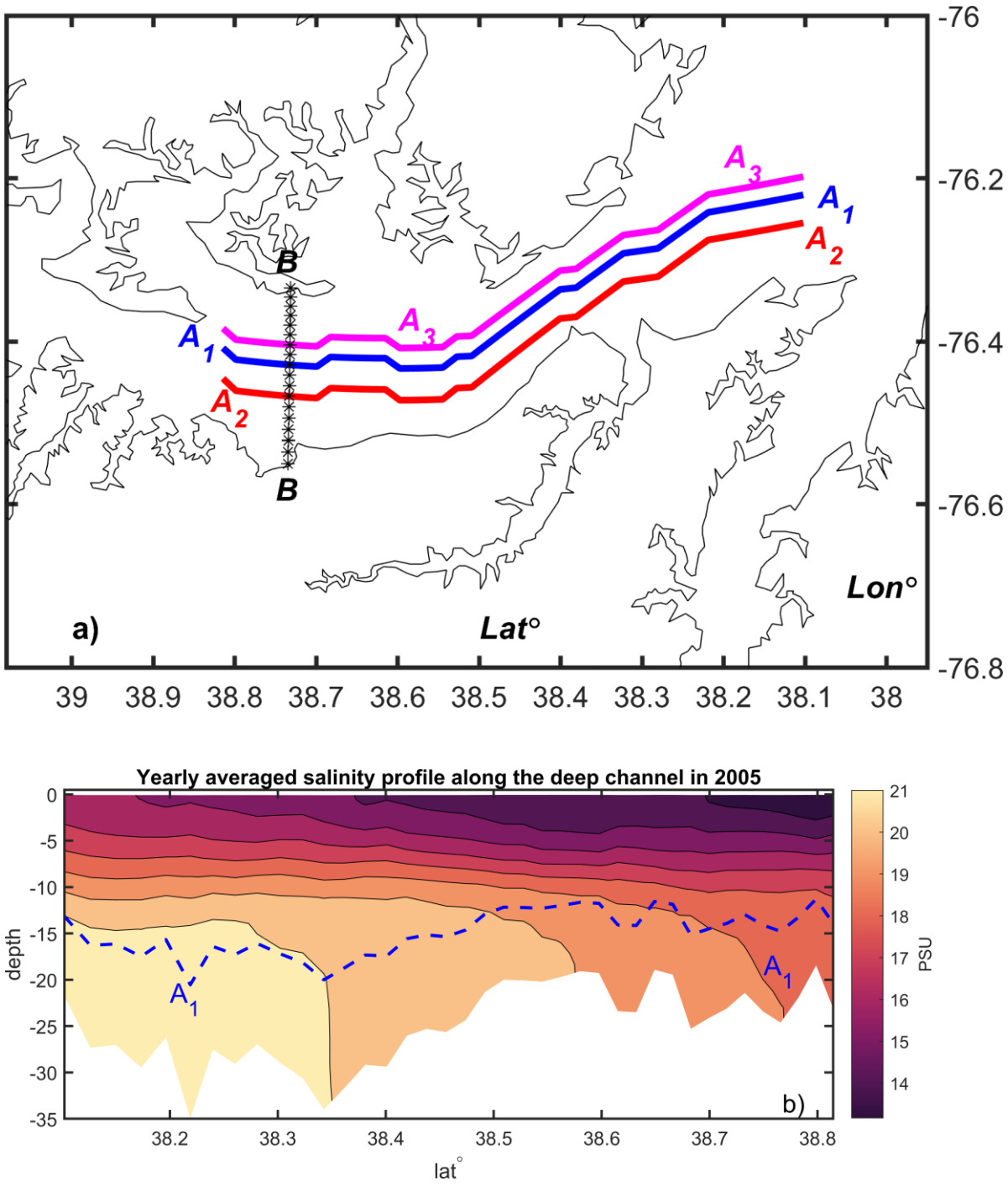

Figure 2.2: a) Location of cross section (B-B, black); deep channel (A_1-A_1), eastern shore (A_2-A_2), and western shore (A_3-A_3) control volumes; b) Along channel view of the control volume location of A_1-A_1 (below the blue dashed line), and background color is the yearly averaged salinity profile in 2005 simulated by the model.

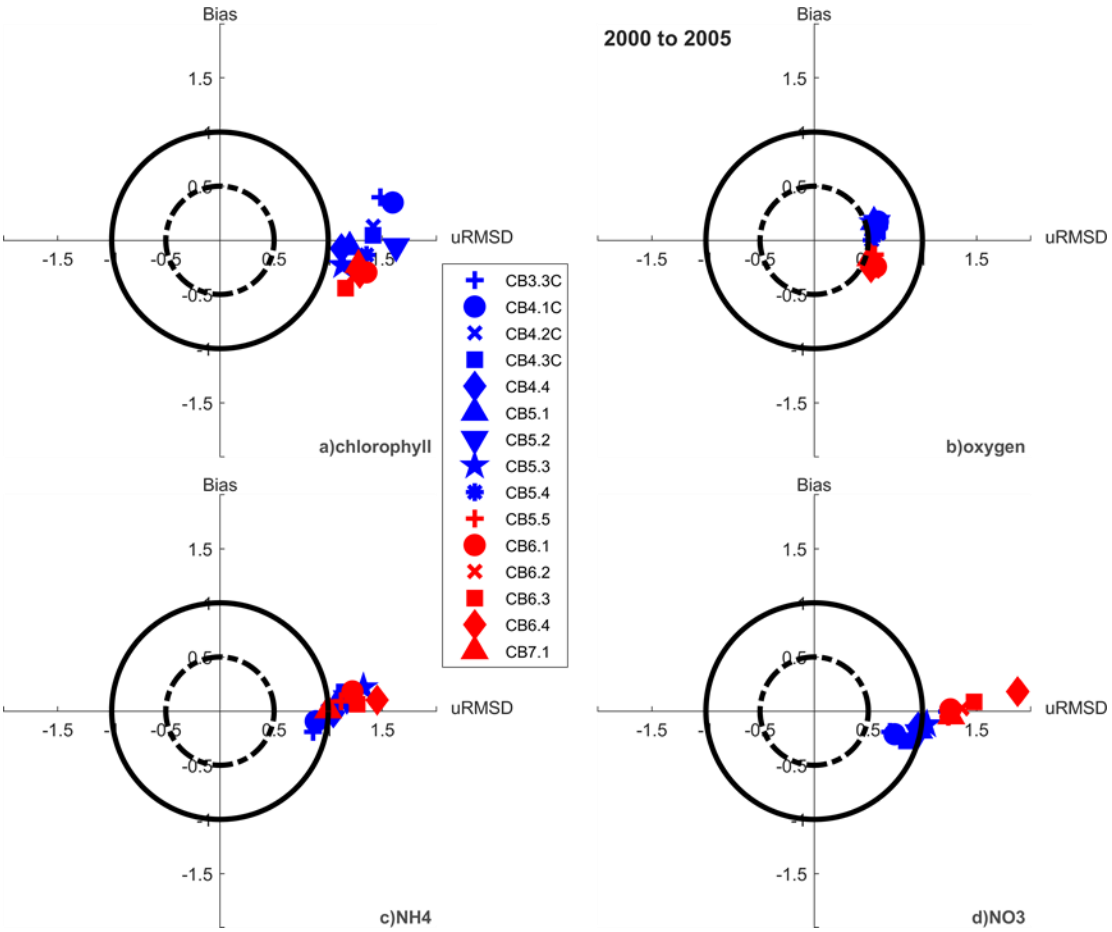

Figure 2.3: Target diagrams for model skill assessment for a) Chlorophyll; b) Oxygen; c) Ammonium; and d) Nitrate for the time frame 2000 through 2005

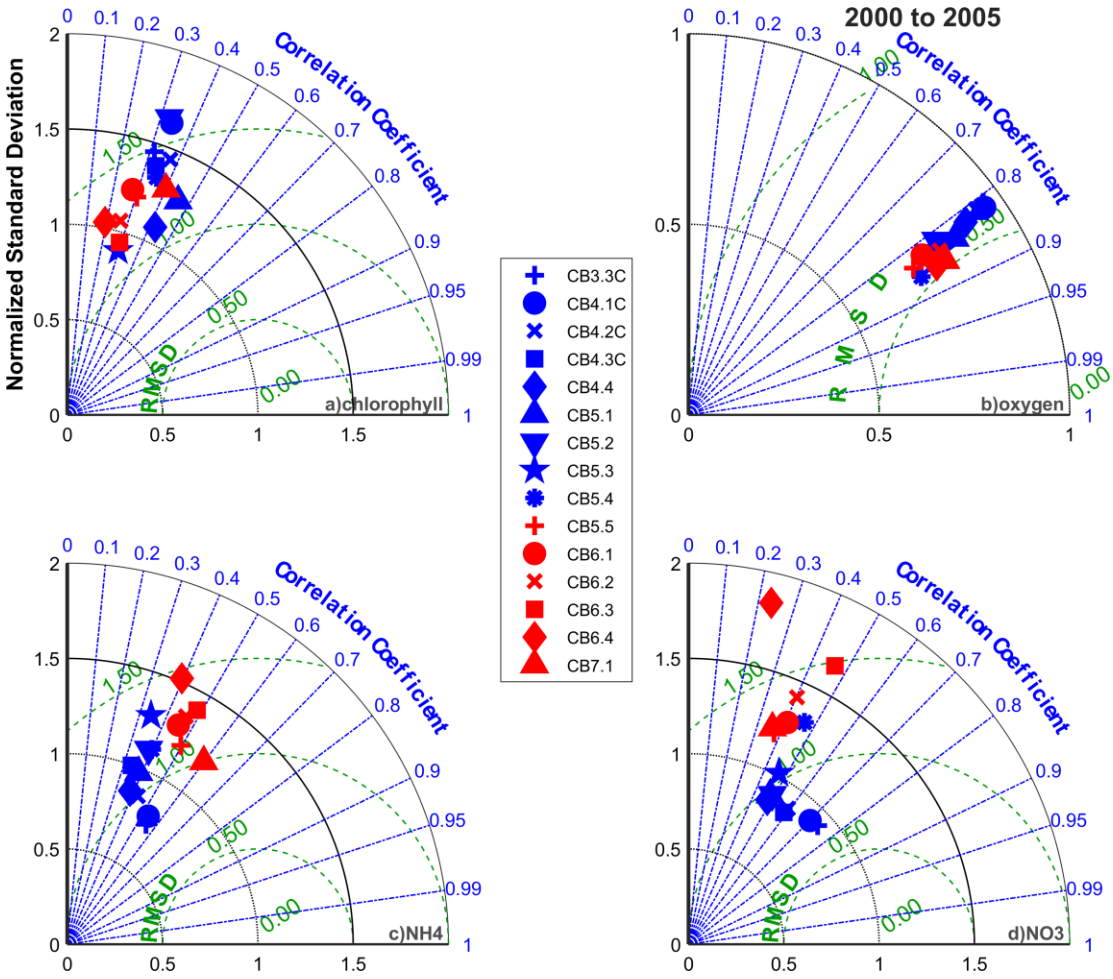

Figure 2.4: Taylor diagrams for model skill assessment for a) Chlorophyll; b) Oxygen; c) Ammonium; and d) Nitrate for the time frame 2000 through 2005.

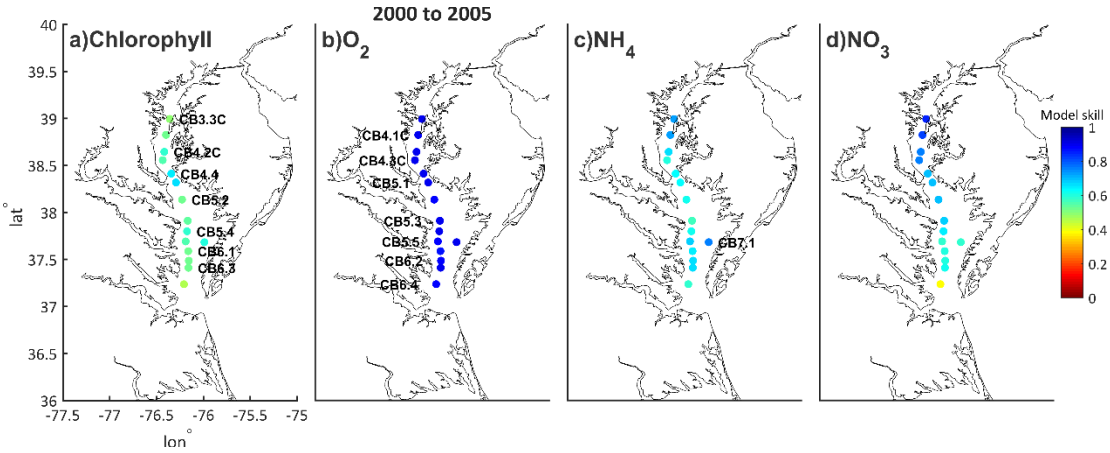

Figure 2.5: Average model skill for a) Chlorophyll; b) Oxygen; c) Ammonium; and d) Nitrate for the time frame 2000 through 2005.

.

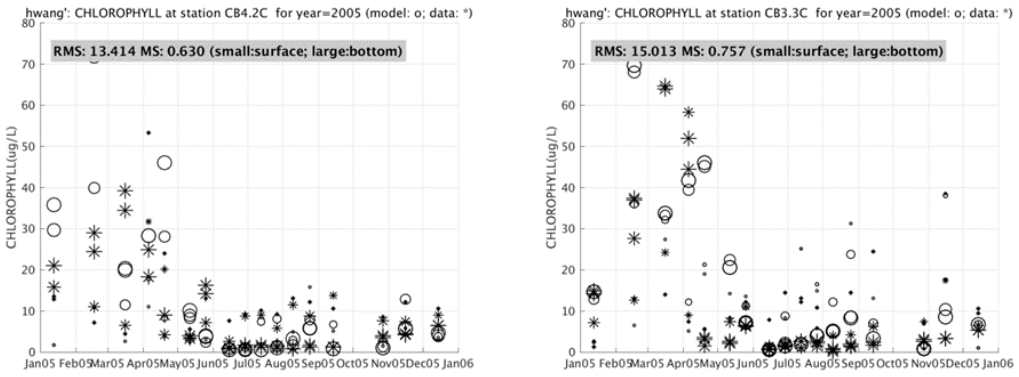

Figure 2.6: Model to measurement comparisons of chlorophyll concentration in 2005 for CB3.3C and CB4.2C. Circles and asterisks represent the model and measurement values, respectively. Larger symbols indicate nearer to the bottom, while smaller symbols indicate nearer to the surface.

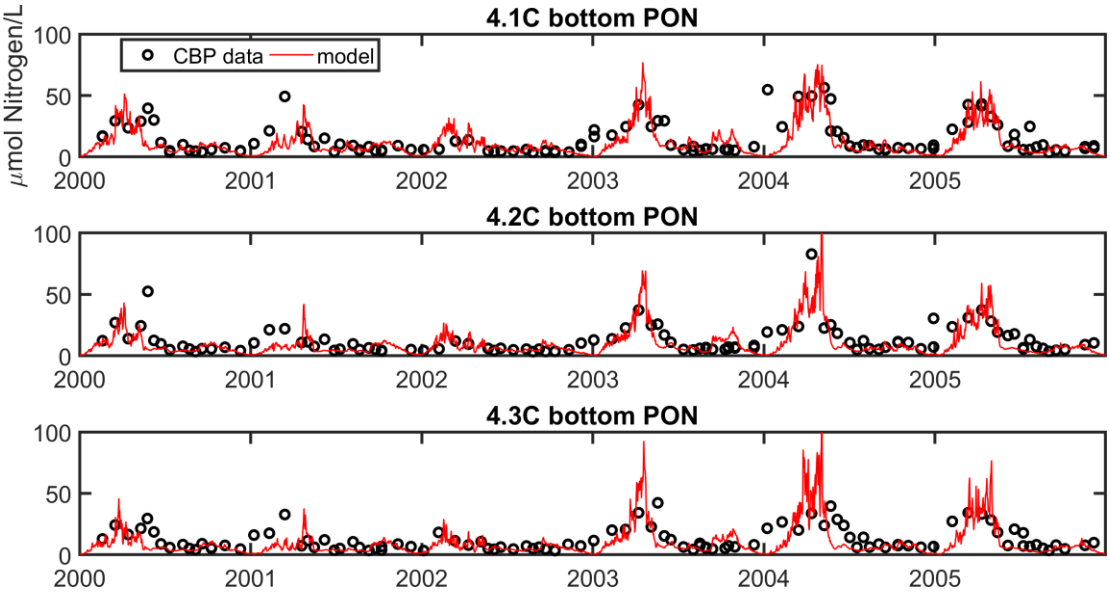

Figure 2.7: Model and measurement comparisons of bottom PON from 2000 to 2005 for CB4.1C, CB4.2C, and CB4.3C.

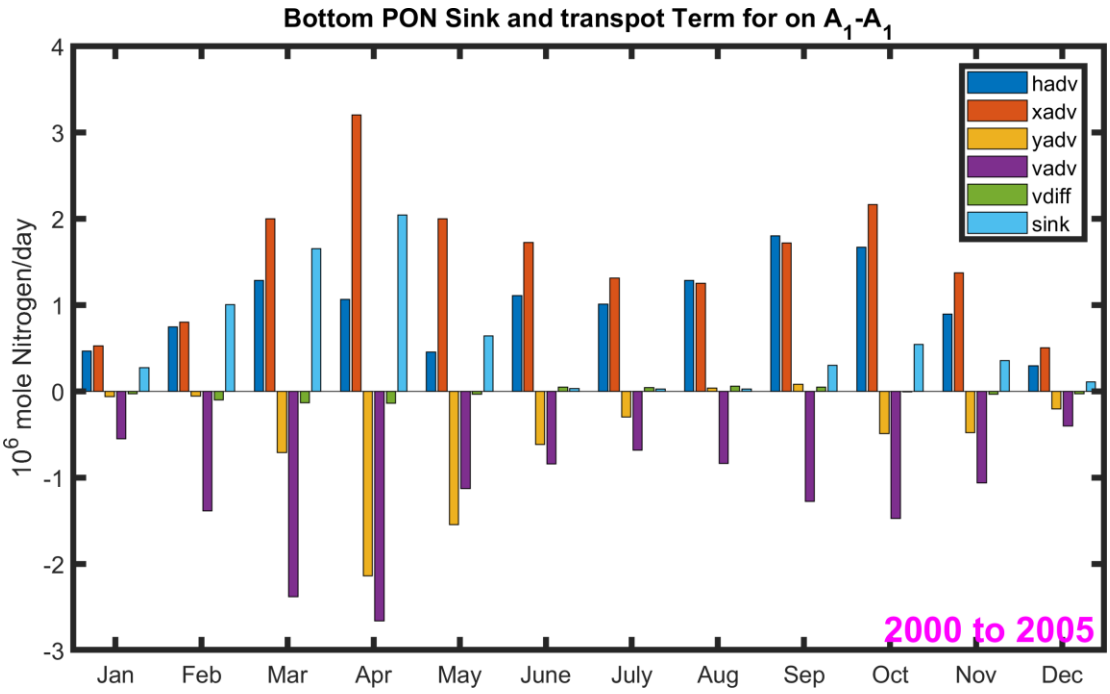

Figure 2.8: Budget of mean sinking and transport terms in the deep channel control volume A_1-A_1. The color bars represent horizontal advection (Hadv, blue), vertical advection (vadv, purple), east-west advection (xadv, red), north-south (yadv, yellow), vertical diffusion (vdiff (green), and

sinking (sink, cyan); Positive values indicate that the process makes the budget increase while negative values represent decreases in A_1-A_1.

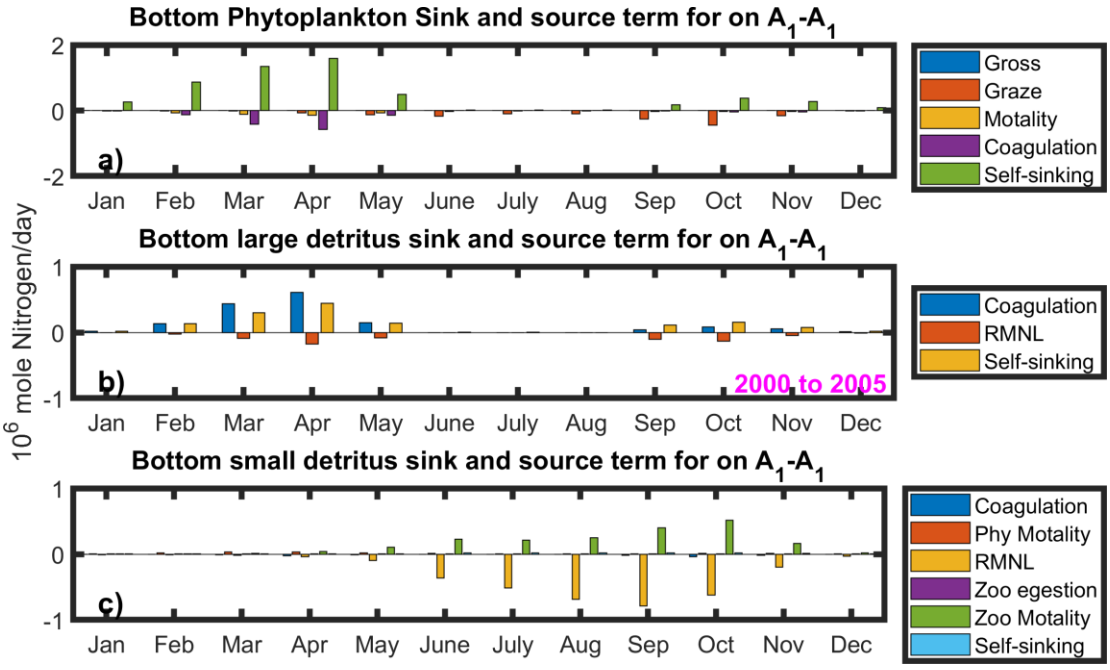

Figure 2.9: Monthly averaged sink and source term in control volume A_1-A_1 for phytoplankton, large detritus and small detritus for years 2000 through 2005.

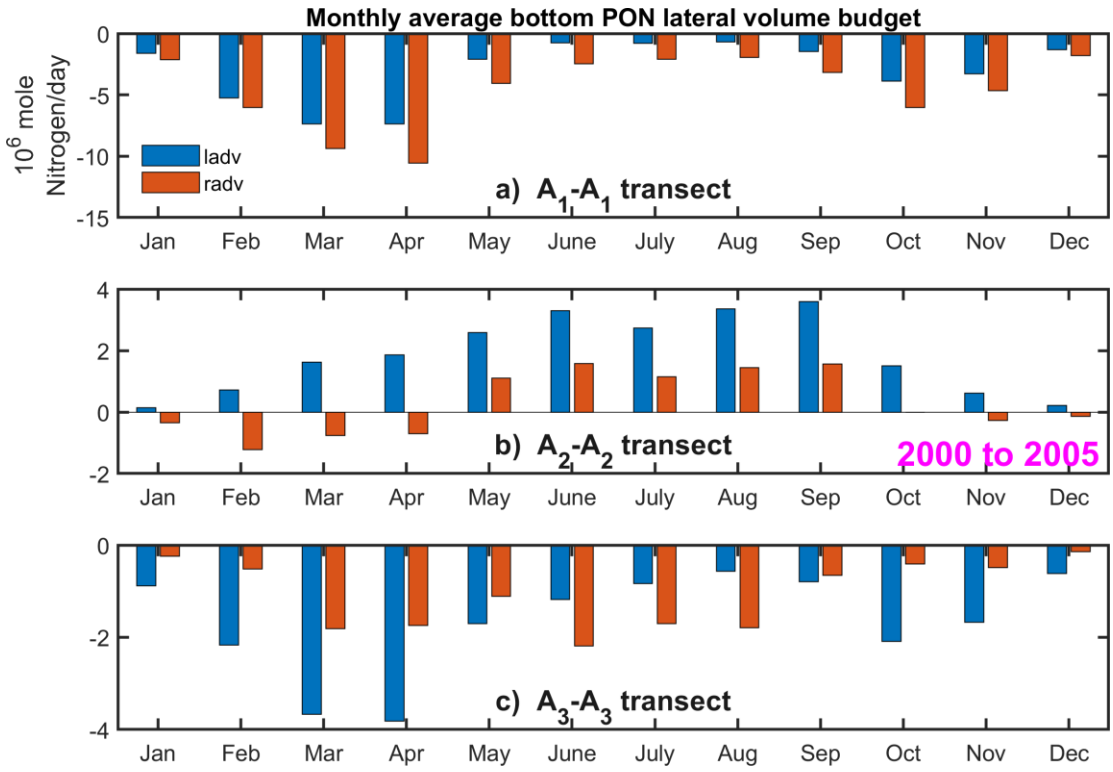

Figure 2.10: PON Budget of lateral transport terms on a) A_1-A_1, b) A_2-A_2 and c) A_3-A_3 control volumes, respectively during years 2000 to 2005. Ladv and radv mean the volumetric flux is from the right hand and left hand side of these control volumes, respectively, looking up bay. Positive values in ladv or radv means the volumetric flux is eastward, while negative means westward.

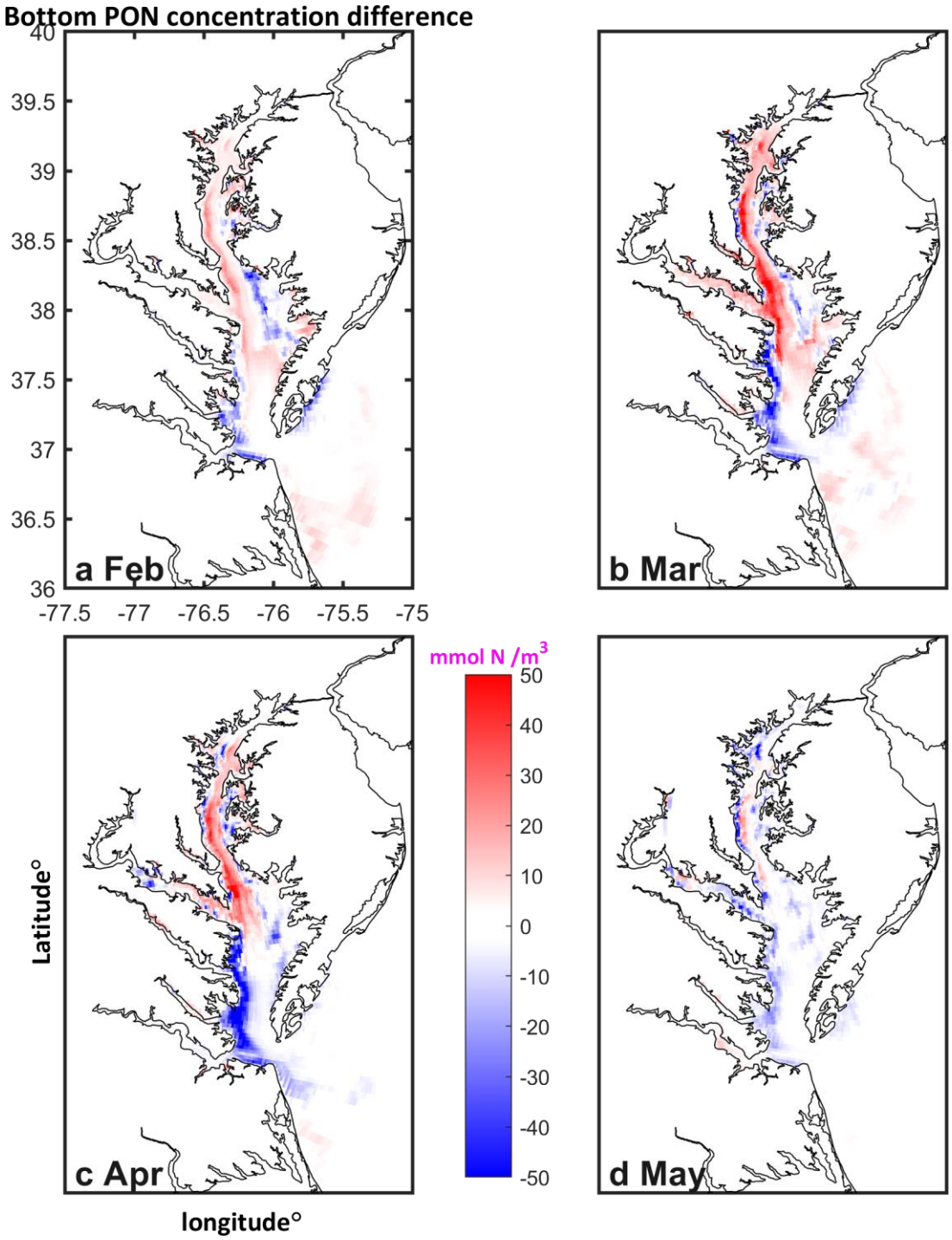

Figure 2.11 Monthly averaged bottom PON differences in late winter and spring between the base run (A1) and a run without the wind forcing (B1) in 2005 (Model run A1 minus model run B1).

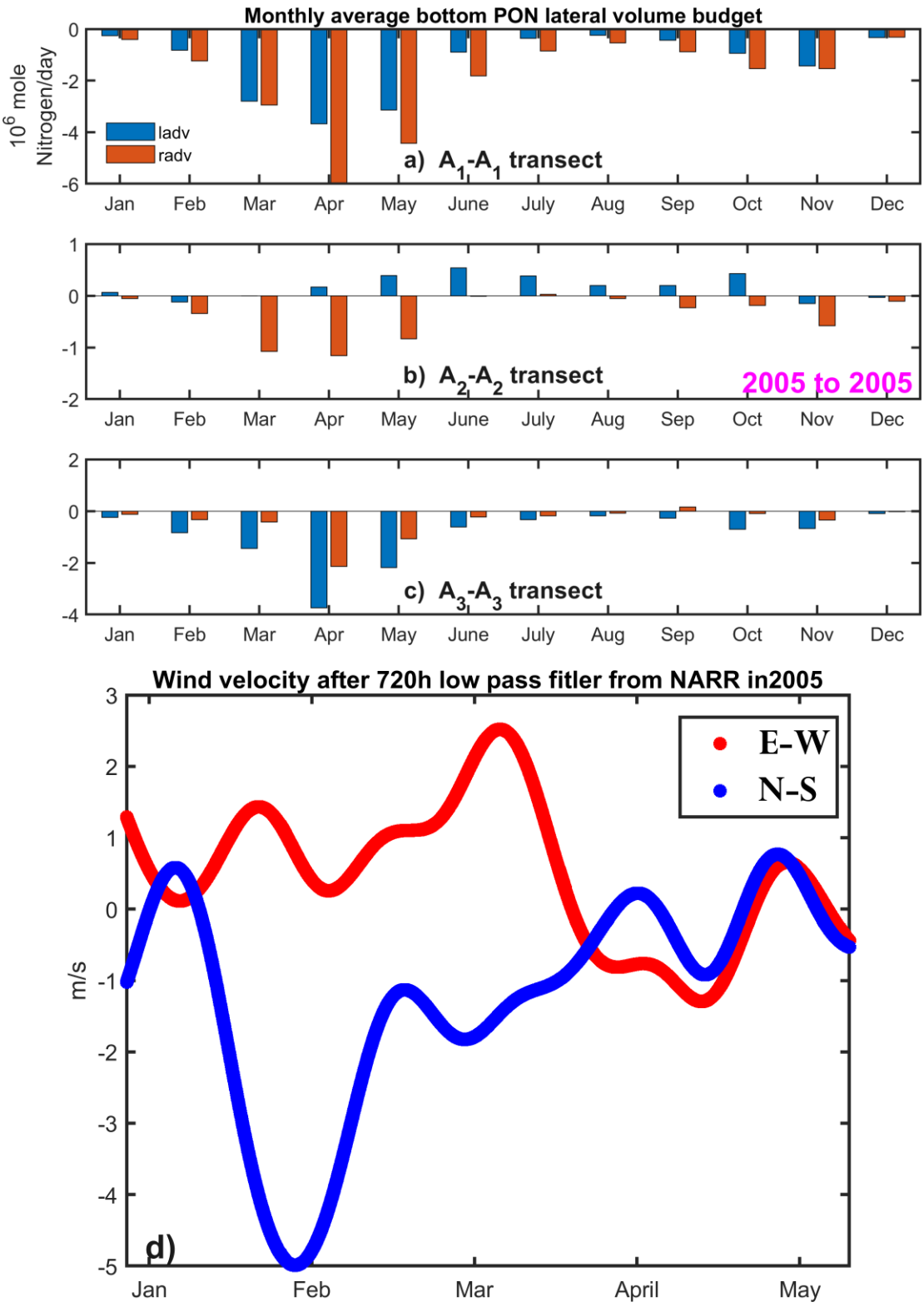
Monthly average bottom PON lateral volume budget
10^6 mole Nitrogen/day
ladv
radv
a) A_1-A_1 transect
b) A_2-A_2 transect
2005 to 2005
c) A_3-A_3 transect
Jan
Feb
Mar
Apr
May
June
July
Aug
Sep
Oct
Nov
Dec
Wind velocity after 720h low pass fitler from NARR in2005
E-W
N-S
m/s
d)
Jan
Feb
Mar
April
May

Figure 2.12 (a-c) Monthly averaged bottom PON lateral flux for run B1 at a) A_1-A_1, b) A_2-A_2 and c) A_3-A_3, respectively; d) 720 hr low pass filtered wind forcing from NARR in 2005.

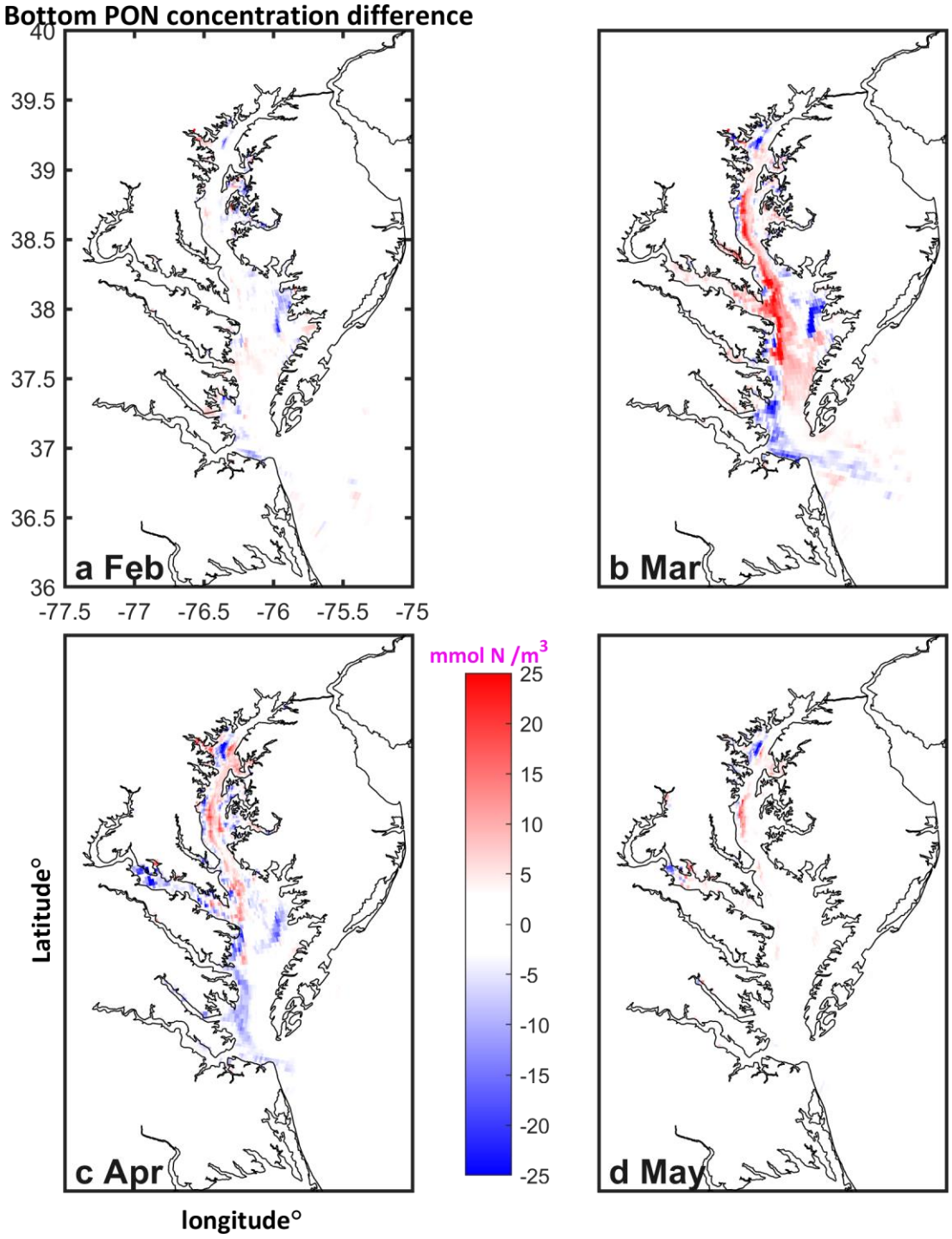

Figure 2.13: Monthly averaged bottom PON differences in late winter and spring between the base run (A1) and a run shutting down N-S wind (B2) in year 2005.

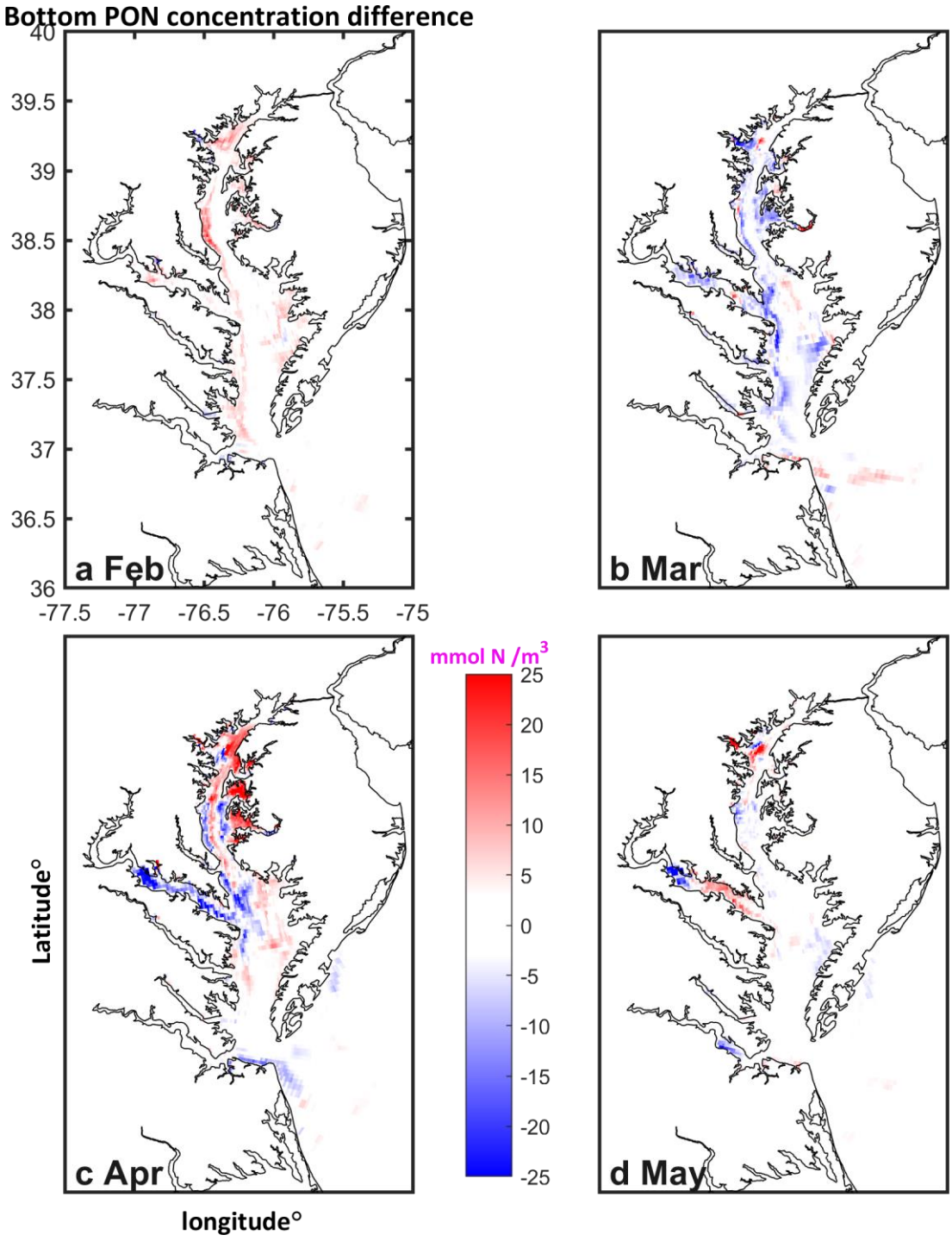

Figure 2.14: Monthly averaged bottom PON differences in late winter and spring between the base run (A1) and run using the year 2001 wind forcing to replace that for the year in 2003 (C1).

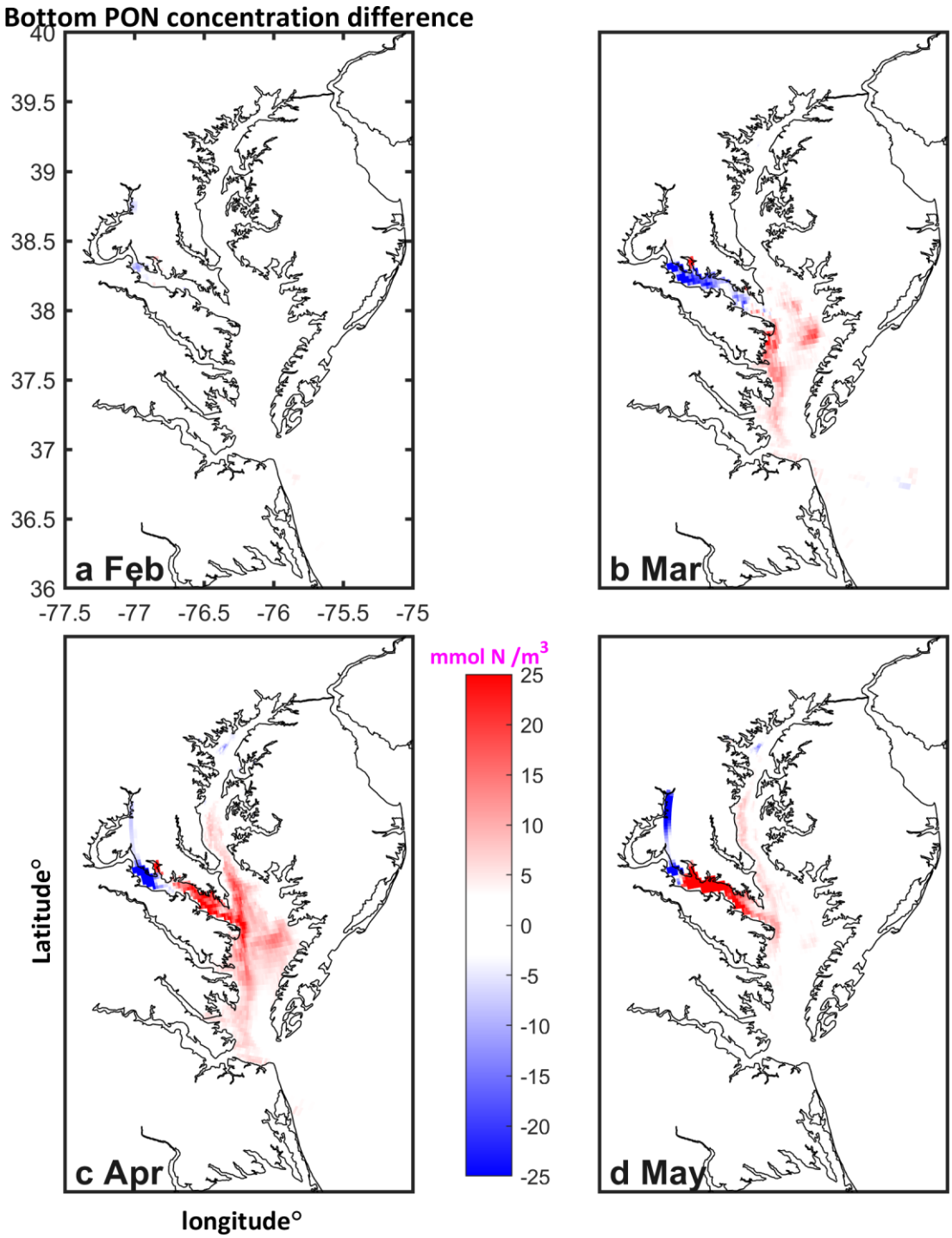

Figure 2.15: Monthly averaged bottom PON differences in late winter and spring between the base run (A1) and a run using the year 2001 Potamc River forcing in in place of the year in 2003 Potomac River forcing (C2).

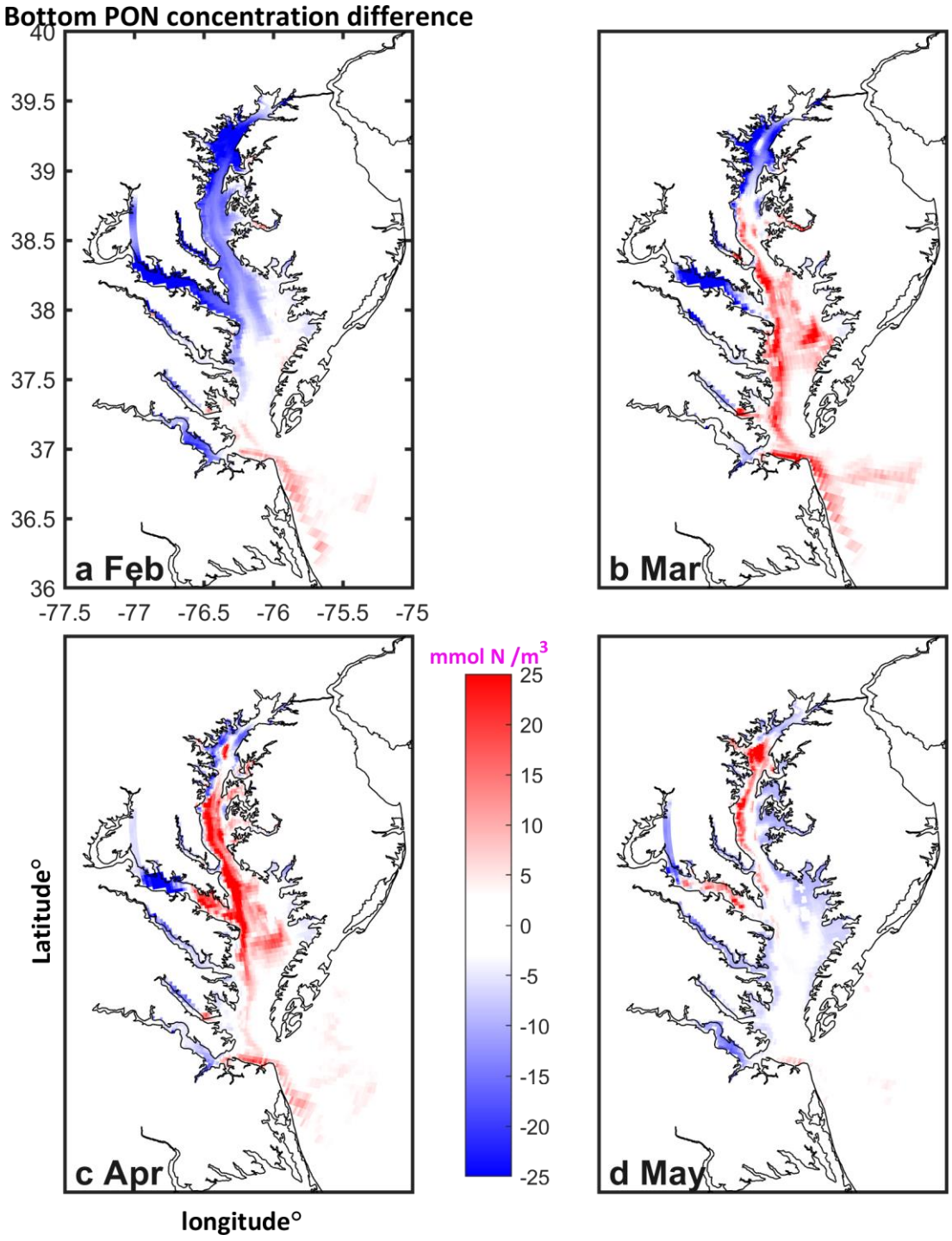

Figure 2.16: Monthly averaged bottom PON differences in late winter and spring between the base run (A1) and run with slow phytoplankton sing speed (C3).

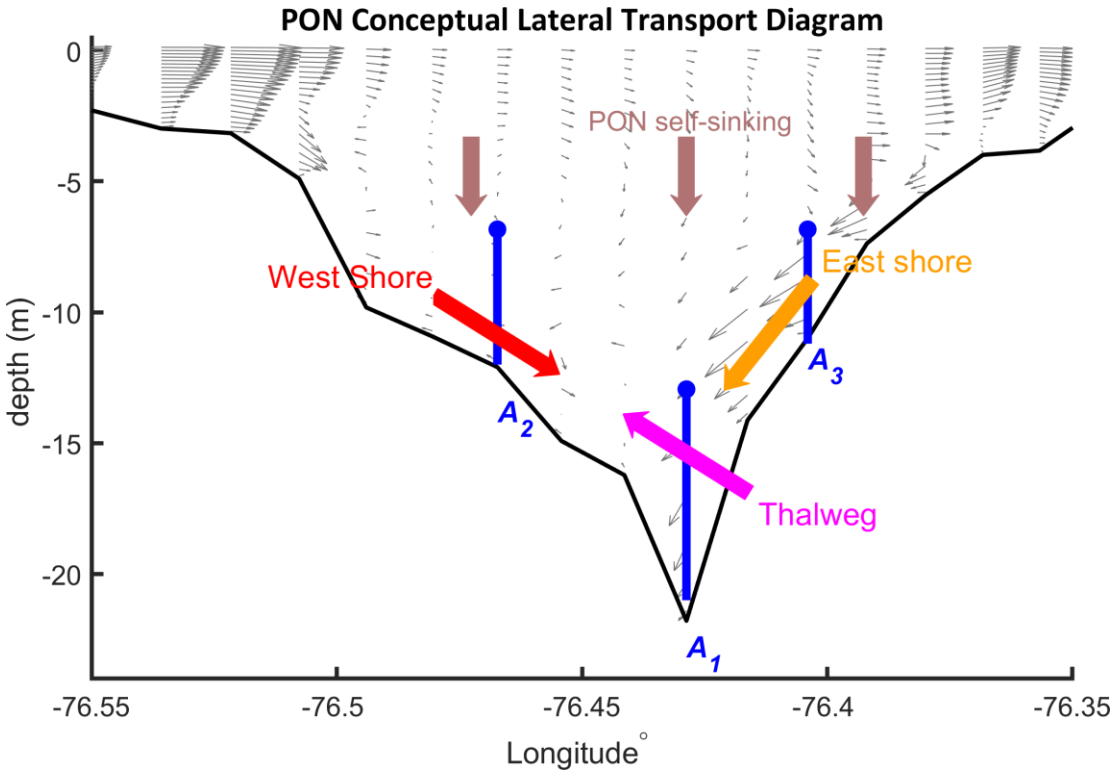

Figure 2.17: Conceptual diagram for PON lateral transport in a transverse section across the bay. Blue line A_1, A_2, and A_3 represent control volumes located in the thalweg, western shore flank, and eastern shore flank, respectively (see Figure 2.2a). Blue points indicate the vertical upper limit location of the control volume analyzed; Grey arrows represented background lateral circulation, while pink, red, and dark yellow arrows represent the residual velocity patterns near the bottom; Brown vertical arrows represented PON aggregation and sinking.

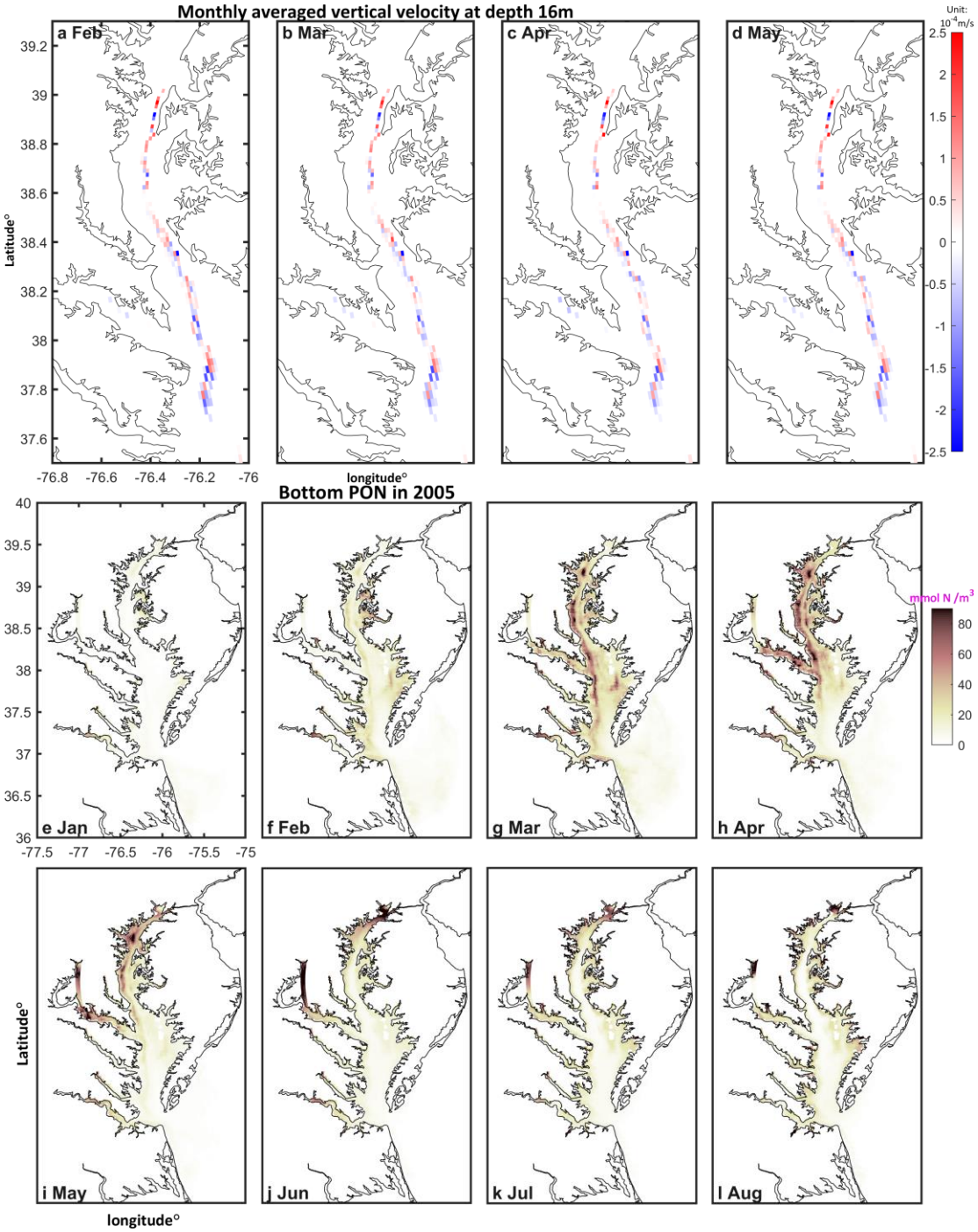

Figure 2.18: 2005 monthly averaged vertical velocity at 16m depth in the deep channel of the bay for February, March, April and May (a,b,c,d, respectively); 2005 bottom PON from January to August (e,f,g,h,i,j,k,l).

Table 2-1 Descriptions of model runs

Model ID	Model description
A1	Base run with realistic forcing
B1	Same as base run realistic forcing, except during year 2005, wind was shut down
B2	Same as base run realistic forcing, except during year 2005, N-S wind was shut down
C1	Same as base run realistic forcing, except 2003 wind forcing was replaced by that the wind forcing in 2001
C2	Same as base run realistic forcing, except year 2003, Potomac River discharge was replaced by Potomac River discharged in 2001
C3	Same as base run realistic forcing, but with phytoplankton sinking speed constant as 0.5m/day in 2005

Table 2-2 Lateral flux through different model run A_1-A_1 thalweg transect. L: left interface lateral flux; R: right interface lateral flux: N:net gain (+) or loss (-) in the control volume.

Run	B1			B2			C1			C2			C3		
	L	R	N	L	R	N	L	R	N	L	R	N	L	R	N
Jan	-0.27	-0.40	0.14	-0.32	-0.47	0.15	-1.22	-1.50	0.28	-1.90	-2.83	0.93	-6.58	-8.81	2.23
Feb	-0.83	-1.24	0.41	-1.32	-1.90	0.58	-4.44	-5.56	1.12	-6.55	-7.43	0.89	-26.49	-32.64	6.15
Mar	-2.79	-2.94	0.15	-5.98	-6.96	0.98	-11.29	-13.27	1.98	-8.45	-9.80	1.35	-10.98	-15.10	4.11
Apr	-3.67	-6.00	2.33	-5.81	-9.58	3.77	-8.72	-14.21	5.49	-12.96	-17.14	4.18	-5.07	-11.08	6.01
May	-3.15	-4.43	1.28	-4.08	-4.83	0.75	-2.37	-3.88	1.51	-1.69	-3.06	1.36	-6.15	-8.97	2.82
June	-0.90	-1.82	0.92	-0.77	-1.96	1.19	-1.17	-3.20	2.02	-1.27	-3.24	1.97	-0.88	-2.77	1.89
July	-0.37	-0.85	0.48	-0.52	-1.11	0.60	-0.58	-2.22	1.65	0.24	-1.60	1.84	-0.98	-2.15	1.17
Aug	-0.24	-0.54	0.30	-0.29	-0.65	0.36	-0.75	-2.05	1.30	-1.23	-2.52	1.29	-0.45	-1.16	0.71
Sep	-0.44	-0.89	0.45	-0.47	-1.14	0.68	-1.92	-3.79	1.88	-1.94	-4.64	2.70	-0.66	-1.87	1.21
Oct	-0.94	-1.54	0.60	-1.39	-2.26	0.87	-4.78	-7.50	2.71	-5.66	-8.67	3.01	-3.93	-6.50	2.57
Nov	-1.43	-1.54	0.11	-2.32	-2.58	0.26	-4.24	-5.71	1.47	-2.79	-4.33	1.53	-9.96	-14.78	4.82
Dec	-0.33	-0.33	-0.01	-0.40	-0.45	0.05	-1.10	-1.26	0.16	-2.18	-2.89	0.71	-12.75	-17.44	4.69

References

Adolf, J.E., C.L. Yeager, W.D. Miller, M.E. Mallonee, and L.W. Harding. 2006. Environmental forcing of phytoplankton floral composition, biomass, and primary productivity in Chesapeake Bay, USA. *Estuarine Coastal and Shelf Science* 67: 108-122. doi: 10.1016/j.ecss.2005.11.030

Boesch, D., E. Burreson, W. Dennison, E. Houde, M. Kemp, V. Kennedy, R. Newell, K. Paynter, R. Orth, and R. Ulanowicz. 2001. Factors in the Decline of Coastal Ecosystems. *Science* 293: 1589. doi: 10.1126/science.293.5535.1589c

Boynton, W., J. Garber, R. Summers, and W. Kemp. 1995. Inputs, transformations, and transport of nitrogen and phosphorus in Chesapeake Bay and selected tributaries. *Estuaries and Coasts* 18: 285-314. doi: 10.2307/1352640

Bradley, P.B., M.P. Sanderson, M.E. Frischer, J. Brofft, M.G. Booth, L.J. Kerkhof, and D.A. Bronk. 2010. Inorganic and organic nitrogen uptake by phytoplankton and heterotrophic bacteria in the stratified Mid-Atlantic Bight. *Estuarine, Coastal and Shelf Science* 88: 429-441. doi: 10.1016/j.ecss.2010.02.001

Breitburg, D., L.A. Levin, A. Oschlies, M. Grégoire, F.P. Chavez, D.J. Conley, V. Garçon, D. Gilbert, D. Gutiérrez, K. Isensee, G.S. Jacinto, K.E. Limburg, I. Montes, S.W.A. Naqvi, G.C. Pitcher, N.N. Rabalais, M.R. Roman, K.A. Rose, B.A. Seibel, M. Telszewski, M. Yasuhara, and J. Zhang. 2018. Declining oxygen in the global ocean and coastal waters. *Science* 359. doi: 10.1126/science.aam7240

Brown, C.W., R.R. Hood, W. Long, J. Jacobs, D.L. Ramers, C. Wazniak, J.D. Wiggert, R. Wood, and J. Xu. 2013. Ecological forecasting in Chesapeake Bay: Using a mechanistic–empirical modeling approach. *Journal of Marine Systems* 125: 113-125. doi: 10.1016/j.jmarsys.2012.12.007

Cerco, C.F., and M.R. Noel. 2004. Process-based primary production modeling in Chesapeake Bay. *Marine Ecology Progress Series* 282: 45-58. doi: 10.3354/meps282045

Chen, S.-N., and L.P. Sanford. 2009. Lateral circulation driven by boundary mixing and the associated transport of sediments in idealized partially mixed estuaries. *Continental Shelf Research* 29: 101-118. doi: 10.1016/j.csr.2008.01.001

Cowan, J.L.W., and W.R. Boynton. 1996. Sediment-water oxygen and nutrient exchanges along the longitudinal axis of Chesapeake Bay: Seasonal patterns, controlling factors and ecological significance. *Estuaries* 19: 562-580. doi: 10.2307/1352518

Da, F., M.A.M. Friedrichs, and P. St-Laurent. 2018. Impacts of Atmospheric Nitrogen Deposition and Coastal Nitrogen Fluxes on Oxygen Concentrations in Chesapeake Bay. *Journal of Geophysical Research-Oceans* 123: 5004-5025. doi: 10.1029/2018jc014009

Deegan, L.A., D.S. Johnson, R.S. Warren, B.J. Peterson, J.W. Fleeger, S. Fagherazzi, and W.M. Wollheim. 2012. Coastal eutrophication as a driver of salt marsh loss. *Nature* 490: 388. doi: 10.1038/nature11533

Diaz, R.J., and R. Rosenberg. 2008. Spreading dead zones and consequences for marine ecosystems. *Science* 321: 926-929. doi: 10.1126/science.1156401

Du, J.B., and J. Shen. 2016. Water residence time in Chesapeake Bay for 1980-2012. *Journal of Marine Systems* 164: 101-111. doi: 10.1016/j.jmarsys.2016.08.011

Du, J.B., and J. Shen. 2017. Transport of riverine material from multiple rivers in the Chesapeake Bay: Important control of estuarine circulation on the material distribution. *Journal of Geophysical Research-Biogeosciences* 122: 2998-3013. doi: 10.1002/2016jg003707

Feng, Y., M.A.M. Friedrichs, J. Wilkin, H.Q. Tian, Q.C. Yang, E.E. Hofmann, J.D. Wiggert, and R.R. Hood. 2015. Chesapeake Bay nitrogen fluxes derived from

a land-estuarine ocean biogeochemical modeling system: Model description, evaluation, and nitrogen budgets. *Journal of Geophysical Research-Biogeosciences* 120: 1666-1695. doi: 10.1002/2015jg002931

Fennel, K., J. Wilkin, J. Levin, J. Moisan, J. O'Reilly, and D. Haidvogel. 2006. Nitrogen cycling in the Middle Atlantic Bight: Results from a three-dimensional model and implications for the North Atlantic nitrogen budget. *Global Biogeochemical Cycles* 20. doi: 10.1029/2005GB002456

Fernandez-Urruzola, I., N. Osma, M. Gomez, F. Pollehne, L. Postel, and T.T. Packard. 2016. Modeling downward particulate organic nitrogen flux from zooplankton ammonium regeneration in the northern Benguela. *Progress in Oceanography* 149: 121-133. doi: 10.1016/j.pocean.2016.10.010

Geyer, W.R., and P. MacCready. 2014. The Estuarine Circulation. *Annual Review of Fluid Mechanics* 46: 175-197. doi: 10.1146/annurev-fluid-010313-141302

Hagy, J.D., W.R. Boynton, and D.A. Jasinski. 2005. Modelling phytoplankton deposition to Chesapeake Bay sediments during winter-spring: interannual variability in relation to river flow. *Estuarine, Coastal and Shelf Science* 62: 25-40. doi: 10.1016/j.ecss.2004.08.004

Hofmann, E., J.N. Druon, K. Fennel, M. Friedrichs, D. Haidvogel, C. Lee, A. Mannino, C. McClain, R. Najjar, J. O'Reilly, D. Pollard, M. Previdi, S. Seitzinger, J. Siewert, S. Signorini, J. Wilkin, and U.S. Team. 2008. Eastern US continental shelf carbon budget: integrating models, data assimilation, and analysis. *Oceanography* 21: 86-104. doi: 10.5670/oceanog.2008.70

Howarth, R., F. Chan, D.J. Conley, J. Garnier, S.C. Doney, R. Marino, and G. Billen. 2011. Coupled biogeochemical cycles: eutrophication and hypoxia in temperate estuaries and coastal marine ecosystems. *Frontiers in Ecology and the Environment* 9: 18-26. doi: 10.1890/100008

Irby, I.D., M.A.M. Friedrichs, C.T. Friedrichs, A.J. Bever, R.R. Hood, L.W.J. Lanerolle, M. Li, L. Linker, M.E. Scully, K. Sellner, J. Shen, J. Testa, H. Wang, P. Wang, and M. Xia. 2016. Challenges associated with modeling low-oxygen waters in Chesapeake Bay: a multiple model comparison. *Biogeosciences* 13: 2011-2028. doi: 10.5194/bg-13-2011-2016

Jolliff, J.K., J.C. Kindle, I. Shulman, B. Penta, M.A.M. Friedrichs, R. Helber, and R.A. Arnone. 2009. Summary diagrams for coupled hydrodynamic-ecosystem model skill assessment. *Journal of Marine Systems* 76: 64-82. doi: 10.1016/j.jmarsys.2008.05.014

Kemp, W.M., W.R. Boynton, J.E. Adolf, D.F. Boesch, W.C. Boicourt, G. Brush, J.C. Cornwell, T.R. Fisher, P.M. Glibert, J.D. Hagy, L.W. Harding, E.D. Houde, D.G. Kimmel, W.D. Miller, R.I.E. Newell, M.R. Roman, E.M. Smith, and J.C. Stevenson. 2005. Eutrophication of Chesapeake Bay: historical trends and ecological interactions. *Marine Ecology Progress Series* 303: 1-29. doi: 10.3354/Meps303001

Kemp, W.M., P.A. Sampou, J. Garber, J. Tuttle, and W.R. Boynton. 1992. Seasonal depletion of oxygen from bottom waters of Chesapeake Bay: Roles of benthic and planktonic respiration and physical exchange processes. *Marine Ecology Progress Series* 85: 137-152. doi: 10.3354/meps085137

Kemp, W.M., E.M. Smith, M. Marvin-DiPasquale, and W.R. Boynton. 1997. Organic carbon balance and net ecosystem metabolism in Chesapeake Bay. *Marine Ecology Progress Series* 150: 229-248. doi: 10.3354/meps150229

Kemp, W.M., J.M. Testa, D.J. Conley, D. Gilbert, and J.D. Hagy. 2009. Temporal responses of coastal hypoxia to nutrient loading and physical controls. *Biogeosciences* 6: 2985-3008. doi: 10.5194/bg-6-2985-2009

Lee, Y.J., W.R. Boynton, M. Li, and Y. Li. 2013. Role of late winter–spring wind influencing summer hypoxia in Chesapeake Bay. *Estuaries and Coasts* 36: 683-696. doi: 10.1007/s12237-013-9592-5

Li, M., L.J. Zhong, and L.W. Harding. 2009. Sensitivity of plankton biomass and productivity to variations in physical forcing and biological parameters in Chesapeake Bay. *Journal of Marine Research* 67: 667-700. doi: 10.1357/002224009791218878

Li, Y., and M. Li. 2011. Effects of winds on stratification and circulation in a partially mixed estuary. *Journal of Geophysical Research-Oceans* 116. doi: 10.1029/2010jc006893

Li, Y., and M. Li. 2012. Wind-driven lateral circulation in a stratified estuary and its effects on the along-channel flow. *Journal of Geophysical Research-Oceans* 117. doi: 10.1029/2011jc007829

Malone, T., L. Crocker, S. Pike, and B. Wendler. 1988. Influences of river flow on the dynamics of phytoplankton production in a partially stratified estuary. *Marine Ecology Progress Series*: 235-249. doi: 10.3354/meps048235

Malone, T.C., W.M. Kemp, H.W. Ducklow, W.R. Boynton, J.H. Tuttle, and R.B. Jonas. 1986. Lateral variation in the production and fate of phytoplankton in a partially stratified estuary *Marine Ecology Progress Series* 32: 149-160. doi: 10.3354/meps032149

Marshall, H.G., and K.K. Nesius. 1996. Phytoplankton composition in relation to primary production in Chesapeake Bay. *Marine Biology* 125: 611-617. doi: 10.1007/BF00353272

Murphy, R.R., W.M. Kemp, and W.P. Ball. 2011. Long-Term Trends in Chesapeake Bay Seasonal Hypoxia, Stratification, and Nutrient Loading. *Estuaries and Coasts* 34: 1293-1309. doi: 10.1007/s12237-011-9413-7

Olabarrieta, M., W.R. Geyer, G. Coco, C.T. Friedrichs, and Z.D. Cao. 2018. Effects of Density-Driven Flows on the Long-Term Morphodynamic Evolution of Funnel-Shaped Estuaries. *Journal Of Geophysical Research-Earth Surface* 123: 2901-2924. doi: 10.1029/2017jf004527

Paerl, H.W., and J.T. Scott. 2010. Throwing Fuel on the Fire: Synergistic Effects of Excessive Nitrogen Inputs and Global Warming on Harmful Algal Blooms. *Environmental Science & Technology* 44: 7756-7758. doi: 10.1021/es102665e

Pan, J.Y., Y.Z. Gu, and D.X. Wang. 2014. Observations and numerical modeling of the Pearl River plume in summer season. *Journal of Geophysical Research-Oceans* 119: 2480-2500. doi: 10.1002/2013jc009042

Rabalais, N.N., R.E. Turner, R.J. Diaz, and D. Justic. 2009. Global change and eutrophication of coastal waters. *Ices Journal of Marine Science* 66: 1528-1537. doi: 10.1093/icesjms/fsp047

Ralston, D.K., W.R. Geyer, J.A. Lerczak, and M. Scully. 2010. Turbulent mixing in a strongly forced salt wedge estuary. *Journal of Geophysical Research* 115. doi: 10.1029/2009jc006061

Scully, M.E. 2010a. The importance of climate variability to wind-driven modulation of hypoxia in Chesapeake Bay. *Journal of Physical Oceanography* 40: 1435-1440. doi: 10.1175/2010jpo4321.1

Scully, M.E. 2010b. Wind modulation of dissolved oxygen in Chesapeake Bay. *Estuaries and Coasts* 33: 1164-1175. doi: 10.1007/s12237-010-9319-9

Scully, M.E. 2013. Physical controls on hypoxia in Chesapeake Bay: A numerical modeling study. *Journal of Geophysical Research: Oceans* 118: 1239-1256. doi: 10.1002/jgrc.20138

Scully, M.E. 2016a. The contribution of physical processes to inter-annual variations of hypoxia in Chesapeake Bay: A 30-yr modeling study. *Limnology and Oceanography* 61: 2243-2260. doi: 10.1002/lno.10372

Scully, M.E. 2016b. Mixing of dissolved oxygen in Chesapeake Bay driven by the interaction between wind-driven circulation and estuarine bathymetry. *Journal of Geophysical Research-Oceans* 121: 5639-5654. doi: 10.1002/2016jc011924

Scully, M.E., and C.T. Friedrichs. 2007. The importance of tidal and lateral asymmetries in stratification to residual circulation in partially mixed estuaries. *Journal of Physical Oceanography* 37: 1496-1511. doi: 10.1175/jpo3071.1

Scully, M.E., and W.R. Geyer. 2012. The role of advection, straining, and mixing on the tidal variability of estuarine stratification. *Journal of Physical Oceanography* 42: 855-868. doi: 10.1175/jpo-d-10-05010.1

Scully, M.E., W.R. Geyer, and J.A. Lerczak. 2009. The influence of lateral advection on the residual estuarine circulation: a numerical modeling study of the Hudson River estuary. *Journal of Physical Oceanography* 39: 107-124. doi: 10.1175/2008jpo3952.1

Shchepetkin, A.F., and J.C. McWilliams. 2005. The regional oceanic modeling system (ROMS): A split-explicit, free-surface, topography-following-coordinate oceanic model. *Ocean Modelling* 9: 347-404. doi: 10.1016/j.ocemod.2004.08.002

Shen, C., J.M. Testa, W. Ni, W.-J. Cai, M. Li, and W.M. Kemp. 2019. Ecosystem Metabolism and Carbon Balance in Chesapeake Bay: A 30-Year Analysis Using a Coupled Hydrodynamic-Biogeochemical Model. *Journal of Geophysical Research: Oceans* 124: 6141-6153. doi: 10.1029/2019jc015296

Shen, X., B.J. Lee, M. Fettweis, and E.A. Toorman. 2018a. A tri-modal flocculation model coupled with TELEMAC for estuarine muds both in the laboratory and in the field. *Water Research* 145: 473-486. doi: 10.1016/j.watres.2018.08.062

Shen, X., E.A. Toorman, B.J. Lee, and M. Fettweis. 2018b. Biophysical flocculation of suspended particulate matters in Belgian coastal zones. *Journal of Hydrology* 567: 238-252. doi: 10.1016/j.jhydrol.2018.10.028

Smetacek, V.S. 1985. Role of sinking in diatom life-history cycles: ecological, evolutionary and geological significance. *Marine Biology* 84: 239-251. doi: 10.1007/BF00392493

Smil, V. 2000. Phosphorus in the environment: Natural flows and human interferences. *Annual Review of Energy and the Environment* 25: 53-88. doi: 10.1146/annurev.energy.25.1.53

Taylor, K.E. 2001. Summarizing multiple aspects of model performance in a single diagram. *Journal of Geophysical Research-Atmospheres* 106: 7183-7192. doi: 10.1029/2000jd900719

Testa, J.M., and W.M. Kemp. 2012. Hypoxia-induced shifts in nitrogen and phosphorus cycling in Chesapeake Bay. *Limnology and Oceanography* 57: 835-850. doi: 10.4319/lo.2012.57.3.0835

Testa, J.M., and W.M. Kemp. 2014. Spatial and temporal patterns in winter-spring oxygen depletion in Chesapeake Bay bottom waters. *Estuaries and Coasts* 37: 1432-1448. doi: 10.1007/s12237-014-9775-8

Testa, J.M., Y. Li, Y.J. Lee, M. Li, D.C. Brady, D.M. Di Toro, W.M. Kemp, and J.J. Fitzpatrick. 2014. Quantifying the effects of nutrient loading on dissolved O2 cycling and hypoxia in Chesapeake Bay using a coupled hydrodynamic–biogeochemical model. *Journal of Marine Systems* 139: 139-158. doi: 10.1016/j.jmarsys.2014.05.018

Testa, J.M., R.R. Murphy, D.C. Brady, and W.M. Kemp. 2018. Nutrient- and Climate-Induced Shifts in the Phenology of Linked Biogeochemical Cycles in a Temperate Estuary. *Frontiers in Marine Science* 5. doi: 10.3389/fmars.2018.00114

Wang, J., H.S. Hong, Y.W. Jiang, F. Chai, and X.H. Yan. 2013. Summer nitrogenous nutrient transport and its fate in the Taiwan Strait: A coupled physical-biological modeling approach. *Journal of Geophysical Research-Oceans* 118: 4184-4200. doi: 10.1002/jgrc.20300

Wang, P., H. Wang, and L. Linker. 2015. Relative Importance of Nutrient Load and Wind on Regulating Interannual Summer Hypoxia in the Chesapeake Bay. *Estuaries and Coasts* 38: 1048-1061. doi: 10.1007/s12237-014-9867-5

Wei, X., M. Kumar, and H.M. Schuttelaars. 2017. Three-Dimensional Salt Dynamics in Well-Mixed Estuaries: Influence of Estuarine Convergence, Coriolis, and Bathymetry. *Journal of Physical Oceanography* 47: 1843-1871. doi: 10.1175/JPO-D-16-0247.1

Wiggert, J.D., R.R. Hood, and C.W. Brown. 2017. Modeling Hypoxia and Its Ecological Consequences in Chesapeake Bay. In *Modeling Coastal Hypoxia*, ed. D. Justic, K. Rose, R. Hetland and K. Fennel, 119-147. Cham: Springer. doi: 10.1007/978-3-319-54571-4_6

Willmott, C.J. 1981. On the validation of models. *Physical Geography* 2: 184-194. doi: 10.1080/02723646.1981.10642213

Xie, X., and M. Li. 2018. Effects of wind straining on estuarine circulation: A combined observational and modeling study. *Journal of Geophysical Research: Oceans* 123: 2363-2380. doi: 10.1002/2017JC013470

Xie, X., M. Li, and W.C. Boicourt. 2017. Baroclinic effects on wind-driven lateral circulation in Chesapeake Bay. *Journal of Physical Oceanography* 47: 433-445. doi: 10.1175/JPO-D-15-0233.1

Xu, J., and R.R. Hood. 2006. Modeling biogeochemical cycles in Chesapeake Bay with a coupled physical–biological model. *Estuarine, Coastal and Shelf Science* 69: 19-46. doi: 10.1016/j.ecss.2006.03.021

Xu, J., R.R. Hood, and S.-Y. Chao. 2005. A simple empirical optical model for simulating light attenuation variability in a partially mixed estuary. *Estuaries* 28: 572-580. doi: 10.1007/BF02696068

Xu, J.T., W. Long, J.D. Wiggert, L.W.J. Lanerolle, C.W. Brown, R. Murtugudde, and R.R. Hood. 2012. Climate forcing and salinity variability in Chesapeake Bay, USA. *Estuaries and Coasts* 35: 237-261. doi: 10.1007/s12237-011-9423-5

Zhang, W., Y. Cao, Y.L. Zhu, J.H. Zheng, X.M. Ji, Y.W. Xu, Y. Wu, and A.J.F. Hoitink. 2018. Unravelling the causes of tidal asymmetry in deltas. *Journal of Hydrology* 564: 588-604. doi: 10.1016/j.jhydrol.2018.07.023

Zhang, X. 2017. Biogeochemistry: A plan for efficient use of nitrogen fertilizers. *Nature* 543: 322-323. doi: 10.1038/543322a

Zhou, Y., D. Scavia, and A.M. Michalak. 2014. Nutrient loading and meteorological conditions explain interannual variability of hypoxia in the Chesapeake Bay. *Limnology and Oceanography* 59: 373-384. doi: 10.4319/lo.2014.59.2.0373

Chapter 3: Modeling Primary Production and Phytoplankton Biomass Variability in Chesapeake Bay

Abstract

In Chesapeake Bay, phytoplankton biomass typically peaks in spring whereas primary production peaks in summer. For this to happen, phytoplankton growth rates must be low in spring and high in summer and very likely there must be low grazing losses in spring and high grazing losses in summer as well. In this research, a three dimensional coupled physical-biological model is used to explore how these seasonal patterns in phytoplankton and primary production arise during the year from 2000 to 2005. It is shown that with the seasonal variation of maximum carbon to chlorophyll ratio, temperature control on phytoplankton growth, and temperature-dependent zooplankton grazing effects, my model can capture the spring peak in phytoplankton biomass and the summer peak in the primary production, agreeing well with the observations. The model simulates high phytoplankton growth rates in the summer, with the maximum growth rates occurring in late summer. The model also reveals that nutrient supply shifts from river-derived nitrate in the springtime to organic matter- derived ammonium during summer. The simulation results also reveal that a substantial fraction of the ammonium that supports the high summer production is derived from allochthonous transport rather than autochthonous ammonium production. The transport process provides as large as 50% ammonium needed for uptake during summertime in the mesohaline Chesapeake Bay. My research also

confirms the importance of nutrient recycling in supporting high summer production in Chesapeake Bay.

Introduction

Estuaries receive substantial inputs of nutrients via the connection to the land that stimulates high rates of primary production (Cloern et al. 2014; Nixon 1995). This primary production forms the base of estuarine food web and so is a key driver of higher trophic level productivity (Blanchard et al. 2012; Cloern and Jassby 2010). Factors governing phytoplankton dynamics in coastal and estuarine systems include water temperature, light availability, salinity, stratification and nutrient availability (Cloern 1996). The strong nutrient, light, and salinity gradients (Gle et al. 2008; Kocum et al. 2002; Lohrenz et al. 1999) along with the three-dimensional estuarine circulation (Geyer and MacCready 2014) give rise to complex variations in primary production in both time and space. There is a growing need to fully comprehend the factors that control primary production, especially in highly eutrophic urbanized estuaries (Kemp et al. 2009) where improving water quality and water security have emerged as important issues (Strokal et al. 2015).

In Chesapeake Bay, the largest estuary in North America, excessive nutrient inputs from major tributaries like the Susquehanna River and Potomac Rivers (Zhou et al. 2014) stimulates excessive phytoplankton growth, which contributes to high biological oxygen demand and the development of large recurring hypoxic and anoxic conditions (Kemp et al. 2005). Yet the current understanding of the factors that control the spatial and temporal variability in primary production and biological oxygen demand in Chesapeake Bay is still rudimentary in many respects. There has

been only a handful of in situ studies of primary production variability in the Chesapeake Bay (Adolf et al. 2006; Harding et al. 2002; Kemp et al. 1997). These studies have revealed that phytoplankton biomass (chlorophyll) and phytoplankton primary production are not tightly linked to one another, with chlorophyll often peaking in spring and primary production usually peaking in summer (Malone et al. 1988). However, the data that have been used to characterize these patterns are relatively sparse and there is tremendous seasonal and interannual variability in the chlorophyll and production patterns. Although ocean color-based measurements of chlorophyll concentration and estimates of primary production provide the potential to help fill the observational gaps, they may not be able to capture the observed disconnection between chlorophyll and primary production, nor can they reveal the underlying mechanisms (Son et al. 2014; Zheng and DiGiacomo 2020). Suffice it to say, there is insufficient observational data available to adequately characterize the seasonal and interannual chlorophyll and primary production variability in Chesapeake Bay, much less determine the factors that control it.

The seasonal variability of phytoplankton biomass and growth rate in coastal and estuarine systems varies substantially (Cloern and Jassby 2010). For example, in the northern Gulf of Mexico, the peak phytoplankton growth rate happens in the late spring and beginning of summer coincident with the phytoplankton biomass peak (Fennel et al. 2011). Nonetheless, several-fold seasonal variations in the phytoplankton growth rate are observed in the Gulf of Mexico. This is in contrast to the aforementioned decoupling of the phytoplankton biomass and production rate peaks in Chesapeake Bay (Malone et al. 1988) which is also indicative of large

seasonal variations in phytoplankton growth rate. Qin and Shen (2017) established a three-dimensional water quality model and introduced a variable growth coefficient that allows the model to simulate observed phytoplankton biomass variations in the James River. Although this parameter is not exactly the same as growth rate, it is interesting to note that at least 2 to 3 fold seasonal variations in this parameter must be imposed from spring to summer to get the model to correctly simulate the seasonal variability in phytoplankton biomass (Qin and Shen 2017). In a related study, Liu and de Swart (2018) established a two dimensional idealized dynamic phytoplankton production model that can simulate the vertical distribution of phytoplankton, and also the spatial distribution of growth rate in spring under different stratification conditions in the Columbia River, but they did not simulate the growth rate variation across the season. Cerco and Noel (2004) established a process-based biogeochemical model that can generally capture the seasonal variability of primary production in Chesapeake Bay as revealed by observations from the 1990s. However, upon close inspection in some years there are large discrepancies between the modeled and observed primary production, and the phytoplankton biomass variability is not shown. None of the previous biogeochemical modeling work conducted in Chesapeake Bay (Cerco and Noel 2004; Feng et al. 2015; Shen et al. 2019; Testa et al. 2014; Xu and Hood 2006) has successfully simulated the observed seasonal transition of both primary production (which generally peaks in summer) and accumulation of biomass (which generally peaks in spring), nor have any of these studies examined how phytoplankton growth rate must vary seasonally to make this happen, or what the environmental factors are that control this growth rate variability. From Adolf et al.

(2006) observations, it can be estimated that the summertime phytoplankton growth rate should be about 3-5 times larger than the growth rate in springtime in order to capture the observed seasonal changes in phytoplankton biomass and primary production.

Although satellite-based primary production results (Son et al. 2014) obtained in recent years provide more large-scale coverage and resolution, the physical, biogeochemical and physiological mechanisms behind the observed patterns are difficult to discern. This difficulty is exacerbated by the fact that satellites tell you very little about what is going on under the surface of the water. However, a processed based physical –biogeochemical model including growth, aggregation and mortality can cover a large spatial scale and multiple years' and potentially provide direct insights into the factors that control the seasonal patterns in phytoplankton biomass and primary production in Chesapeake Bay if the model can be formulated and parameterized to capture these patterns.

The aim of this research is to answer the following questions: 1) Can a simple nitrogen-based ecosystem model capture the observed seasonal patterns of phytoplankton biomass and primary production in Chesapeake Bay? And 2) what are the physical, biogeochemical and physiological factors that give rise to these patterns?

Methods

The physical and biogeochemical model components that are used in this study are consistent with previous chapter. Research region, its sub-regions and monitoring stations are presented in Figure 3.1. For the gross primary production (GPP), I use the

first term in the phytoplankton budget equation as shown in Table 0-2. $L_{NO_3^-}$, $L_{NH_4^+}$, L_I are the light, nitrate and ammonium limitations in this term, respectively. The modeled primary production is converted to carbon units using the Redfield ratio for comparison to ^{14}C primary production measurements. The light formula is based on Xu et al. (2005). I used the 1% light level as a critical value to estimate daily averaged euphotic zone thickness, thus removing euphotic zone thickness fluctuations at short time scales. In ChesROMS, the salinity background vertical diffusion coefficient was set to $10^{-5}m^2/s$ as in Scully (2013). I defined the mixed layer depth as the location where the salt vertical diffusion is $10^{-4}m^2/s$, which is an order of magnitude larger than Scully (2018) for better visualization (10^{-5} is hard to detect). The F-ratio defined in this research is the ratio of locally generated NH_4^+, uptake over the sum of NH_4^+, uptake and NO_3^- uptake in the euphotic zone.

All the measurement data presented in this paper is from the Chesapeake Bay Program (CBP) (https://www.chesapeakebay.net/what/data). I conducted simulations with the same parameter sets for the year 1991 and a six-year simulation from 2000 to 2005. The 1991 simulation was carried to validate the model against primary production as measurements (Kemp et al. 1997) while also aiming at providing the best simulation results simultaneously for GPP, chlorophyll and phytoplankton growth rate. The 2000 to 2005 results were used for climatological analysis. In addition, year 2005 was also used for additional process analysis.

In order to elucidate the processes that control primary production, especially the ammonium remineralization, uptake, and transport during the summer, the original ROMS code diagnostic terms were modified to include biogeochemical source and

sink terms, as well as the transport terms, for example, the horizontal advection, vertical advection and vertical diffusion. With these terms,I could distinguish the allochthonous and autochthonous sources of ammonium. For evaluation of the contribution of allochthonous transport on summertime nutrients, I defined the ratio of transport and total uptake as presented in Equation 3-2. Sensitivity runs were also conduced to examine the factors controlling the summertime GPP. Run descriptions are provided in Table 3-1. Particulate organic nitrogen (PON) is defined as the sum of the phytoplankton, zooplankton, large organic detritus and small organic detritus in nitrogen units (Feng et al. 2015). Model skill assessment follows Willmott (1981).

$$GPP = \mu_0 L_I \left(L_{NO_3} + L_{NH_4}\right) P$$

Equation 3-1

$$\frac{\partial NH_4}{\partial t} + \text{transport} = Production - uptake$$

Equation 3-2

Results and Discussions

Model performance in Biomass and GPP

The model results were validated using GPP measurements from 1991 (Figure 3.2). The model generates a clear seasonal pattern of GPP, and the model results capture the observed seasonal variations, but generally underestimate GPP values in the middle and lower bay regions, but overestimate GPP in the upper bay. For example, the summertime measurements indicate more than 3.5g Carbon/m^2/day(Kemp et al. 1997), both in the middle and lower bay, but the model generates around ~2 - 3g Carbon/m^2/day in these regions. The model also overestimates the upper bay GPP,

where measurements indicate ~0.5g Carbon/m^2/day during summertime but model predicts >1.5 g Carbon/m^2/day (Figure 3.2). Surprisingly, observations indicate that the lower Bay GPP is higher than it is in the middle Bay (Kemp et al. 1997). My model fails to capture this pattern of elevated GPP in lower Bay (Figure 3.2).

Figure 3.3 and Figure 3.4 compare modeled and observed bottom and surface particulate organic nitrogen (PON) levels, respectively. Clear seasonal variation was observed in the bottom PON in both the observations and the model, with accumulation occurring primarily in the springtime followed by PON disappearance in the summer (Figure 3.3). Interannual PON variability was also observed in both the observations and the model with higher PON concentrations in wet years, like 2003, compared to drier years like 2002 (Figure 3.3). In both the observations and the model, the surface PON concentrations are higher during the summer compared to spring due to high productivity in the surface during summer. The model also overpredicted the surface PON concentrations in some years, for example 2004 (Figure 3.4).

Figure 3.5 shows point to point comparisons between the modeled and observed chlorophyll concentrations over all depths at several stations along the mainstem of Chesapeake Bay for a selected year: 2005. Larger symbols represent deeper water values while smaller symbols represent more shallow water values. These plots clearly reveal that the model captures the observed bottom chlorophyll accumulation during the spring season. Figure 3.5 also reveals that the model generally captures the seasonal variations in chlorophyll concentration throughout the bay, with chlorophyll concentrations higher in the spring and lower in the summer. The model chlorophyll

skill for all of the monitoring stations is 0.6 or higher, except for CB5.2. The model chlorophyll skill for other years is consistent with the previous Chapter.

Figure 3.6 shows the modeled spatial patterns in vertically integrated chlorophyll for March, April, July and August. As observed, the model generates a well-defined spring bloom and chlorophyll concentrations decline in summer. Observations show that during summer, the species composition of the phytoplankton is dominated by dinoflagellates and cyanobacteria (Adolf et al. 2006; Marshall and Nesius 1996), and that there is very little bottom chlorophyll or PON accumulation due to the impacts of high zooplankton grazing, low sinking speed, and a more stratified water column. Parameter adjustments can be made to lower chlorophyll concentration during summer to obtain better model skill, but this comes at the price of degrading the model's GPP performance. In general, the model somewhat overestimates chlorophyll concentrations in the surface during summer (Figure 3.5). But the model does clearly capture the seasonal pattern in chlorophyll concentration (Figure 3.5), i.e., the chlorophyll biomass peak occurs during the springtime, with more than 500 mg/m^2 in the mesohaline region of the Bay (Figure 3.6). In contrast, the model maintains a relatively low amount of chlorophyll biomass in the summer, around 200 mg/m^2 and even less in the upper mainstem Bay in August (Figure 3.6). The biomass accumulation occurs during the spring season resulting in the spring chlorophyll peak even though the growth rate is relatively low at this time due to the low temperatures. Figure 3.7 shows the climatological, depth-integrated gross primary production for 2000 to 2005. In general, the model simulates the seasonal patterns in primary production reasonably well in the upper, middle, and lower bay regions. The model

also captures the observed lower GPP in the upper bay compared to the middle bay region due to the turbidity/light limitation effects. However, the model fails to capture the elevated primary production in the lower bay discussed above. Scully (2018) also failed to capture this pattern. In Scully (2018) the highest simulated GPP is in the mid-Bay region as in this study. Interestingly, satellite remote sensing estimates of primary production also indicated relatively higher net primary production in the middle bay compared to the lower bay (Son et al. 2014).

In summary, the comparisons presented here reveal that the model provides a reasonable simulation of the seasonal variability of the GPP in Chesapeake Bay with an acceptable chlorophyll skill as well. Although GPP is underestimated by the model, the results clearly show that the model can reproduce the observed summer GPP peak. It should also be noted that the model GPP is averaged over the middle Bay sub-domain, which is a large region. At specific locations in the middle Bay in the spring, the maximum monthly averaged GPP in the model is around 1 to1.5 g carbon/m^2/day, whereas when the summer approaches, it can exceed 4.0 g carbon/m^2/day in some places. The latter is compared to the sub-domain summer average of ~2 g carbon/m^2/day. Thus, the averaging can significantly lower the maximum simulated summertime GPP values. A pronounced spatial gradient in GPP is also simulated by the model during summer with low GPP in the upper bay, much higher GPP in the middle Bay, followed by a gradual decrease in GPP in the lower Bay (Figure 3.7). The same spatial distribution in GPP has been observed in other investigations (Scully 2018; Son et al. 2014).

Growth rate estimation

The modeled near-surface (0.5m depth) and subsurface (1.5m) from 2000 to 2005 averaged phytoplankton growth rate, in units of d^{-1}, is plotted in Figure 3.8 and Figure 3.9, respectively. Assuming a carbon to chlorophyll ratio of 40, this growth rate is reasonable compared to previous research (Adolf et al. 2006). For example, in Adolf et al. (2006), the multiple year averaged summertime GPP is around 2200 $mg/m^2/day$ with chlorophyll around $85mg/m^2$ and, assuming a carbon to chlorophyll ratio 40, the euphotic zone growth rate is ~0.64 d^{-1}. Though, obviously, the growth rate estimated from Adolf et al. (2006) will vary depending on the assumed carbon to chlorophyll ratio. My model generates similar growth rates, although for different years. These modeled growth rates are lower than the rates estimated by Scully (2018) using the diel oxygen method but they have a similar seasonal distribution (See Figure 7 in Scully, 2018). It should also be noted that the growth rates estimate in Scully (2018) are based on surface oxygen measurements. The average growth rate in the euphotic zone will be much lower due to the light attenuation effect that rapidly reduces the growth rate with depth, as shown in Figure 3.8 and Figure 3.9. The high modeled growth rate at 0.5 m depth of ~2-2.5 d^{-1} in August and September drops to ~1.2 d^{-1} at 1.5 m depth. Field measurements have shown that the in-situ growth rates, which include the effects of light and nutrient limitations, can vary by more than a factor of 4 (Harding et al. 2002). Our modeled growth rates also vary by a factor of 4 at 0.5 m depth from spring to summer compared to a factor of 2 at 1.5 meter depth. Previous research (Harding et al. 2002) has shown that the primary factor controlling the

phytoplankton grow rate Bay wide is temperature. The model results are broadly consistent with these findings as present in Figure 3.10a.

Figure 3.10 shows the variability in phytoplankton growth rate for different locations along the estuarine gradient and different water depths. The growth rate at CB3.1 is lower than at CB4.1 during spring at 1.5m, largely due to the increased light limitation at the northern station. In contrast, the growth rate is only slightly lower for CB3.1 compared to CB4.1C at 0.5m depth because the light levels are more similar at shallower depths. During springtime the phytoplankton growth rates at the northern bay location CB4.1C are much higher than further south at CB5.3C and CB6.2C, due to nutrient limitation effects. However, in the summer, the growth rates are more similar throughout the, Bay except at CB3.1C at 1.5 depth, which is reduced by light limitation as discussed above. During summertime phytoplankton growth rates at CB5.3 are higher than the CB4.1C, likely due to the greater water clarity at CB5.3 due to reduced CDOM.

It should be noted, however, that the model probably underestimates the phytoplankton growth rate in early summer (May and June), i.e., in the modeled growth rates are relatively low at this time (Figures 3.8 – 3.10) whereas previous studies indicate that they should be fairly high (Harding et al. 2002; Scully 2018). This likely happens because the nitrate and ammonium concentrations are near zero at the surface during this time in the model. This problem might be solved in the future by increasing nutrient recycling in the surface layers. In addition, the model probably overestimates the phytoplankton growth rates in September, i.e., in the model the growth rates are highest in September (Figures 3.8 - 3.10) whereas previous studies

indicate that they should peak in mid-summer (Harding et al. 2002; Scully 2018). This may be the result of having too much zooplankton grazing and nutrient recycling during the late summer and early fall in the model.

In Scully (2018)'s diel method of estimating gross primary production, the maximum chlorophyll specific production rate (assimilation number) is as high as 28 to 30 $[\mu gC/\mu g\ Chl\ h]^{-1}$ at stations in the Patapsco River and near Annapolis during July to August for the period 2010–2016 (see Figure 7 in Scully, 2018). Assuming a carbon to chlorophyll ratio of 50, this gives growth rates as high as 13.4 day^{-1}, much higher than the surface values generated by the model (~2.5 day^{-1}, Figure 3.10a). This monthly surface growth rate inferred from Scully (2018) is even larger than the instantaneous grow rate, 7 day^{-1}suggested by Cerco and Noel (2004). During summertime the phytoplankton growth rates in the model are more similar from north to south, which is consistent with the phytoplankton growth rate patterns reported in Scully (2018) (see his Figure 7).

Figure 3.11 shows the vertical diffusion coefficient for salinity, plotted on a log scale, in July (Figure 3.11a) and October (Figure 3.11b) in 2005. The -4 value (Figure 3.11a,b) near the surface was used to represent the mixed layer depth. These plots reveal that the mixed layer depth is varies substantially from July to October. For example, during the summertime, mixed layer depth is around 1.5 to 2.5 meters depth, while in the October, it is more than 8 meters depth. It is expected that average phytoplankton growth rate in the mixed layer will decline from summer to fall due to the increase in the mixed layer depth due to increasing light limitation, which is not apparent in Figures 3.8 and 3.9 where the growth rates are plotted as specific depths.

Allochthonous and autochthonous NH_4^+, effects on Primary production

Figure 3.12 shows that the F-ratio shifts from 1 to zero from spring to summer, revealing that nitrate fuels the spring phytoplankton bloom whereas ammonium fuels the high summertime primary production. Previous studies have emphasized the importance of NH_4^+, recycling in supporting high summertime primary production in Chesapeake Bay, with the source of this ammonium derived from remineralization of detritus deposited on the bottom in the spring (Testa and Kemp 2012). Presumably, remineralization of organic matter generated during summer also plays a significant role in supporting high summertime primary production. Thus, it is important to investigate the sources of NH_4^+ production in the summer in order to understand how high summer GPP is supported. Results presented in Figure 3.13g, which reveal the allochthonous contributions in the total ammonium uptake during the summertime along the white dashed line in Figure 3.11a, indicate that the allochthonous supply contributes 20% to 50% of NH_4^+ uptake during the summertime. This also reveals the importance of autochthonous ammonium supplied from organic matter remineralization which constitutes 50% to 80% of the uptake. Indeed, the magnitude of these two processes become approximately equal as one moves northward in the mesohaline region of the mainstem Bay (Figure 3.13g). Thus, this analysis supports the classic conceptual model which asserts that the nutrients that support high summer primary production in the mainstem, mesohaline Chesapeake Bay are supplied by transport processes (allochthonous) that move ammonium derived from remineralization of organic matter deposited on the bottom into the euphotic zone (Kemp et al. 1992; Kemp et al. 1997). Also, an equally important source of

ammonium comes from organic matter remineralization within the euphotic zone itself (autochthonous). These findings are also consistent with classical research on the nitrogen budget in Chesapeake Bay (Boynton and Kemp 1985), i.e., Boynton and Kemp (1985) estimated that benthic remineralization of organic matter supplies about 50% of the water column ammonium budget.

A significant amount of both new production and recycled production occurs in many upwelling (Hahm et al. 2019; Ji et al. 2019; Kadko 2017) and estuarine systems (Boynton and Kemp 1985; Qin and Shen 2019). There is a long-held belief that estuarine primary production is high, in part, due to trapping and recycling of nutrients (Kemp et al. 2009; Testa and Kemp 2012). An examination of the NH_4^+ volume flux, along the subsurface pink transect in Figure 3.11b, revealed that much more NH_4^+ was transported upward (~ 500 to 1200 mmol/m^3/day) north of 39° N in the bay, through vertical advection compared to vertical diffusion (Figure 3.14f,g). Diffusion plays an important role in supplying nutrient the surface water only in May and June (Figure 3.14d,e). Negative (downward) advective ammonium flux was observed in the southern Bay region (Figure 3.14a-j), but the magnitude was small compared to the northern Bay. This small downward flux is due to the effects of downward gravitational circulation combined with low NH_4^+ concentrations in the polyhaline region of the Bay (e.g. Figure 3.14f,g). It is widely accepted that in estuaries high primary production is driven by the new production. The model results show that the nitrogen was recycled and reused as a result of the estuarine circulation.

Sensitively analysis on the primary production

The results presented in this paper reveal that my model is capable of capturing the observed phytoplankton chlorophyll and primary production patterns in Chesapeake Bay, where phytoplankton chlorophyll concentrations typically peak in spring and primary production typically peaks in summer. The model's ability to capture these patterns is related to four key attributes: 1) the temperature dependence of phytoplankton growth rate which allows the phytoplankton growth rate to increase substantially in the summer compared to spring; 2) the temperature dependence of the zooplankton grazing rate which allows phytoplankton biomass accumulation in spring when grazing rates are low and prevents phytoplankton biomass accumulation in summer when grazing rates are high; 3) a variable carbon to chlorophyll ratio which reduces the amount of chlorophyll per unit phytoplankton nitrogen in summer compared to spring; and 4) a seasonally variable sinking speed for phytoplankton and detritus which results in rapid export of PON to the bottom in spring while retaining PON in the surface in summer where it can be recycled to ammonium.

In order to examine the relative impacts of these three attributes I conducted an additional four runs where each of these features of the model were turned off to determine their relative importance (Table 3-1). Model run B, where the temperature dependence of phytoplankton growth rate was turned off, shows the model skill for simulating chlorophyll concentration remained relatively high (> 0.65) in many main stem Bay stations, but the maximum summertime GPP dropped to < 1.4 g C/m^2/day compared to the base Run A where GPP is > 3 g C/m^2/day. This indicates that the high primary production during summertime is largely driven by the impact of

temperature on the phytoplankton growth rate. Model run C, where the carbon to chlorophyll ratio in the model was held constant from spring through summer, also gave a similar chlorophyll skill and high GPP (~2.9 g/m^2/day) compared to the base run, but the surface chlorophyll is much higher than observed during summer (Figure 3.15). This suggests that simulating changes in the carbon to chlorophyll ratio associated with seasonal changes in phytoplankton species composition (spring dominance of diatoms versus summertime dominance of dinoflagellates and cyanobacteria), and/or the carbon to chlorophyll ratio response to light, are very important for capturing the relatively low chlorophyll concentrations that are observed in summer in Chesapeake Bay. Model run D, where grazing rate was held constant from spring to summer, gave a high summer GPP (~ 3.5 g/m^2/day), but the chlorophyll skill was substantially lowered. Without temperature-controlled zooplankton grazing, the surface chlorophyll was much higher than the base run during summer (Figure 3.15), which allowed the model to achieve the high GPP during summer even with same phytoplankton growth rate. Model run E, where the sinking speed of phytoplankton and detritus was held at the high springtime (diatom) value throughout the year, gave a low GPP during summer because phytoplankton biomass in the euphotic zone was too low to support the high observed GPP. Rather, in model run E the phytoplankton and PON quickly dropped to the bottom during summer, which also inhibited PON remineralization to ammonium in the surface layers that also supports high summertime GPP.

Conclusion

In this research, a 3-dimensional coupled physical-biological model was used to simulate seasonal and spatial patterns in phytoplankton biomass (chlorophyll) and primary production in Chesapeake Bay, USA. It is shown that the model can capture the seasonal variability of both chlorophyll and primary production and that it can reproduce the observed spring maximum in depth-integrated chlorophyll and summer maximum in depth-integrated primary production that has been reported in many observational studies. The key to reproducing these patterns is related to following key attributes of my model: 1) the temperature dependence of phytoplankton growth rate on temperature which allows the phytoplankton growth rate to increase substantially in the summer compared to spring; 2) the temperature dependence of the zooplankton grazing rate which allows phytoplankton biomass accumulation in spring when grazing rates are low and prevents phytoplankton biomass accumulation in summer when grazing rates are high; 3) a variable carbon to chlorophyll ratio which reduces the amount of chlorophyll per unit phytoplankton nitrogen in summer compared to spring; and 4) a seasonally varying sinking speed which allows the model to represent the predominance of fast-sinking diatoms in the spring and slow-sinking flagellates and dinoflagellates in the summer.

These results highlight the idea that that multiple factors are involved in generating the seasonal patterns in chlorophyll concentration and primary production that are observed in Chesapeake Bay which conspire to keep phytoplankton growth rates low and chlorophyll concentrations high in spring and phytoplankton growth rates high and chlorophyll concentrations low in summer.

It should also be emphasized that the summertime high primary production (and growth rate) is the result of the combined effects of high temperature, light availability, and nutrient supplements in the form of ammonium that is provided through both transport and mixing processes (new nitrogen) and euphotic zone recycling (old nitrogen). The control volume budget analysis revealed substantial nutrient inputs via upward transport of NH_4^+ flux during the summer in the mesohaline region of the Bay, while there was more downward flux in the southern Bay region, consistent with the expected influence of gravitational circulation on nutrient transport, retention and recycling. The model indicated that the vertical transport processes make a large contribution (as much as 50%) to the total ammonium uptake in northern Bay region. This model-estimated transport contribution to total nitrogen uptake was also consistent with previous nutrient cycling and budget research in the Chesapeake Bay and it provides an explanation for the conundrum revealed in previous studies that nutrients remineralized from bottom detritus can only support about half of the summer primary production. The explanation emerging from this study is that the remaining nutrients are supplied through euphotic zone recycling (old nitrogen).

Acknowledgement

This research was funded in part by NOAA's U.S. Integrated Ocean Observing System (IOOS) Program Office as a subcontract to the University of Maryland Center for Environmental Science from the Southeastern University Research Association (award no. NA13NOS120139). Lead author Wang was also supported by a Bay and Rivers Scholarship from Horn Point Laboratory, University of Maryland Center for

Environmental Science, and by the China Scholarship Council (CSC, File 201206710006). This is University of Maryland Center for Environmental Science contribution XXXX.

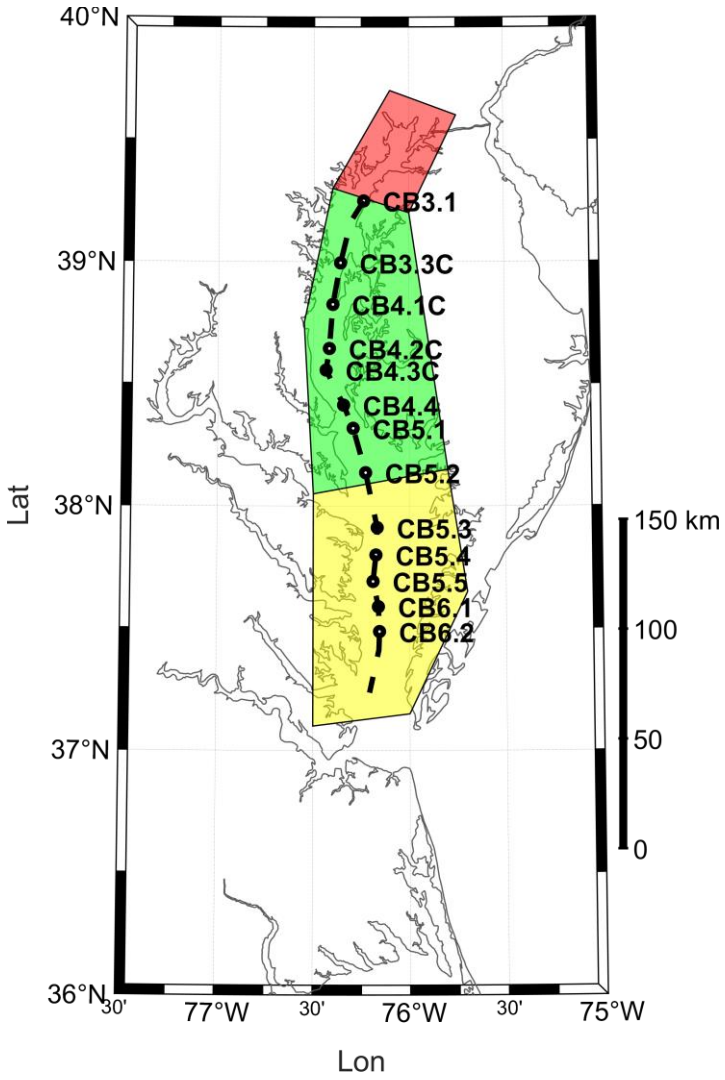

Figure 3.1: Research region and monitoring station locations. The black circles represent the CBP stations that provided biogeochemical data for validation. The black line represents the deep channel transect along estuarine salinity gradient. The light red, light green and light yellow regions represent the upper, middle and lower bay regions, respectively, that were used for averaging.

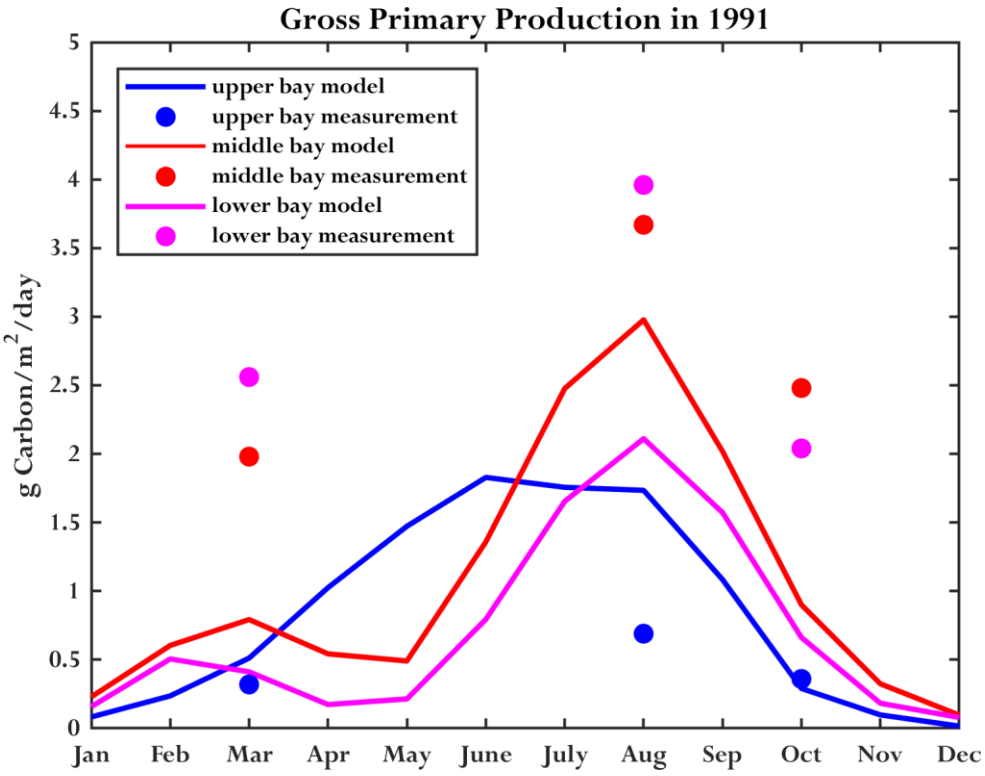

Figure 3.2: Seasonal whole Bay-averaged and monthly-averaged gross primary production comparison between the model and observations. The plot shows averages for the upper Bay, middle Bay and lower Bay for the year 1991. The circles represent observed production and the lines represent the modeled production.

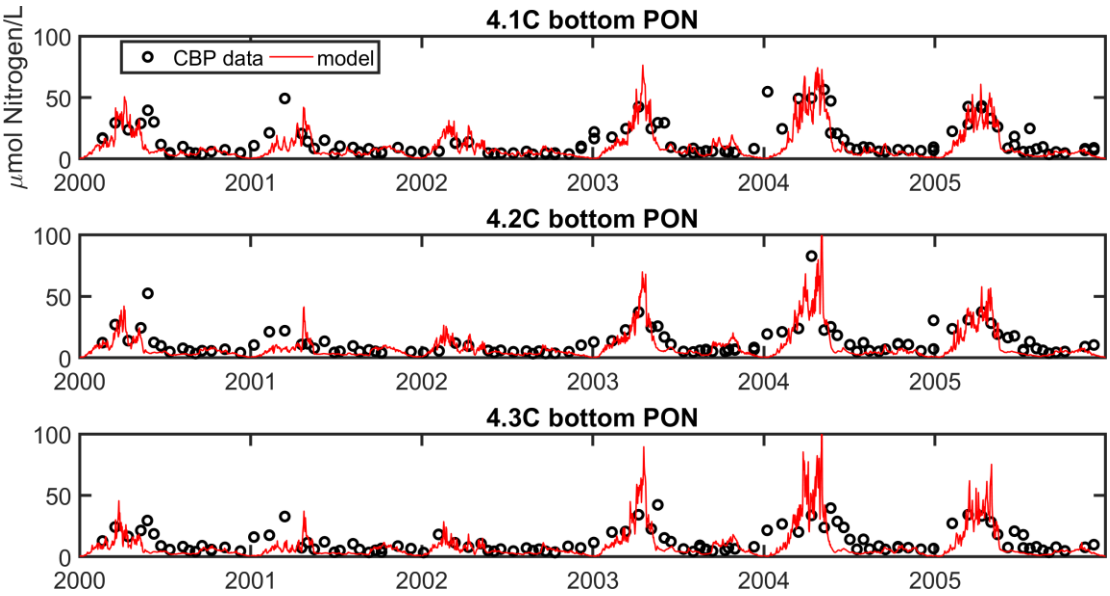

Figure 3.3: Surface PON from the model (red line) versus measurements (black points) at stations CB 4.1C, CB 4.2C, CB4 .3C from 2000 to 2005.

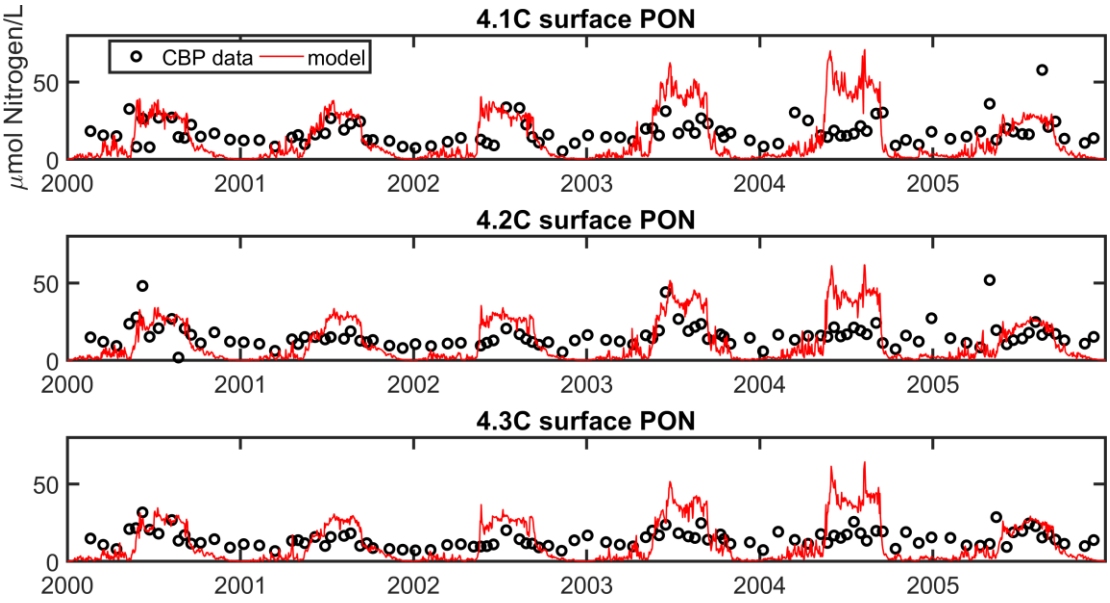

Figure 3.4: Bottom PON from the model (red line) versus measurements (black points) at stations CB 4.1C, CB 4.2C, CB4 .3C from 2000 to 2005.

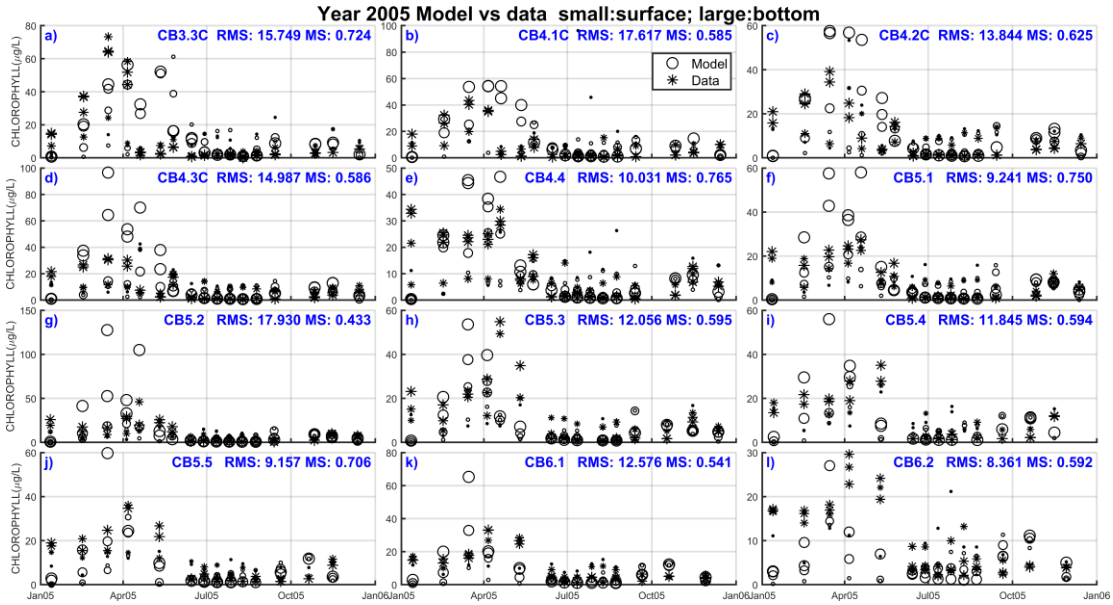

Figure 3.5: Point to point modeled (circles) vs. measurements (stars) comparisons of chlorophyll in the deep channel stations; the larger symbols represent deeper water.

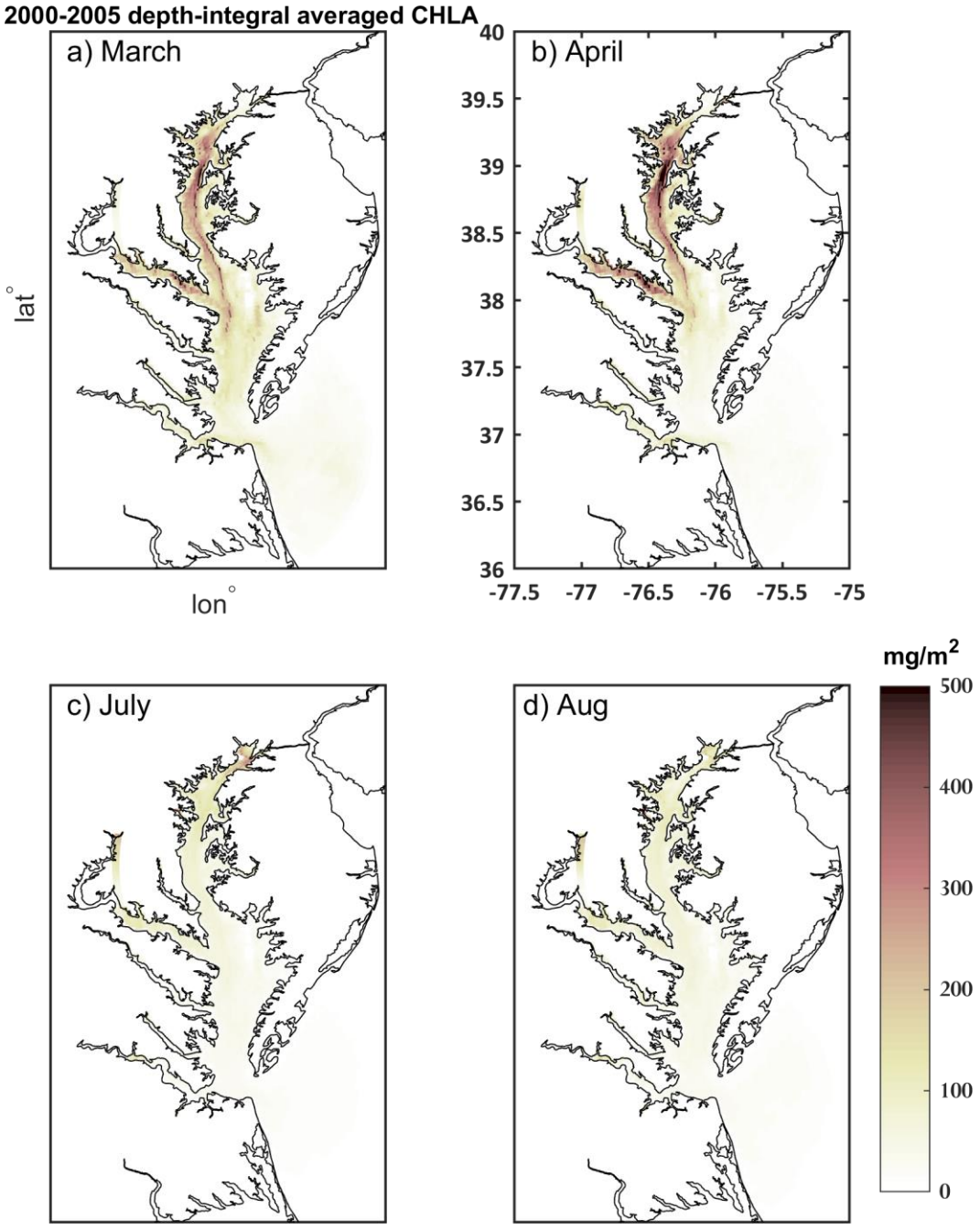

Figure 3.6: Model-simulated Bay-wide depth-integrated and monthly averaged chlorophyll concentration for March, April, July and August of 2000 to 2005.

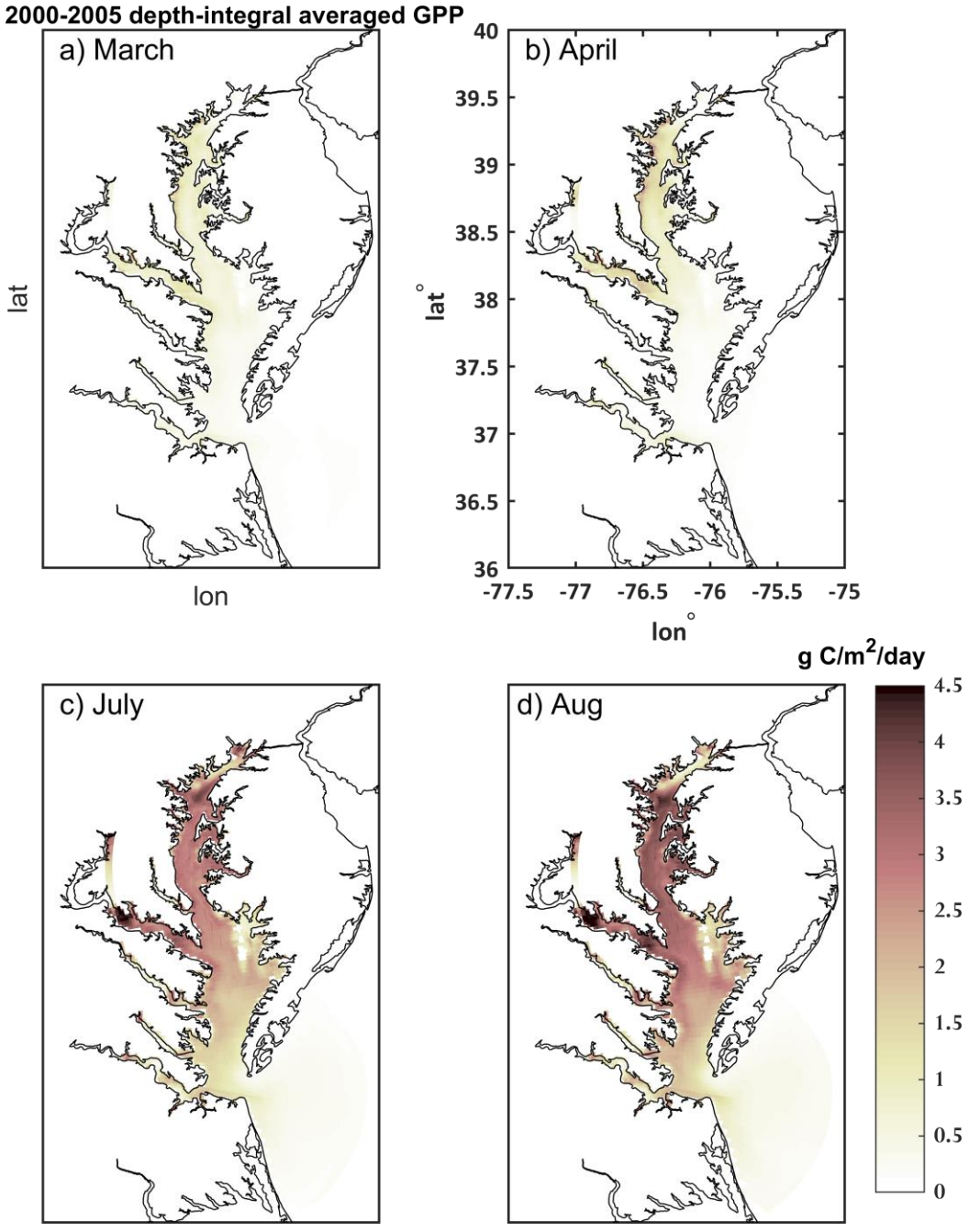

Figure 3.7: Model-simulated Bay-wide depth-integrated and monthly averaged gross primary production for March, April, July and August of 2000-2005.

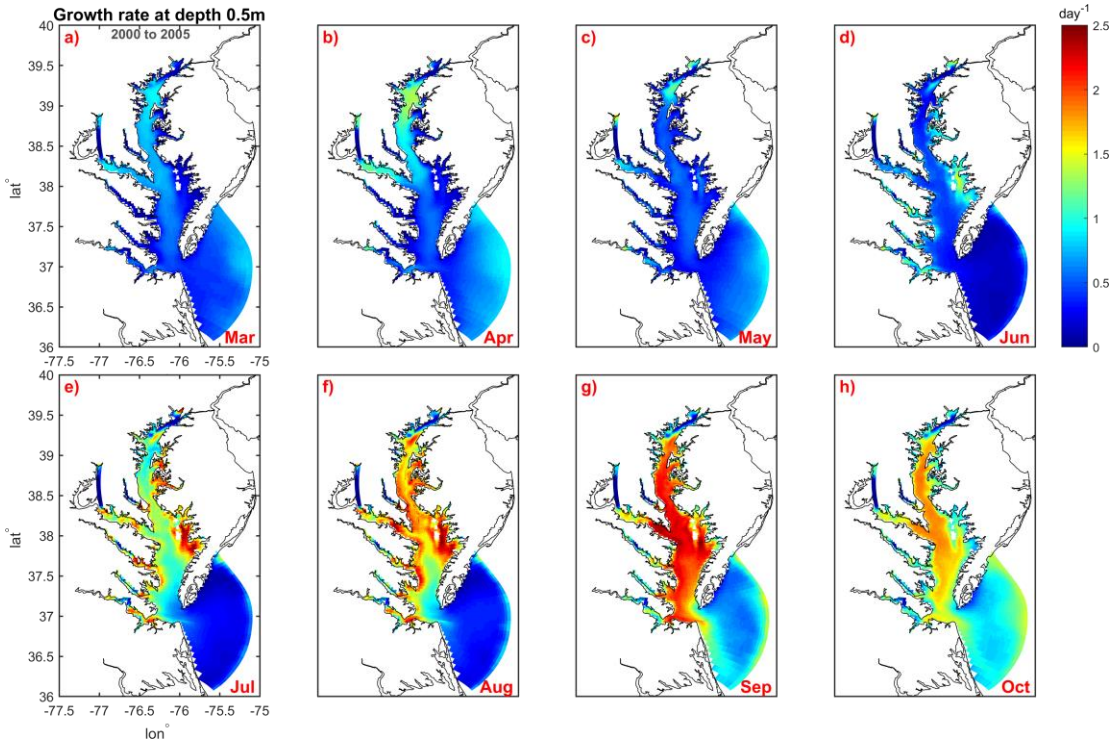

Figure 3.8: Bay-wide monthly averaged phytoplankton growth rate at 0.5 meters depth for 2000-2005.

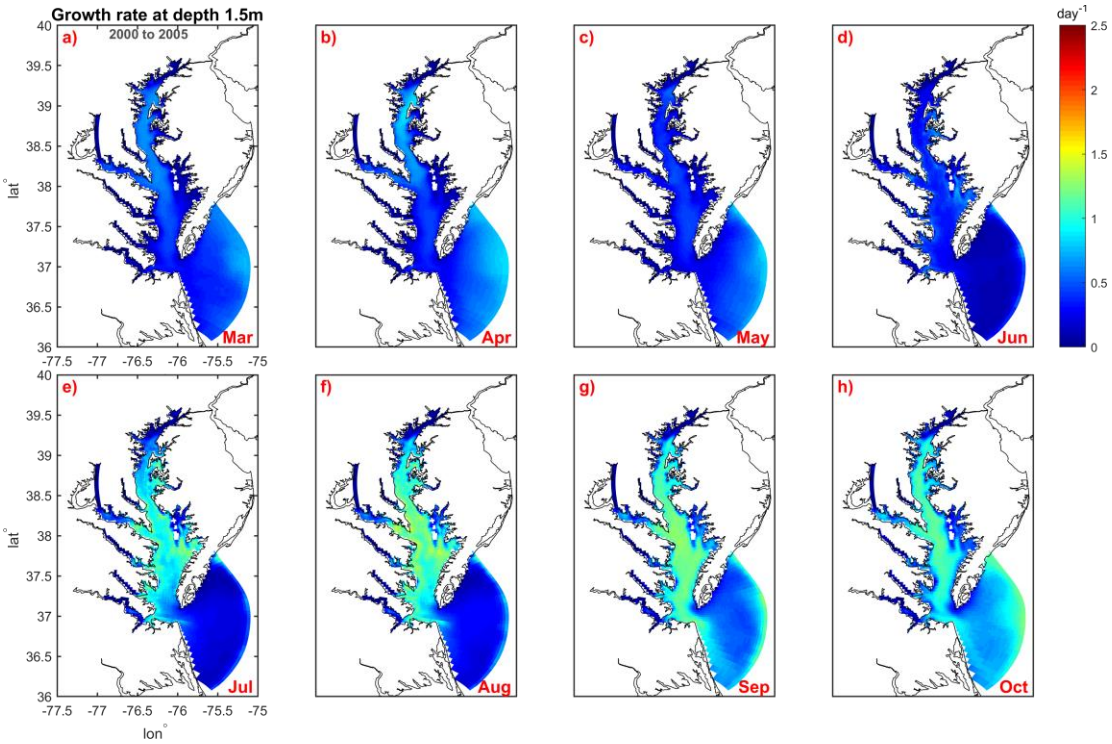

Figure 3.9: Bay-wide monthly averaged phytoplankton growth rate at 1.5 meters depth for 2000-2005.

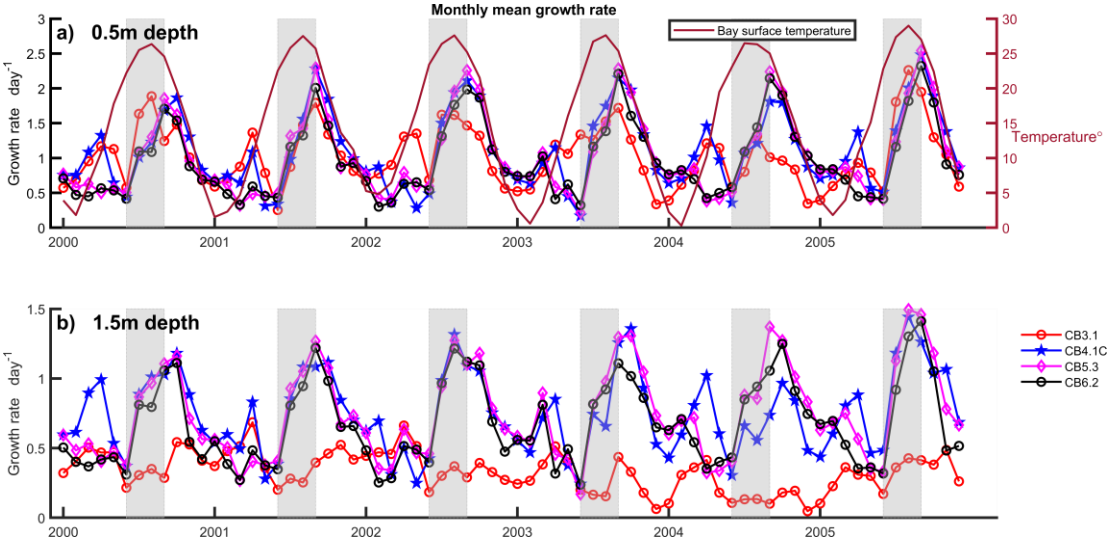

Figure 3.10: Monthly-averaged phytoplankton growth rate at different CBP station locations from the model: a) at 0.5m depth, b) at 1.5m depth; the shaded region present June to September.

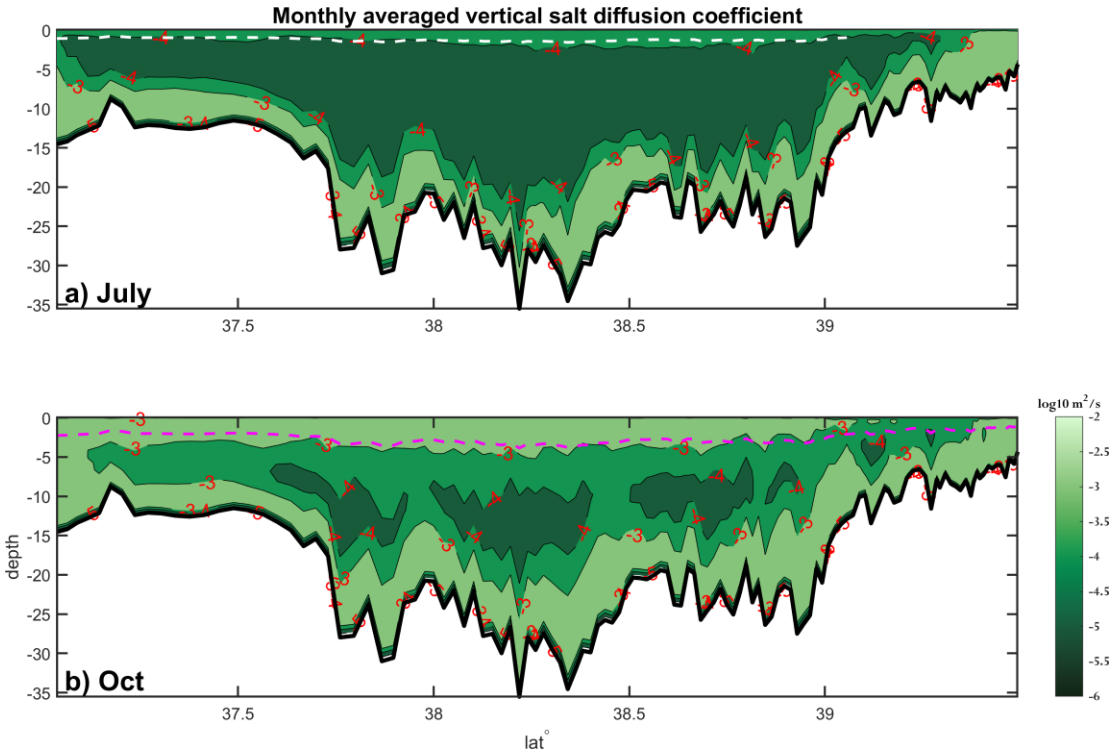

Figure 3.11: Model-simulated monthly averaged salt vertical diffusion coefficients for July (a) and October (b) in 2005. The white dashed line(chosen fixed trhougt out the year) in the top panel is the location for allochthonous/autochthonous ratio (Figure 3.13). The pink dashed line (chosen fixed trhoutout the year)in the bottom panel is the location for allochthonous/uptake ratio and the contribution of ammonium flux analysis below (Figure 3.14).

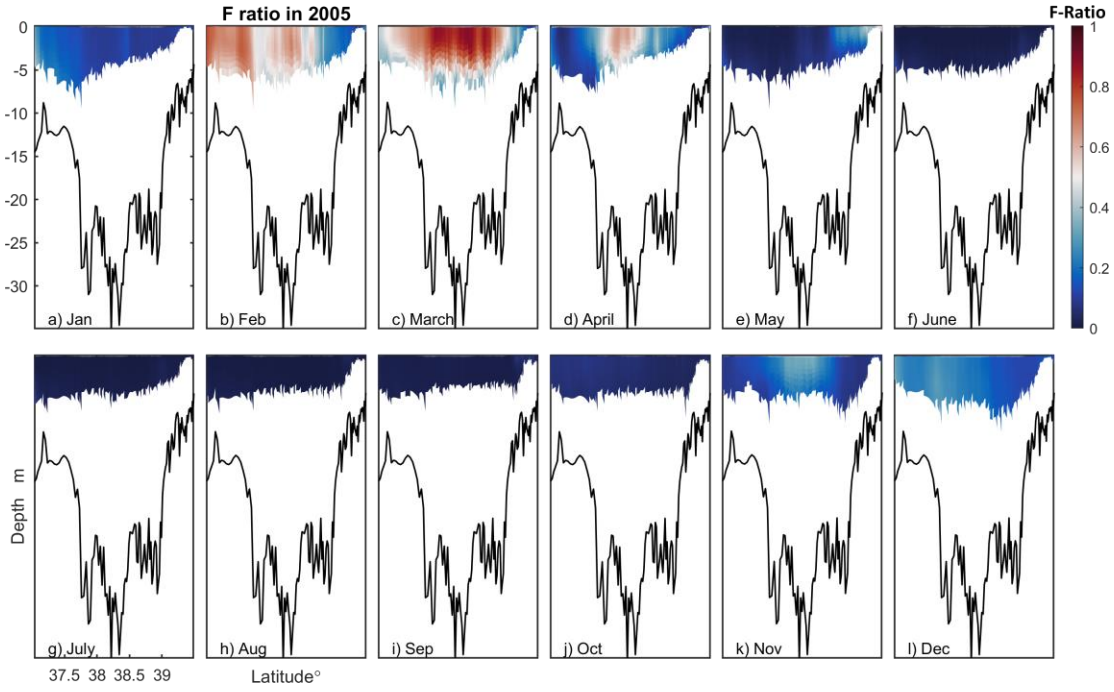

Figure 3.12: Monthly averaged F ratio values along the deep channel of the bay for the euphotic zone in 2005. The red color indicates nitrate uptake while the blue color indicates ammonium uptake.

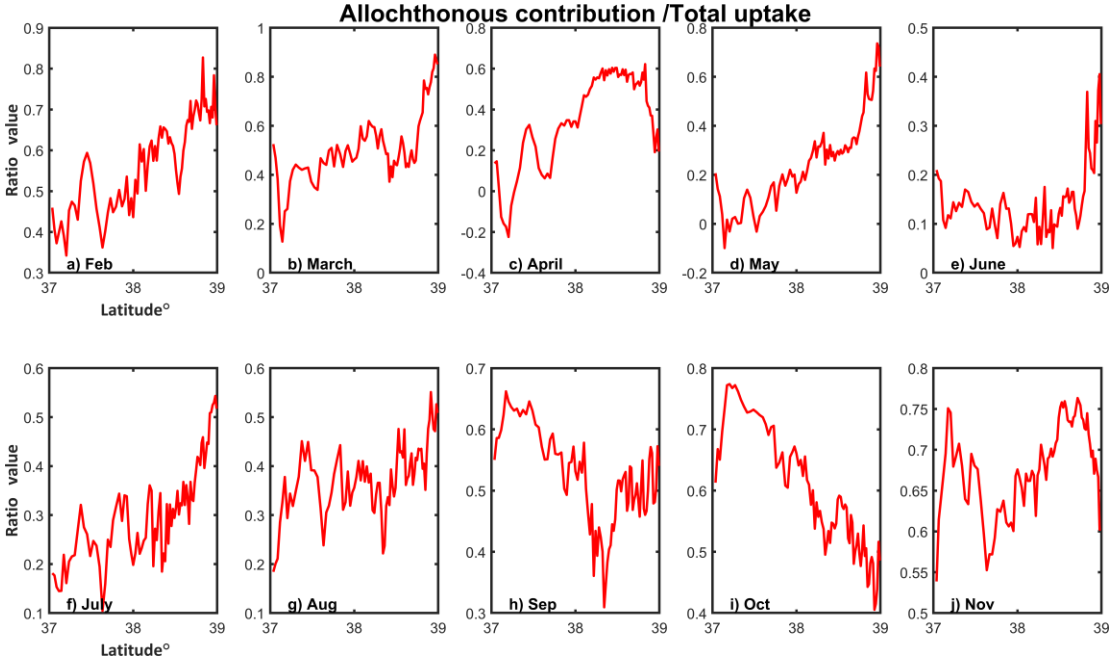

Figure 3.13: Monthly averaged ratio of the allochthonous contribution to total ammonium uptake along the deep channel of the bay (see white dotted line in figure 3.11a).

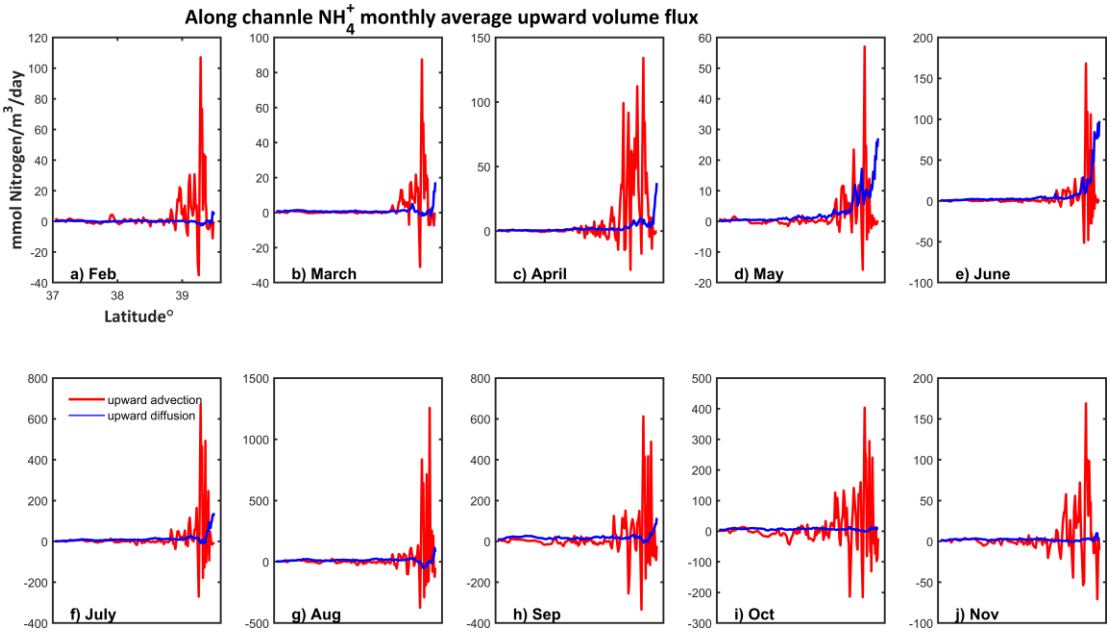

Figure 3.14: Monthly averaged volume upward vertical advection flux (red) and upward diffusion flux (blue) of ammonium along the deep channel of the Bay (see pink dotted line in figure 3.11b) from the model in 2005.

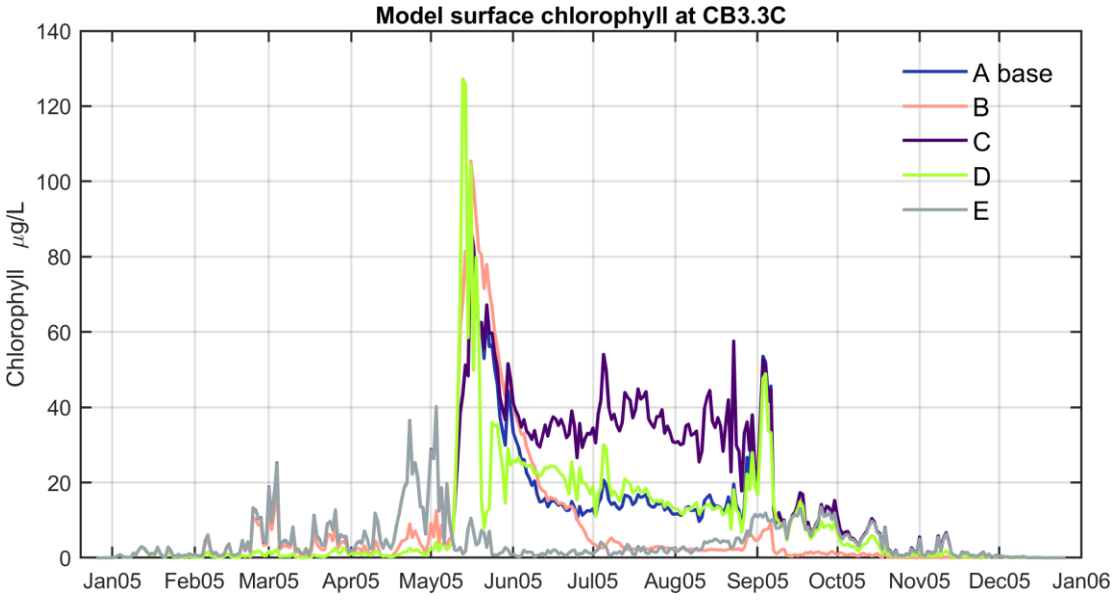

Figure 3.15 Surface chlorophyll comparison at CB3.3C for the base and sensitivity runs in Table 3-1.

Table 3-1: Skill and GPP results for the model sensitivity runs.

RUN A	Base run				
RUN B	Temperature-independence on growth rate				
RUN C	Turn off carbon to chlorophyll maximum varying in summer				
RUN D	Turn off the grazing control in summer				
RUN E	Invariant sinking speed throughout the year (3 m/day)				
Station name	CHLA skill run A	B	C	D	E
CB3.3C	0.72	0.69	0.66	0.36	0.76
CB4.1C	0.59	0.54	0.68	0.43	0.54
CB4.2C	0.63	0.62	0.60	0.42	0.62
CB4.3C	0.59	0.63	0.56	0.43	0.57
CB4.4	0.77	0.68	0.76	0.48	0.75
CB5.1	0.75	0.70	0.72	0.48	0.74
CB5.2	0.43	0.50	0.41	0.43	0.44
CB5.3	0.60	0.77	0.59	0.43	0.60
CB5.4	0.59	0.73	0.55	0.46	0.59
CB5.5	0.71	0.79	0.67	0.45	0.69
CB6.1	0.54	0.77	0.54	0.47	0.57
CB6.2	0.59	0.75	0.60	0.5	0.6
Peak GPP in Middle Bay ($g/m^2/day$)	3.05, Aug	1.34, June	2.86, Aug	3.5, June	1.09, Aug

Table 3-2: Depth-integrated primary production from the model and measurements (Kemp et al. 1997).

	Location	season	Model results	Measured results
Gross primary production ($g\ C \cdot m^2 \cdot day^{-1}$)	Upper Bay	spring	1.5	0.32
		Summer	2.95	0.69
		Autumn	1.7	0.36
	Middle Bay	Spring	0.65	1.98
		Summer	2.55	3.67
		Autumn	1.45	2.48
	Lower Bay	Spring	0.29	2.56
		Summer	1.76	3.96
		Autumn	1.32	2.04

References

Adolf, J.E., C.L. Yeager, W.D. Miller, M.E. Mallonee, and L.W. Harding. 2006. Environmental forcing of phytoplankton floral composition, biomass, and primary productivity in Chesapeake Bay, USA. *Estuarine Coastal and Shelf Science* 67: 108-122. doi: 10.1016/j.ecss.2005.11.030

Blanchard, J.L., S. Jennings, R. Holmes, J. Harle, G. Merino, J.I. Allen, J. Holt, N.K. Dulvy, and M. Barange. 2012. Potential consequences of climate change for primary production and fish production in large marine ecosystems. *Philosophical Transactions of the Royal Society B-Biological Sciences* 367: 2979-2989. doi: 10.1098/rstb.2012.0231

Boynton, W.R., and W.M. Kemp. 1985. Nutrient Regeneration and Oxygen Consumption Along an Estuarine Salinity Gradient Estuarine. *Marine Ecology Progress Series* 23: 45-55. doi: 10.3354/meps023045

Cerco, C.F., and M.R. Noel. 2004. Process-based primary production modeling in Chesapeake Bay. *Marine Ecology Progress Series* 282: 45-58. doi: 10.3354/meps282045

Cloern, J.E. 1996. Phytoplankton bloom dynamics in coastal ecosystems: A review with some general lessons from sustained investigation of San Francisco Bay, California. *Reviews of Geophysics* 34: 127-168. doi: 10.1029/96rg00986

Cloern, J.E., S.Q. Foster, and A.E. Kleckner. 2014. Phytoplankton primary production in the world's estuarine-coastal ecosystems. *Biogeosciences* 11: 2477-2501. doi: 10.5194/bg-11-2477-2014

Cloern, J.E., and A.D. Jassby. 2010. Patterns and Scales of Phytoplankton Variability in Estuarine-Coastal Ecosystems. *Estuaries and Coasts* 33: 230-241. doi: 10.1007/s12237-009-9195-3

Feng, Y., M.A.M. Friedrichs, J. Wilkin, H.Q. Tian, Q.C. Yang, E.E. Hofmann, J.D. Wiggert, and R.R. Hood. 2015. Chesapeake Bay nitrogen fluxes derived from a land-estuarine ocean biogeochemical modeling system: Model description, evaluation, and nitrogen budgets. *Journal of Geophysical Research-Biogeosciences* 120: 1666-1695. doi: 10.1002/2015jg002931

Fennel, K., R. Hetland, Y. Feng, and S. DiMarco. 2011. A coupled physical-biological model of the Northern Gulf of Mexico shelf: model description, validation and analysis of phytoplankton variability. *Biogeosciences* 8: 1881-1899. doi: 10.5194/bg-8-1881-2011

Geyer, W.R., and P. MacCready. 2014. The Estuarine Circulation. *Annual Review of Fluid Mechanics* 46: 175-197. doi: 10.1146/annurev-fluid-010313-141302

Gle, C., Y. Del Amo, B. Sautour, P. Laborde, and P. Chardy. 2008. Variability of nutrients and phytoplankton primary production in a shallow macrotidal

coastal ecosystem (Arcachon Bay, France). *Estuarine Coastal and Shelf Science* 76: 642-656. doi: 10.1016/j.ecss.2007.07.043

Hahm, D., T.S. Rhee, H.C. Kim, C.J. Jang, Y.S. Kim, and J.H. Park. 2019. An observation of primary production enhanced by coastal upwelling in the southwest East/Japan Sea. *Journal of Marine Systems* 195: 30-37. doi: 10.1016/j.jmarsys.2019.03.005

Harding, L.W., M.E. Mallonee, and E.S. Perry. 2002. Toward a Predictive Understanding of Primary Productivity in a Temperate, Partially Stratified Estuary. *Estuarine, Coastal and Shelf Science* 55: 437-463. doi: 10.1006/ecss.2001.0917

Ji, R., M. Jin, Y. Li, Y.-H. Kang, and C.-K. Kang. 2019. Variability of primary production among basins in the East/Japan Sea: Role of water column stability in modulating nutrient and light availability. *Progress in Oceanography* 178: 102173. doi: 10.1016/j.pocean.2019.102173

Kadko, D. 2017. Upwelling and primary production during the US GEOTRACES East Pacific Zonal Transect. *Global Biogeochemical Cycles* 31: 218-232. doi: 10.1002/2016gb005554

Kemp, W.M., W.R. Boynton, J.E. Adolf, D.F. Boesch, W.C. Boicourt, G. Brush, J.C. Cornwell, T.R. Fisher, P.M. Glibert, J.D. Hagy, L.W. Harding, E.D. Houde, D.G. Kimmel, W.D. Miller, R.I.E. Newell, M.R. Roman, E.M. Smith, and J.C. Stevenson. 2005. Eutrophication of Chesapeake Bay: historical trends and ecological interactions. *Marine Ecology Progress Series* 303: 1-29. doi: 10.3354/Meps303001

Kemp, W.M., P.A. Sampou, J. Garber, J. Tuttle, and W.R. Boynton. 1992. Seasonal depletion of oxygen from bottom waters of Chesapeake Bay: Roles of benthic and planktonic respiration and physical exchange processes. *Marine Ecology Progress Series* 85: 137-152. doi: 10.3354/meps085137

Kemp, W.M., E.M. Smith, M. Marvin-DiPasquale, and W.R. Boynton. 1997. Organic carbon balance and net ecosystem metabolism in Chesapeake Bay. *Marine Ecology Progress Series* 150: 229-248. doi: 10.3354/meps150229

Kemp, W.M., J.M. Testa, D.J. Conley, D. Gilbert, and J.D. Hagy. 2009. Temporal responses of coastal hypoxia to nutrient loading and physical controls. *Biogeosciences* 6: 2985-3008. doi: 10.5194/bg-6-2985-2009

Kocum, E., G.J.C. Underwood, and D.B. Nedwell. 2002. Simultaneous measurement of phytoplanktonic primary production, nutrient and light availability along a turbid, eutrophic UK east coast estuary (the Colne Estuary). *Marine Ecology Progress Series* 231: 1-12. doi: 10.3354/meps231001

Liu, B., and H.E. de Swart. 2018. Quantifying the Effect of Salinity Stratification on Phytoplankton Density Patterns in Estuaries. *Estuaries and Coasts* 41: 453-470. doi: 10.1007/s12237-017-0276-4

Lohrenz, S.E., G.L. Fahnenstiel, D.G. Redalje, G.A. Lang, M.J. Dagg, T.E. Whitledge, and Q. Dortch. 1999. Nutrients, irradiance, and mixing as factors regulating primary production in coastal waters impacted by the Mississippi River plume. *Continental Shelf Research* 19: 1113-1141. doi: 10.1016/s0278-4343(99)00012-6

Malone, T., L. Crocker, S. Pike, and B. Wendler. 1988. Influences of river flow on the dynamics of phytoplankton production in a partially stratified estuary. *Marine Ecology Progress Series*: 235-249. doi: 10.3354/meps048235

Marshall, H.G., and K.K. Nesius. 1996. Phytoplankton composition in relation to primary production in Chesapeake Bay. *Marine Biology* 125: 611-617. doi: 10.1007/BF00353272

Nixon, S.W. 1995. Coastal marine eutrophication: A definition, social causes, and future concerns. *Ophelia* 41: 199-219. doi: 10.1080/00785236.1995.10422044

Qin, Q., and J. Shen. 2017. The contribution of local and transport processes to phytoplankton biomass variability over different timescales in the Upper James River, Virginia. *Estuarine Coastal and Shelf Science* 196: 123-133. doi: 10.1016/j.ecss.2017.06.037

Qin, Q.B., and J. Shen. 2019. Pelagic contribution to gross primary production dynamics in shallow areas of York River, VA, USA. *Limnology and Oceanography* 64: 1484-1499. doi: 10.1002/lno.11129

Scully, M.E. 2013. Physical controls on hypoxia in Chesapeake Bay: A numerical modeling study. *Journal of Geophysical Research: Oceans* 118: 1239-1256. doi: 10.1002/jgrc.20138

Scully, M.E. 2018. A Diel Method of Estimating Gross Primary Production: 2. Application to 7 Years of Near-Surface Dissolved Oxygen Data in Chesapeake Bay. *Journal of Geophysical Research: Oceans* 123: 8430-8443. doi: 10.1029/2018JC014179

Shen, C.Q., J.M. Testa, M. Li, W.J. Cai, G.G. Waldbusser, W.F. Ni, W.M. Kemp, J. Cornwell, B.S. Chen, J. Brodeur, and J.Z. Su. 2019. Controls on Carbonate System Dynamics in a Coastal Plain Estuary: A Modeling Study. *Journal of Geophysical Research-Biogeosciences* 124: 61-78. doi: 10.1029/2018jg004802

Son, S., M. Wang, and L.W. Harding. 2014. Satellite-measured net primary production in the Chesapeake Bay. *Remote Sensing of Environment* 144: 109-119. doi: 10.1016/j.rse.2014.01.018

Strokal, M., C. Kroeze, L.L. Li, S.J. Luan, H.Z. Wang, S.S. Yang, and Y.S. Zhang. 2015. Increasing dissolved nitrogen and phosphorus export by the Pearl River (Zhujiang): a modeling approach at the sub-basin scale to assess effective nutrient management. *Biogeochemistry* 125: 221-242. doi: 10.1007/s10533-015-0124-1

Testa, J.M., and W.M. Kemp. 2012. Hypoxia-induced shifts in nitrogen and phosphorus cycling in Chesapeake Bay. *Limnology and Oceanography* 57: 835-850. doi: 10.4319/lo.2012.57.3.0835

Testa, J.M., Y. Li, Y.J. Lee, M. Li, D.C. Brady, D.M. Di Toro, W.M. Kemp, and J.J. Fitzpatrick. 2014. Quantifying the effects of nutrient loading on dissolved O2 cycling and hypoxia in Chesapeake Bay using a coupled hydrodynamic–biogeochemical model. *Journal of Marine Systems* 139: 139-158. doi: 10.1016/j.jmarsys.2014.05.018

Willmott, C.J. 1981. On the validation of models. *Physical Geography* 2: 184-194. doi: 10.1080/02723646.1981.10642213

Xu, J., and R.R. Hood. 2006. Modeling biogeochemical cycles in Chesapeake Bay with a coupled physical–biological model. *Estuarine, Coastal and Shelf Science* 69: 19-46. doi: 10.1016/j.ecss.2006.03.021

Xu, J., R.R. Hood, and S.-Y. Chao. 2005. A simple empirical optical model for simulating light attenuation variability in a partially mixed estuary. *Estuaries* 28: 572-580. doi: 10.1007/BF02696068

Zheng, G.M., and P.M. DiGiacomo. 2020. Linkages Between Phytoplankton and Bottom Oxygen in the Chesapeake Bay. *Journal of Geophysical Research-Oceans* 125: 15. doi: 10.1029/2019jc015650

Zhou, Y., D. Scavia, and A.M. Michalak. 2014. Nutrient loading and meteorological conditions explain interannual variability of hypoxia in the Chesapeake Bay. *Limnology and Oceanography* 59: 373-384. doi: 10.4319/lo.2014.59.2.0373

Chapter 4: A Numerical Investigation of Denitrification Variability in Chesapeake Bay

Abstract

Denitrification is an essential process in the marine nitrogen cycle because it removes bioavailable nitrogen from the aquatic system. Current understanding of denitrification variability in Chesapeake Bay is severely constrained by the sparse observations that provide insufficient coverage in both space and time. In this research, denitrification variability is examined in the Chesapeake Bay using a three dimensional coupled physical-biogeochemical model based on the Regional Ocean Modelling System (ROMS). Model simulations indicate that denitrification occurs not only in the sediment but also in the water column at significant, though somewhat lower rates. Model results indicated that the water column accounts for around 7.5% of the total denitrification amount that occurred in the system during the 2001 and 2002 period of this study. This conflicts with the historical assumption that water column denitrification in Chesapeake Bay is negligible. The model also reveals the spatial patterns in denitrification with more denitrification occurring in the upper to middle bay due to higher availability of organic matter in these areas compared to the lower bay. In terms of temporal variability, denitrification peaks in the sediment in spring while in the water column it peaks in the summer. The reason for this difference in the timing is related to the availability of oxygen: In the spring oxygen levels in the water column are too high to allow denitrification so it happens only in the sediment where low oxygen levels persist all year around. In summer low oxygen

and depletion of nitrate below the pycnocline completely shuts down denitrification in the sediment in the mesohaline and polyhaline region of the by. However, water column denitrification continues at the interface between oxygenated waters near the surface and oxygen-depleted waters below where coupled nitrification-denitrification happens. The model also reveals that denitrification removes significant quantities of biologically available nitrogen, meaning that without this process, more summertime primary production would occur in the form of more surface chlorophyll, increasing as much as 10ug/L in the middle bay region, which would, in turn, lead to more oxygen depletion.

Introduction

Agricultural application of nitrogen fertilizer (Mueller et al. 2017; Zhang 2017) combined with NOx emissions from auto and industrial fuel combustion, release of both organic and inorganic nitrogen from septic systems and release of nitrogen in municipal wastewater have resulted in significant nitrogen loading worldwide and this has had a considerable impact on the global nitrogen cycle (Bouwman et al. 2009). Denitrification, which is he biologically-mediated sequential reduction of nitrate to nitrite, then to nitric oxide and nitrous oxide and ultimately dinitrogen gas (Zumft 1997) has long been considered to be the primary sink process in the nitrogen cycle that can help to mitigate the effects of excessive fixed nitrogen loading (Cowan and Boynton 1996) in aquatic ecosystems that suffer from eutrophication (Christensen et al. 1987; Seitzinger and Giblin 1996). Given the magnitude of the ecological and economic problems that are caused by eutrophication (Bonaglia et al. 2014; Dodds et al. 2009; Kemp et al. 2005; Smith 2003), it is essential to understand

the nitrogen cycle in aquatic ecosystems, and especially nitrogen removal processes like denitrification for its potential role in nutrient management.

At the global scale both shelf sediments (Seitzinger et al. 2006) and open ocean oxygen minimum zones, which include the Arabian Sea (Bulow et al. 2010; Ward et al. 2009), the eastern tropical South Pacific (Chang et al. 2010; Lam et al. 2009) and eastern tropical North Pacific (Horak et al. 2016), are well-studied hot spots for nitrogen loss via denitrification. In contrast, denitrification in estuarine systems and the relative importance of sediment versus water column denitrification has not been extensively studied (Cornwell et al. 2016; Deek et al. 2013; Fear et al. 2005; Weston et al. 2010).

Chesapeake Bay (Figure 4.1), which is the largest estuary in United States, suffers from eutrophication due to excessive nitrogen loading as in other coastal waters (Kemp et al. 2005; Kemp et al. 2009). During the summertime, the chronic oxygen depletion in bottom water (Testa and Kemp 2014; Testa et al. 2018a; Testa et al. 2018b) promotes denitrification that transforms nitrate to nitrogen gas (Cornwell et al. 1999; Cowan and Boynton 1996; Kana et al. 2006), which is then released to the atmosphere. Therefore, understanding the spatial and temporal variability of denitrification in Chesapeake Bay is of great importance for understanding the Chesapeake Bay nitrogen cycle, budget, and for nutrient management efforts. An example of the importance of denitrification can be seen in measurements of bottom water NO_3 in the main stem mesohaline Bay (CB3.3C) almost every year when values drop from 10-30 μmol/L in early summer to zero in less than one month (Figure 4.2a,b). This happens after bottom water oxygen levels are depleted forcing

facultative heterotrophic bacteria to switch to using NO_3 as an alternative elector acceptor (Seitzinger 1988). This loss of nitrogen via generation of dinitrogen gas represents a substantial term in the Chesapeake Bay nitrogen cycle, yet the number of measurements that have been collected to characterize denitrification rates in the Bay are surprisingly sparse and, remarkably, they are restricted almost entirely to the benthos (Boynton et al. 1995). There are no reported direct measurements of water column denitrification in Chesapeake Bay. This is in contrast to the open ocean where water column denitrification rates have been routinely measured for many years (Fuchsman et al. 2017; Yang et al. 2017). Since a large volume of the bay becomes anoxic during summer (Fennel and Testa 2019; Testa et al. 2018a), there must be some water column denitrification as observed in the open ocean, yet this was ignored in the nitrogen budget that was estimated by Boynton et al. (1995). Using a global model, DeVries et al. (2012) estimated that about 28% of the oceanic nitrogen loss occurs in the ocean water column oxygen minimum zones. In contrast, the relative importance of water column versus benthic denitrification in Chesapeake Bay is still unknown.

In addition to denitrification, there is another pathway of nitrogen loss in marine systems through anaerobic ammonium oxidation (ANAMMOX) (Bulow et al. 2010; Dalsgaard et al. 2003; Dalsgaard and Thamdrup 2002; Lam et al. 2009; Thamdrup and Dalsgaard 2002). As with denitrification, there are also a very limited number of reported rates of dinitrogen gas production due to the ANAMMOX process in Chesapeake Bay (Babbin et al. 2016; Babbin and Ward 2013; Rich et al. 2008). Babbin and Ward (2013) suggested that the stoichiometry of organic matter, rather

than the total amount of organic matter, regulates the relative contributions of ANAMMOX and denitrification to overall nitrogen loss in Chesapeake Bay. Rich et al. (2008) found that the percent of N_2 production due to ANAMMOX ranged from 0 to 22% in Chesapeake Bay, with the highest percentages occurring in the freshwater portion of the main stem of the upper bay. Due to the controversy and uncertainty surrounding the role of ANNAMOX in driving nitrogen loss in marine systems, combined with the difficulty of representing ANNAMOX in marine biogeochemical models, I only consider heterotrophic denitrification in this research.

Modeling technology provides a powerful tool to help us quantify the nitrogen cycle and denitrification variability over a wide range of space and time scales (Bianucci et al. 2012; Fennel et al. 2009; Fennel et al. 2006; Testa et al. 2013). Feng et al. (2015) used a coupled physical-biogeochemical model to determine a five-year average nitrogen budget for the entire Chesapeake Bay, that suggest that there is ~ 34×10^9 gram nitrogen/year removal from the whole bay via denitrification, which is consistent with previous research (Boynton et al. 1995), but they did not report the spatial and temporal variability in the rates or the relative contribution between the water column and sediment.

In this research, a nitrogen-based biogeochemical model coupled with a 3-dimensional estuarine circulation model is used to study denitrification variability in Chesapeake Bay. The model, which is based on Fennel et al. (2006), has been modified for application to Chesapeake Bay allowing the sediments and the water column to go fully anoxic with commensurate changes in denitrification. The general approach used here is to use the available measurements of sediment denitrification

rate, as well as other biogeochemical variables in the sub-euphotic water column, to validate the model. Once validated, the model can be used as a dynamic interpolator to study the spatial and temporal variability of denitrification. My overarching goal is to determine the relative amounts of water column and sediment denitrification and the spatial and temporal variability of both in Chesapeake Bay. In addition, I examine and quantify the crucial factors that control the denitrification rate in both the water column and the sediments. I also highlight the role of water column denitrification in the thalweg region of the bay, as well as the impacts of external forcing such as wind effects on water column denitrification.

Methods

In this research, I use a nitrogen-based three-dimensional coupled physical-biogeochemical model to simulate benthic and water column denitrification variability in Chesapeake Bay as in the previous chapter, except for here we use a better parameterization for simulating oxygen levels while maintaining the model's skill in simulating chlorophyll and particulate organic nitrogen.

The biogeochemical model has been modified to include both water column and sediment denitrification. These modifications build upon Fennel et al. (2006) simplified sediment diagenesis model that assumes coupled nitrification-denitrification with a fixed anaerobic and aerobic respiration percentage (14% anaerobic and 86% aerobic) in the sediments beneath a fully oxic water column. Under this condition no NO_3 is taken up from the water column. Rather denitrification (and the associated loss of nitrogen via formation of N_2 gas) proceeds though coupled nitrification-denitrification with NO_3 supplied via nitrification in the

sediments, following the stoichiometry specified in Appendix A in Fennel et al. (2006). The Chesapeake Bay model has been modified to allow the ratio of anaerobic to aerobic remineralization to change in response to changes in the oxygen concentrations in the overlying water column extending all the way to a fully anoxic overlying water column with the remineralization process in bottom sediment transitioning to fully anaerobic remineralization. In addition, for this Chesapeake Bay application it is assumed that under a fully oxic water column 90% of the remineralization is anerobic and 10% is aerobic. The higher anaerobic respiration percentage was chosen based on the fact that the sediment composition in Chesapeake Bay is different than it is in the Middle Atlantic Bight, i.e., sediment in Chesapeake Bay is more prone to anoxic conditions because it has a more cohesive sediment composition (Hagy et al. 2005; Russ and Palinkas 2020; Sanford et al. 1991). Under this assumption nitrification in the sediments cannot supply all of the NO_3 for denitrification and, as a result, the sediments take up nitrate under the fully oxic water column condition. The sediment demand for nitrate increases as oxygen levels in the water column and the sediments decline and sediment nitrification shuts down. In addition, the Fennel et al. (2006) model has been modified so that as oxygen concentrations in the water column become depleted, nitrification and zooplankton grazing/metabolism are shut down and aerobic remineralization of dissolved and particulate organic matter transitions to anaerobic denitrification. As in the sediments, the demand for nitrate increases as oxygen levels in the water column decline and nitrification shuts down. For additional details on these model formulations see Chapter 2 of this thesis.

Given the importance of reproducing the observed O_2 concentrations for simulating denitrification, a background respiration rate for, a 62.5 mmol O_2/m^2/day was applied uniformly in the bottom layer of the model. This background rate is similar to sediment oxygen consumption rates applied in other studies (Grosse et al. 2019; Yu et al. 2015) to properly simulate observed O_2 concentrations in the deep and bottom waters of Chesapeake Bay (Li et al. 2015; Shen et al. 2013).

It should also be noted that in this model remineralization of organic matter is allowed to proceed in the sediments and in the water column after NO_3 is depleted. This is allowed because, in nature, organic matter remineralization in the sediments and the water column proceeds after depletion of NO_3 via sulfate reduction where sulfate-reducing bacteria use SO_4 as their terminal electron acceptor for respiration. One caveat with this approach is that the stoichiometry for SO_4 reduction results in half as much ammonium production per mole of organic matter that is remineralized compared to oxic remineralization and denitrification. Thus, the model overestimates the NH_4 production from organic matter remineralization under fully anoxic conditions.

In the original Fennel et al. (2006) model organic detritus sinks with a constant rate and it is instantaneously remineralized when it hits the bottom, and there is no sediment burial or resuspension. In my Chesapeake Bay implementation, organic detritus is also instantaneously remineralized when it hits the bottom, but a burial term is also included as in Feng et al. (2015). In addition, by reducing the sinking rate in the bottom layer of the model by 90% I trap organic detritus near the bottom

which provides a simplified representation of near-bottom sediment accumulation, resuspension and transport.

The model was forced from the year 2000 through 2002, with the year 2000 used for spinning up. Due to the limited denitrification data availability, only the modeled time period of 2001 to 2002 was validated and analyzed. Sensitivity model runs were carried out with different background oxygen consumption rates during summertime, along with different oxygen half saturation coefficients, to evaluate the effects of oxygen level on the amount of denitrification in the system. A sensitivity model run with a reduced large detritus sinking speed, as in Fennel et al. (2006), was also conducted to evaluate the sensitivity of the model to this parameter and how the system responds to the resulting reduced denitrification and nitrogen removal from the estuary. To evaluate the effects of the assumed sediment anaerobic respiration percentage on denitrification a model sensitivity run was also carried out using the original assumption of 14% anaerobic respiration in the sediments under a fully oxic water column (based on Fennel et al. 2006) to contrast the results obtained from assuming 90% anaerobic respiration in the sediments under a fully oxic water column Di Toro (2001). Finally, a model sensitivity run was also carried out with wind direction shifted during summertime to evaluation the potential role of wind on denitrification. More information on these runs is presented in Table 4-1. It should also be noted that the model was tuned differently for the years 2001 and 2002 to maximize agreement with the measurement. The differences between the 2001 and 2002 parameter sets and how these differ from the previous Primary Production Chapter 3 are given in Table 4-2.

The in situ sediment denitrification data used for validation in this paper are derived form Testa et al. (2013).

Results

Model validation on NO_3, NH_4 and oxygen

Figure 4.3 shows the 3-D model spatial model skill assessment (Willmott 1981) for chlorophyll, NH_4 and O_2 along the estuarine gradient during the 2001 and 2002. Chlorophyll skill is high (>0.6) at stations CB4.2C to CB5.2, but lower at other stations (Figure 4.3a). The model skill is very high for oxygen (> 0.9), from stations CB3.3C to CB5.3, and the skill decreases (>0.7) in the southern bay (Figure 4.3a). Ammonium skill is also high (Figure 4.3b) with most stations > 0.6. Figure 4.4 shows the modeled and observed bottom particulate organic nitrogen (PON) at stations CB4.1C, CB4.2C and CB4.3C. For example, at CB4.1C, the model captures the high PON during springtime (~50µmol nitrogen/L) in 2001 but the peak in the model is somewhat lagged. The PON concentration then significantly decline due to remineralization during summertime. The model captures the pronounced interannual variability in bottom PON associated with transition from a wetter year (2001) to a drier year (2002), i.e., the peak of peak bottom PON is lower in 2002. Overall, I consider that the model captures the biogeochemical variability in the system.

Model validation for the denitrification in the sediment and water

As discussed above, the denitrification rate measurements that are available for model validation are sparse. Therefore, the approach I have taken to ensure that the model is simulating biogeochemical cycling and denitrification is to, first, validate the model's

simulation of the state variables O_2, NH_4 as discussed above. Second, I compare the model's bay-wide denitrification budget with previously published budgets derived from observations by Boynton et al. (1995) and a biogeochemical model by Feng et al. (2015). And, third, I compare the model-simulated denitrification rates with sparse measured denitrification rates.

In Boynton et al. (1995), they gave a denitrification amount of 39.55×10^9g nitrogen/year based on data from 1984 to 1988 (Figure 4.5a). This rate was used for the model validation in Feng et al. (2015), which gave a similar value (Figure 4.5b). Our model was tuned to give similar results, but also provides, for the first time, estimates of the relative amounts of water column and sediment denitrification. The model indicates that the water column contributes 7.53% of the total denitrification rate (Figure 4.5c).

Our model also provides information about the temporal variability in the water column and sediment denitrification rates. For example, in 2001 it is estimated that maximum sediment denitrification rate occurred in the springtime with rates as large as 0.23×10^9g nitrogen/day and the minimum sediment denitrification rate occurred in August with rates as low as 0.05×10^9g nitrogen/day, thus defining a clear seasonal pattern, with peak rates in the spring and the lowest rates in the summer. The sediment denitrification rates are not completely zero in summer because the upper bay region still has a supply of NO_3 (results presented in below). In contrast, the model indicates that the highest denitrification rates in the water column occur in the summertime with the highest rates (~0.05×10^9g nitrogen/day) occurring in August.

Observed versus model point to point comparisons of sediment denitrification rates at stations R-64 (mesohaline zone) and Sill Pond (oligohaline zone) are presented in Figure 4.6a and Figure 4.6b, respectively. At station R-64, the model gives a high skill score (0.59) and also reproduces the clear seasonal patterns that are observed 2001 and 2002. The denitrification rates in both the model and the observations peak at ~50-100 μmol/nitrogen/m^2 in spring (April) drop to zero in summer (August) and then increase again in fall (October) to ~50-100 μmol/nitrogen/m^2. For the Sill Pond in the oligohaline zone of the bay, the model skill score is lower (~.3) and the model tends to overestimate denitrification rates during springtime and underestimate denitrification rates during the summertime. Nonetheless, in both the model and the observations the summertime denitrification rate at Sill Pond is not zero in both 2001 and 2002, which accounts for the model-estimated non-zero total denitrification rate during summer as shown in (Figure 4.5c). The discrepancy between the model and the observations at Sill Pond indicates that the model may underestimate summertime sediment denitrification bay wide (Figure 4.5c).

Climatological (2001 to 2002) monthly averaged Bay wide sediment denitrification rates from the model are plotted in Figure 4.7. This plot shows that substantial denitrification occurs in the upper bay and tributaries in association with the spring phytoplankton bloom in March, April and May. This happens because the spring bloom produces organic matter that is then denitrified in the anoxic sediments while there is still oxygen and nitrate available in the overlying water column. As summer approaches, although the increasingly anoxic conditions in the bottom water should

facilitate denitrification, depletion of NO_3 in the deep water limits the denitrification rate in the deep channel of the mesohaline mainstem Chesapeake Bay.

There are no available direct water column denitrification measurements in the mainstem Chesapeake Bay. However, a recent analysis of water column nitrous oxide production provides an alternative means to estimate the denitrification rate in the water column (Beaulieu et al. 2011). It was estimated that 1 % of total denitrified nitrogen is converted to N_2O in river networks of the Bay (Beaulieu et al. 2011). This implies that the ratio of N_2O:N_2 production during denitrification is 1:100 as suggested and utilized by Ji et al. (2018). Based on this ratio, Ji et al. (2018) estimate the nitrogen removal from water column denitrification to be ~140 μmol/m^2/h, which occurs in a 0.2m thick oxic-anoxic transition zone across the pycnocline. In contrast, Laperriere et al. (2019) estimate that there is 21 μmol/m^2/day of N_2O production, which gives a denitrification rate of ~175 μmol nitrogen/m^2/h in the oxic-anoxic transition zone across the pycnocline. These two recent indirect estimates clearly indicate that significant amounts of water column denitrification can happen during summer compared to spring sediment denitrification (Testa et al. 2013).

The model-estimated water column denitrification rates are the same magnitude as these indirect estimates and they can be as large as 200 μmol nitrogen/m^2/h in the mesohaline thalweg region (Figure 4.8a,b).

In the model, water column denitrification not only occurs at the oxic-anoxic transition zone across the pycnocline (Figure 4.9a), but also below the pycnocline before oxygen is depleted (Figure 4.10f,g). The model also shows that as the oxygen is drawn down in summer in 2001 (Figure 4.10a-d), the water column denitrification

becomes enhanced, to >25μmol N/m^2/h in the middle water column (Figure 4.10g,h). The vertical integral of water column denitrification over the deep channel (add vertically-integrated rates from the model) is comparable to limited indirect measurement conducted in this region (Ji et al. 2018; Laperriere et al. 2019).

It is well known that nitrification rates are significant in the middle water column of Chesapeake Bay during summer, producing substantial amounts of NO_3 that can fuel denitrification. In the model, denitrification is, indeed, fueled by nitrification in the oxic-anoxic transition zone across the pycnocline in the water column and is therefore similar to the coupled nitrification-denitrification process (Figure 4.9a,b) in sediment (Cornwell et al. 1999; Kemp et al. 1990).

Model Sensitivity Experiments

Several model runs were carried out to determine how sensitive the model-generated denitrification rates are to different parameterizations and assumptions (Table 4-2). Model run B showed that the simulated denitrification rates are very sensitive to the oxygen half saturation coefficient and also the simulated water column oxygen concentrations. When the model was run with the oxygen half saturation coefficient set as in Feng et al. (2015) and with a lower summertime background oxygen consumption rate (31.25 O_2 mmol/m^2/day which is half the rate used in the base run A) the percentage of water column denitrification increased from ~8% to 27.7% (Table 4-2). However, the total amount of denitrification (water column plus sediment) in run B is similar in magnitude to the base run A. This increase in water column denitrification percentage can be offset by decreasing the oxygen half-saturation coefficient (results not shown).

As implied in the previous paragraph, the relative amounts of sediment and water denitrification that are predicted by the model are sensitive to the O_2 half-saturation coefficient for water column denitrification. Indeed, if I use the water column O_2 half-saturation coefficient adopted by Feng et al. (2015) the Bay wide water column denitrification rate increases substantially because their value allows water column denitrification to occur under much lower oxygen concentrations. Given that the model-estimated denitrification rates are fairly sensitive to these assumptions, efforts should be undertaken to better constrain these parameters.

Model run C (No Di Toro, which assumed 14% anaerobic respiration under a fully oxic overlying water column as in Fennel et al., 2006) was carried out to examine the sensitivity of the model to the assumed anaerobic respiration percentage in the sediments under a fully oxic overlying water column. The results presented in Figure 4.11a,b show that model run C had much higher sediment denitrification, increasing from 33.76×10^9 gram nitrogen/year to 44.87×10^9 gram Nitrogen/year, while the water column contribution to denitrification decreased. The total denitrification budget increase to 47.7×10^9 gram nitrogen/year. Figure 4.11a,b shows that more denitrification happened in the down bay region while less denitrification occurred in the upper bay region in model run C compared with the base model run A. That is, decreasing the amount of anoxic remineralization that is assumed to occur under a fully oxic overlying water column to 14% (compared to 90% in the base run) resulted in a spatial shift in the denitrification removal and a lower percentage of water column denitrification.

Model run D was carried out to show the impact of reducing denitrification which results in reducing the amount of nitrogen that is removed from the system (Fennel et al. 2006). In this run the sinking speed of detritus in the bottom layer was reduced by 99%, compared with the 90% reduction of the base run A. Figure 4.11c,d shows that this change resulted in less denitrification in the system during April 2001, especially in the upper bay region where the decrease was as large as 350µmol/m^2/h (Figure 4.11c). The region where the change in denitrification is large is consistent with the region in the bay where high concentrations of organic matter are produced during the spring bloom. The greater reduction of the sinking speed of detritus in the bottom layer of the model results in less denitrification and loss of nitrogen from the system in the form of N_2 gas. This, in turn, results in a substantial increase in surface chlorophyll concentrations, especially in the northern bay where chlorophyll increased by more 10µg/L in June (Figure 4.11d). The changes in the chlorophyll concentrations are much smaller down bay because the additional nutrients that are retained due to the reduced denitrification rates in the upper bay are consumed before they reach the lower bay.

Model run E (Wind rotates by 180° during May-Aug in 2001) was carried out to examine the effect of wind direction on denitrification because winds are an important factor in controlling estuarine transport (Li and Li 2011; Li and Li 2012) and oxygen levels (Scully 2013; Scully 2016) in Chesapeake Bay. Model run E shows that although the total amount of denitrification remains roughly the same (Table 4-3), the lateral distribution of the water column denitrification is altered (Figure 4.12). This study suggests that water column denitrification can also be influenced by the wind

indirectly. In model run D, where I shifted the wind direction by 180° during summertime, changes the dominant wind direction so that it blows from the north rather than the south. Winds from the north should promote more oxygen transport from the west flank to the deep channel, bringing higher oxygen water to the thalweg. This results in more nitrification which promotes more denitrification in the bottom water (Figure 4.12k,o) compared with the base run (Figure 4.12c,g). Although the total change in denitrification was small, this highlights how physical processes like wind direction can influence spatial distribution of biogeochemical processes in a partially mixed estuary with chronic bottom oxygen depletion (Testa and Kemp 2012).

Discussion

Water column denitrification along thalweg

Water column denitrification has long term been ignored in Chesapeake Bay (Boynton et al. 1995) and in other estuaries worldwide. Our model results, which are supported by indirect measurements on N_2O production rate, indicate that, contrary to previous studies, water column denitrification accounts as much as 7.53% of total denitrification occuring in the system during the 2001 and 2002 period. My model suggests that this water column denitrification occurs in the transition zone between oxic surface water and anoxic deep-water during summertime in the mesohaline region of Chesapeake Bay (Figure 4.9) and also in the oxygen depleted region below (Figure 4.10). My model also suggests that nitrification in this zone supplies nitrate for this denitrification (Figure 4.9b). The highest denitrification rates occur in the

middle of the water column, but these elevated rates also extend towards the bottom. The deep anoxic water in the mainstem, mesohaline Chesapeake Bay has close to zero nitrate during summer due to denitrification so any denitrification that happens in these waters must be supported by nitrification. On a monthly scale, the water column denitrification steadily increases as summer approaches along with the oxygen depletion, with the highest rates (as large as 25μmol/m^3/h) occurring around 38.75° N in August (Figure 4.10f). It spreads across the deep-water column due to downward nitrate mixing and transport. The region of elevated denitrification rates spread southward in July and August (Figure 4.10g,h). My model results clearly reveal the couple nitrification-denitrification process in the water column. If one considers only the deep channel transect (Figure 4.1, black line) it can be seen that contribution from water column denitrification is substantial and even exceeds sediment denitrification during the summer months (Figure 4.13f,g,h). During spring time, the sediment dominates over water column denitrification in the deep channel (Figure 4.13c, d) while in summer time, the denitrification in the sediment decreases noticeably except in the northern bay region (Figure 4.13f,g,h) due to nitrate limitation (Cowan and Boynton 1996; Kemp et al. 1990). In the northern tidal fresh region of the main stem bay, there is still significant nitrate and oxygen in the bottom water supplied via river input during summer which allows some amount of denitrification in summer (Figure 4.13f,g,h). This elevated denitrification during summer in the upper bay is also observed and modeled at Still Pond (Figure 4.6b) as discussed above. Figure 4.13, also shows how water column denitrification occurs primarily in the summertime in the mesohaline region of the bay, with vertically-

integrated rates as large as 200-250 μmol/m^2/h, (Figure 4.13f, g, h). These rates are comparable to and can even exceed sediment denitrification during summer. Future research aimed at better quantifying water column denitrification in Chesapeake Bay (Ji et al. 2018; Laperriere et al. 2018) should be strongly encouraged as in other systems (Fuchsman et al. 2019; Ma et al. 2019).

Effects of denitrification on the nitrogen cycle in Chesapeake Bay

Denitrification promotes the removal of bio-available nitrogen from the aquatic the system. Numerical experiment D shows that reducing sinking speed of particulate organic matter in the bottom layer of the model changes nitrogen inventory in the system substantially. Due to reduced denitrification, more nitrogen was retained in the system and this increased summertime primary production. The sinking speed selection was based on previous literature (Fennel et al. 2006; Xu and Hood 2006). However, it should be noted that this approach does not take into account the effects of organic matter flocculation with inorganic suspended solids (Shen et al. 2018; Shen et al. 2019). Our research indicates these sinking processes are important for determining the denitrification budget.

Conclusion

In this research, a coupled physical-biogeochemical model was used to estimate denitrification variability in Chesapeake Bay. The model was validated using observed O_2 and NH_4 concentrations combined with sparse measurements of sediment denitrification and estimates of water column denitrification derived from measurements of N_2O production. The model-estimated Bay wide denitrification rate

is consistent with previously derived estimates (Boynton et al. 1995; Feng et al. 2015). The model predicts that sediment denitrification rates are highest in late spring after the spring bloom when organic matter fluxes to the bottom are high. These results are consistent with previous modeling studies and observations. During the summer, sediment denitrification is shut down due to NO_3 depletion even though anoxic conditions should facilitate the anaerobic respiration. In contrast, rates of water column denitrification are highest in summertime (June, July and August) when the deep water goes anoxic. This water column denitrification happens in the transition zone between oxygenated waters near the surface and oxygen depleted waters at depth where NO_3 is supplied by nitrification.

That model predicts that water column denitrification is about 7.53% of that compared with the sediment denitrification, which is consistent with the idea that water column denitrification rates in Chesapeake Bay are small (Boynton et al. 1995), but they are not insignificant. Water column denitrification can exceed sediment denitrification during summertime in the mesohaline region of the mainstem bay, replacing the role of sediment denitrification that dominates in the spring. During the summertime, sediment denitrification only occurs in the northern tidal fresh region of the bay where it is supported by nitrate and oxygen supplied via riverine sources. It is also shown that water column denitrification is reduced by slowing the sinking rate of organic matter near the bottom. This, in turn, reduces nitrogen losses due to denitrification which results in significantly elevated chlorophyll concentration in the middle to upper Bay region.

Finally, an examination of the sensitivity of the model-predicted denitrification rates to key model parameters reveals that the relative amounts of water column and sediment denitrification are sensitive to the assumed percentage of aerobic and anaerobic respiration in the sediments under a fully oxic overlying water column. In addition, the relative amounts of sediment and water column denitrification that are predicted by the model are sensitive to the O_2 half-saturation coefficient for water column denitrification. Winds can have a significant influence on the spatial distribution of denitrification in Chesapeake Bay. Efforts to better constrain these parameters should be undertaken and more in situ measurements of sediment and water column denitrification are needed to better constrain the model.

Acknowledgement

This research was supported by NOAA COMT project (Luettich et al. 2013). The COMT project was supported by NOAA via the IOOS Office, awards NA10NOS0120063 and NA11NOS0120141. The first author was also supported by the China Scholarship Council (201206710006) and University of Maryland Center for Environmental Science Education Committee. This paper is University of Maryland Center for Environmental Science contribution XXXX.

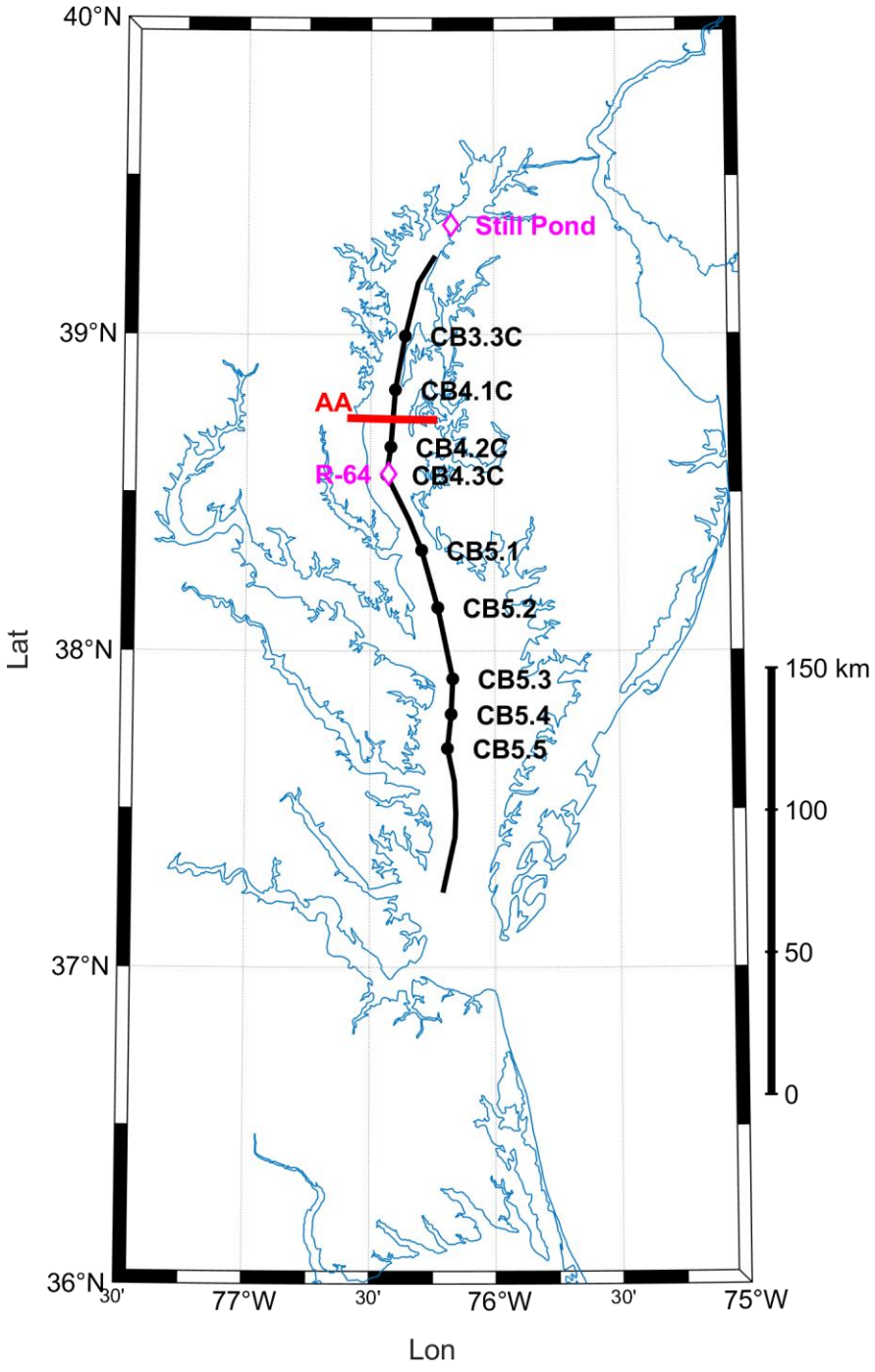

Figure 4.1 Research domain and Chesapeake Bay Program monitoring station locations. Black circles show the locations of CBP biogeochemical data that were used for model validation, and pink diamonds show the locations of the denitrification measurements that were used for validation. The black line represents a deep channel transect along estuarine salinity gradient and the red line represents cross section location where model results are plotted.

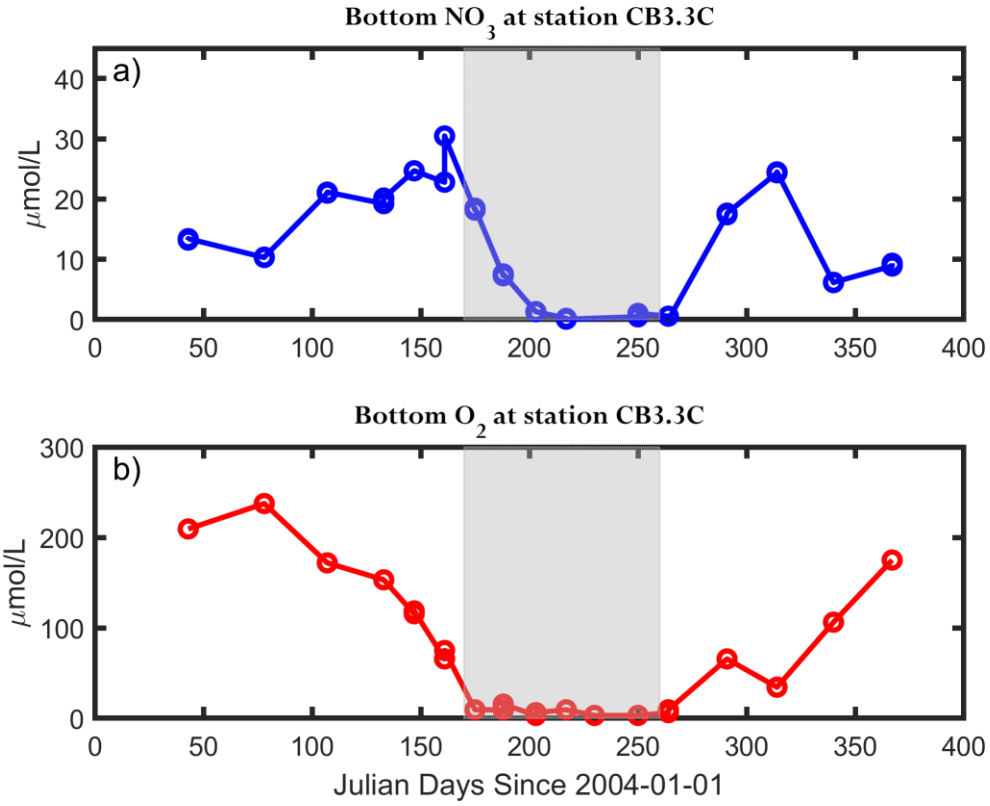

Figure 4.2 Bottom water nitrate and bottom water oxygen concentrations from Chesapeake Bay Program measurements. Shading region represents summertime period.

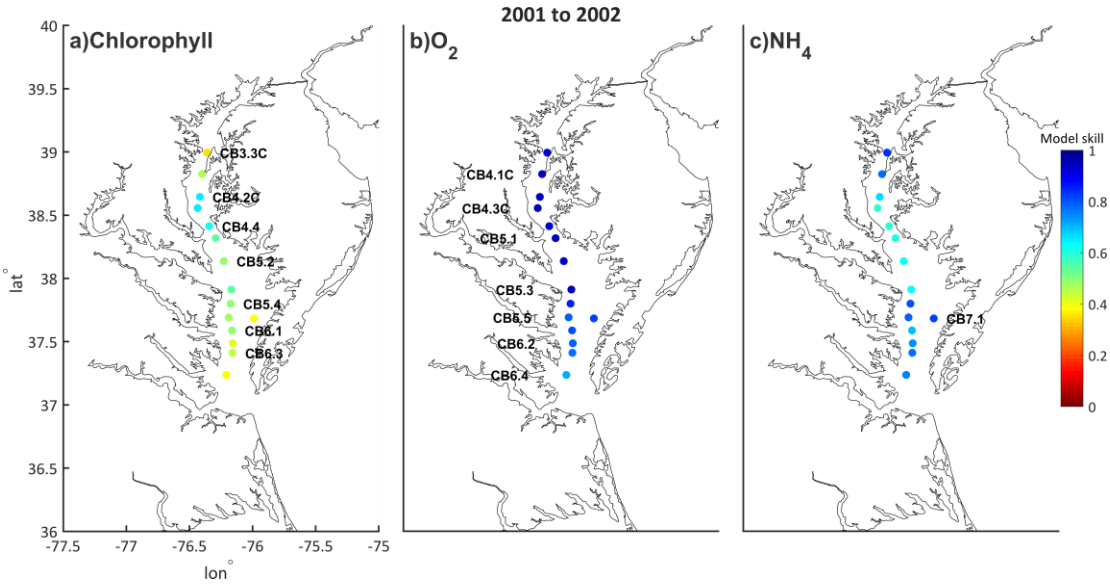

Figure 4.3 Model skill for chlorophyll (a), oxygen (b) and ammonium (c).

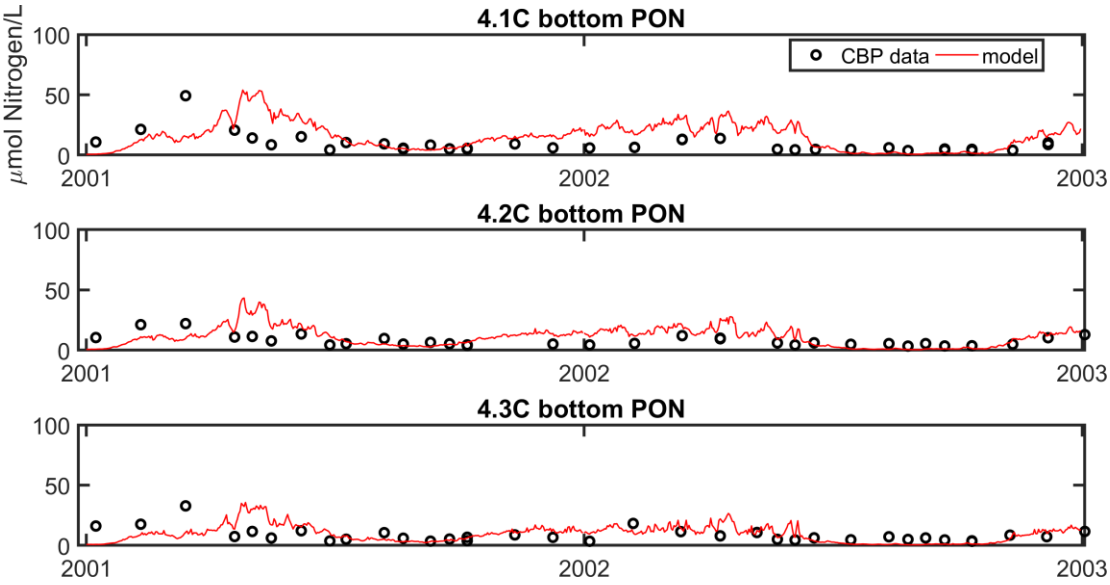

Figure 4.4 Bottom particulate organic nitrogen validation for the year 2001 to 2002. The black circles represent CBP measurements and the black line shows the model.

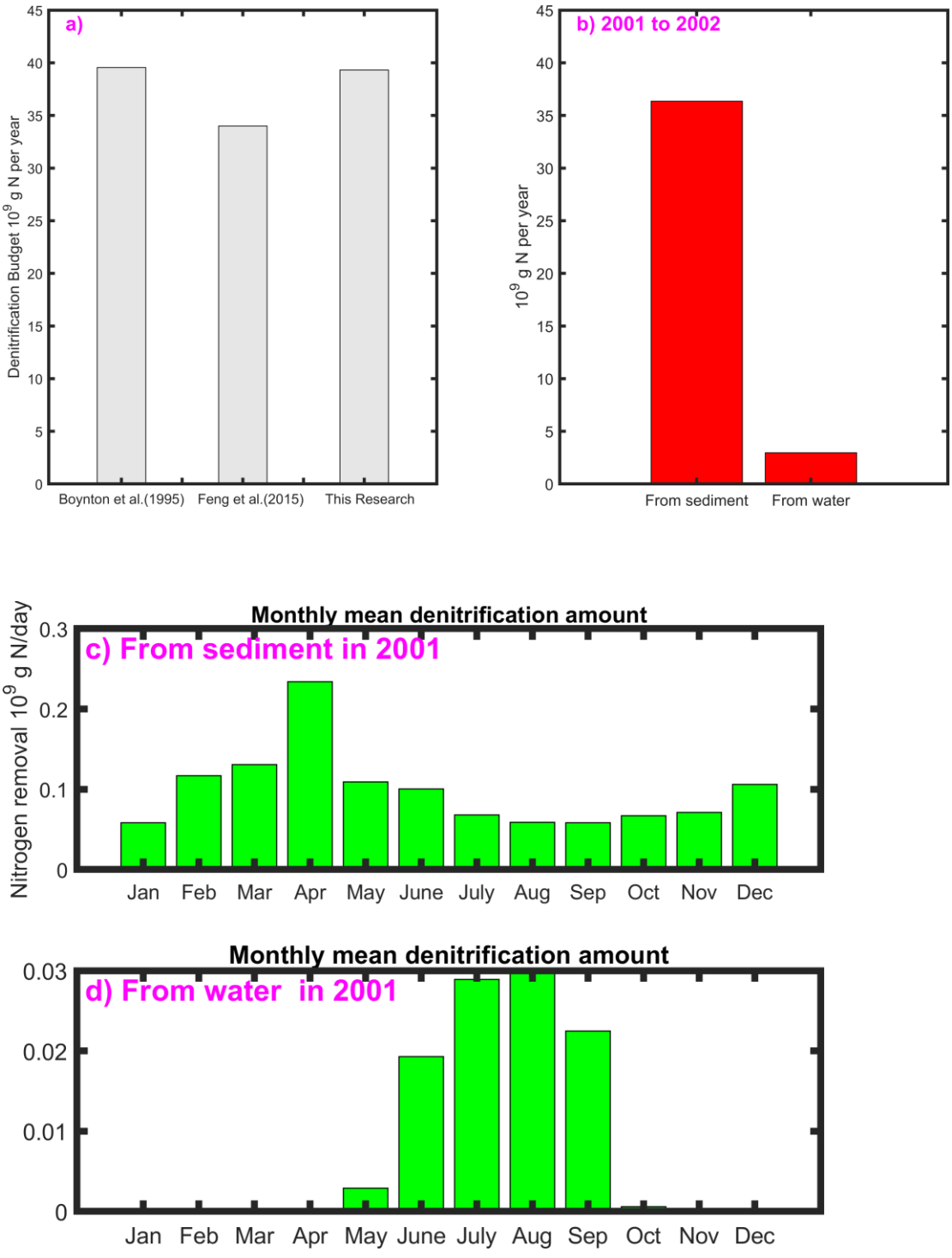

Figure 4.5 Top Left Panel: Estimated total Bay wide denitrification rates from Boynton et al. (1995), Feng et al. (2015) and this study; Top Right Panel: Total baywide denitrification amount

in water column and sediment; Bottom Panels: Monthly averaged nitrogen removal in 2001 for the sediment (top) and the water column (bottom).

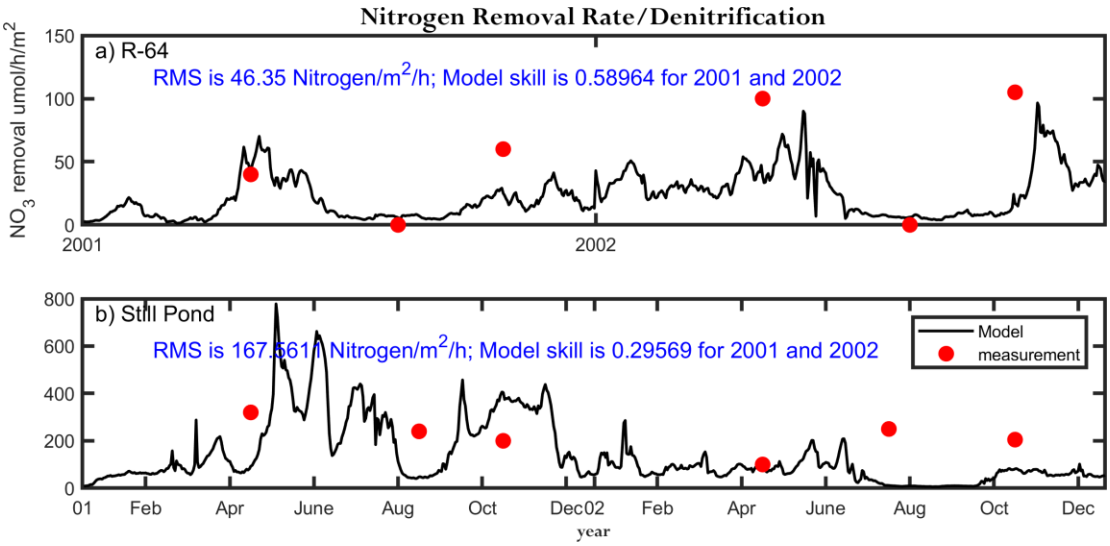

Figure 4.6 Denitrification validation for R-64 (a, mesohaline zone) and Sill Pond (b, oligohaline zone). The red circles represent measurements and the black line shows the model.

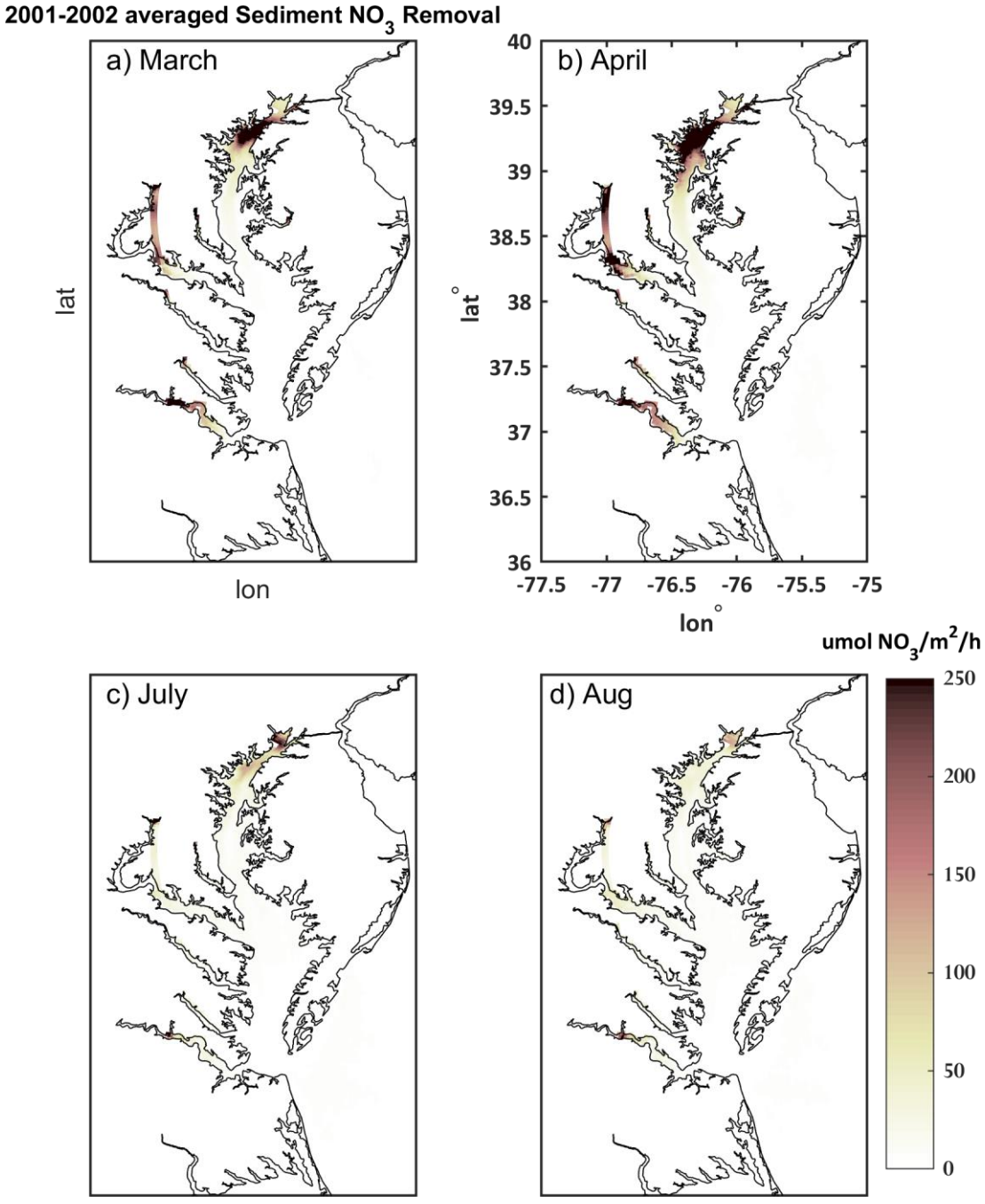

Figure 4.7: Monthly averaged sediment nitrogen removal in Chesapeake Bay for the period between 2001-2002 for March (a), April (b), July (c) and August (d).

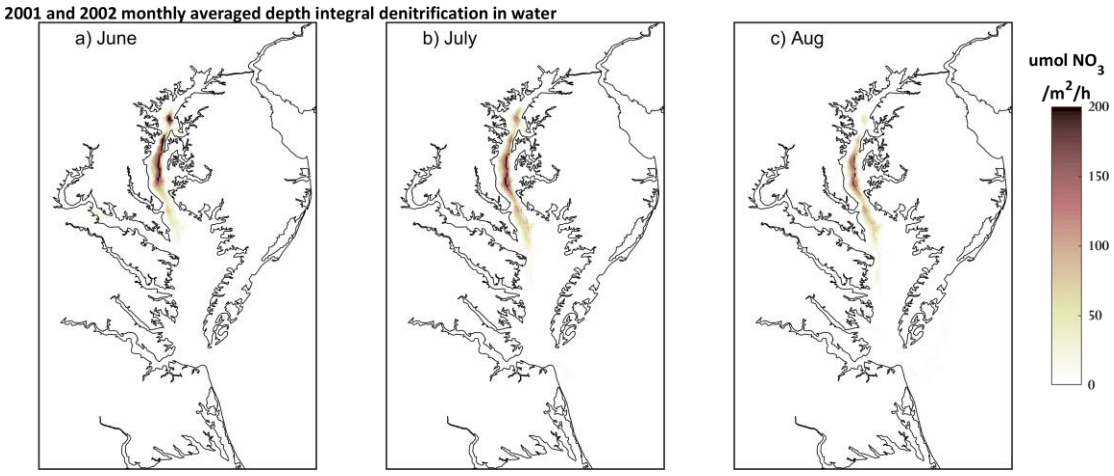

Figure 4.8: Monthly averaged water column-integrated nitrogen removal rate in Chesapeake Bay for 2001 and 2002 in a) June, b) July and c) August.

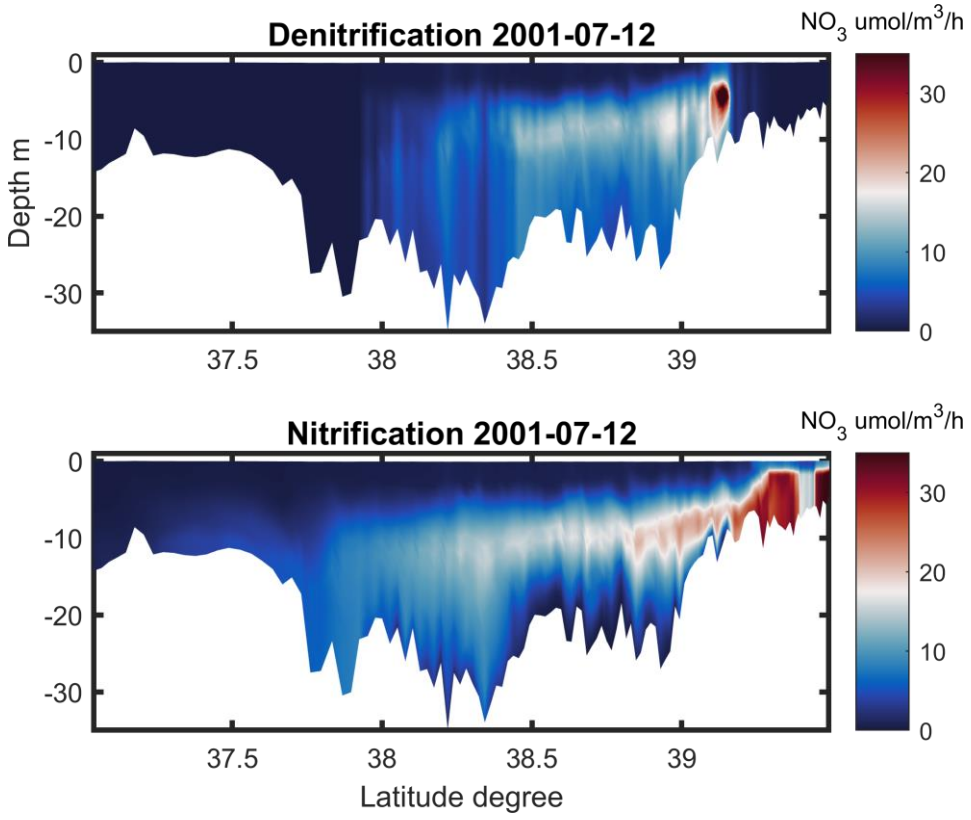

Figure 4.9 Along channel model-estimated denitrification rate (top panel) and nitrification rate (bottom panel) distributions for July-12th 2001.

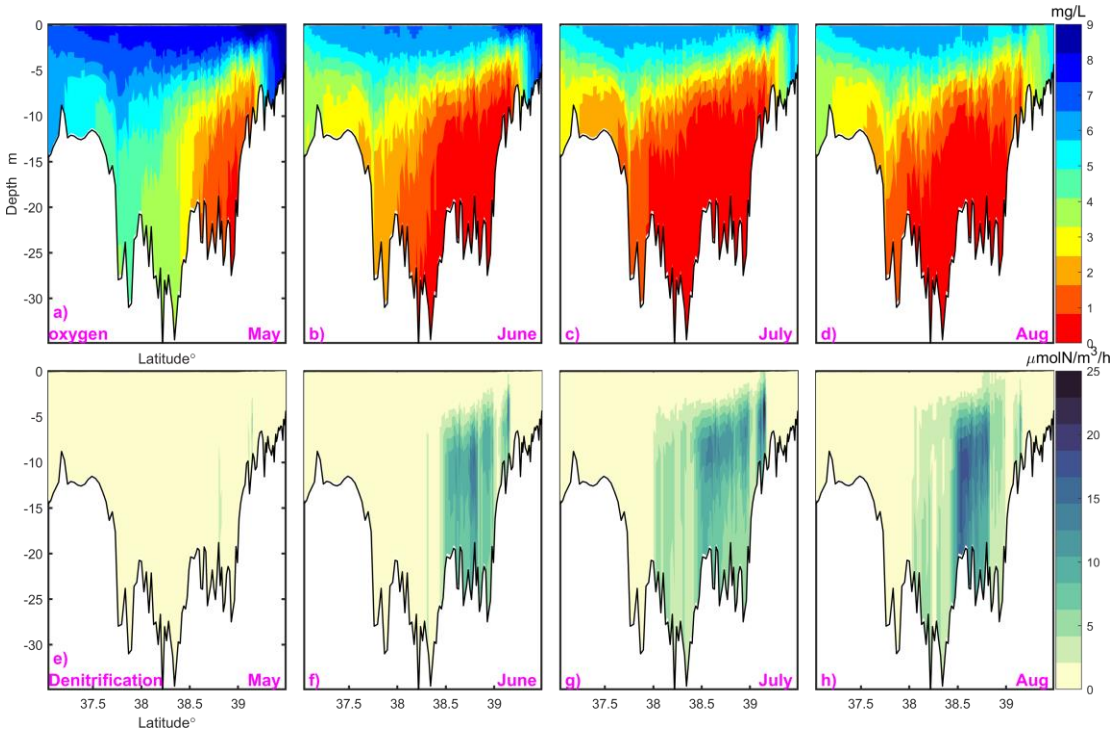

Figure 4.10: Along channel model-estimated oxygen level (a-d); and denitrification rate (e-h).

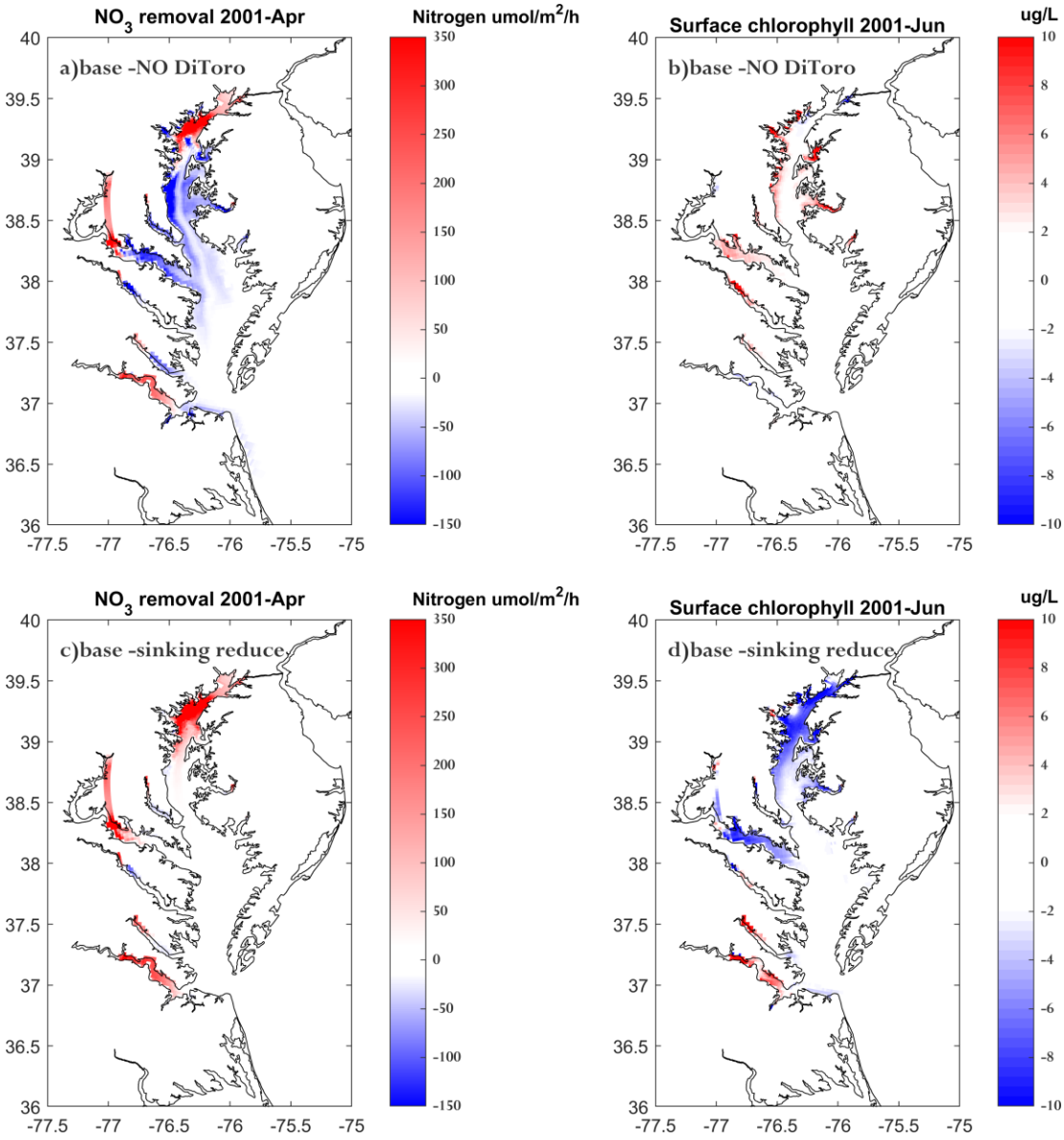

Figure 4.11 Nitrate removal difference (a) and surface chlorophyll difference (b) between the large sinking rate run A – slower sinking rate run C ; same but for run A – run D.

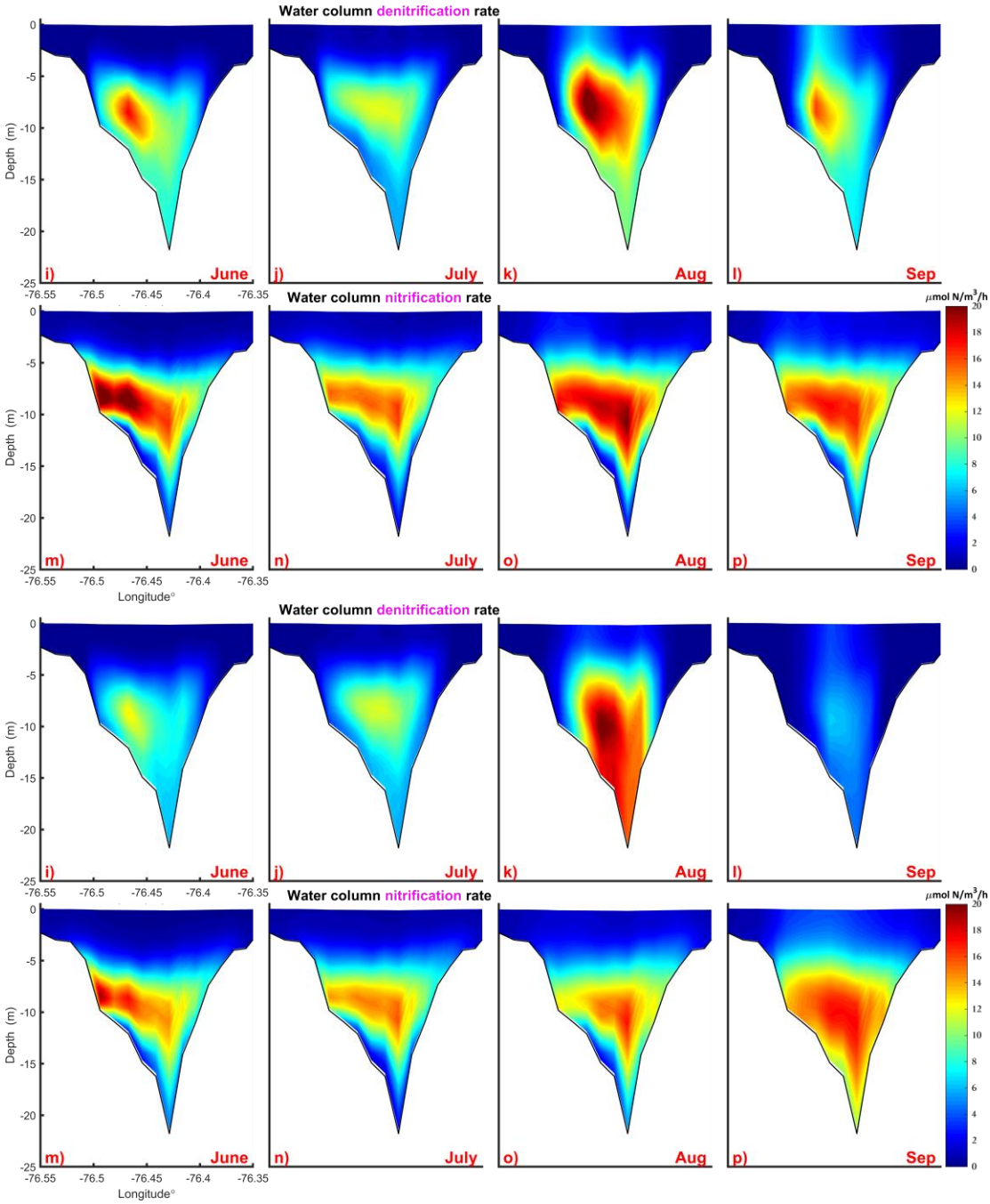

Figure 4.12: Cross channel base run A denitrification (a-d), nitrification (e-h); and sensitivity run E for wind has been rotated 180°during during 2001 May to August in 2001, denitrification (i-l), nitrification (m-p).

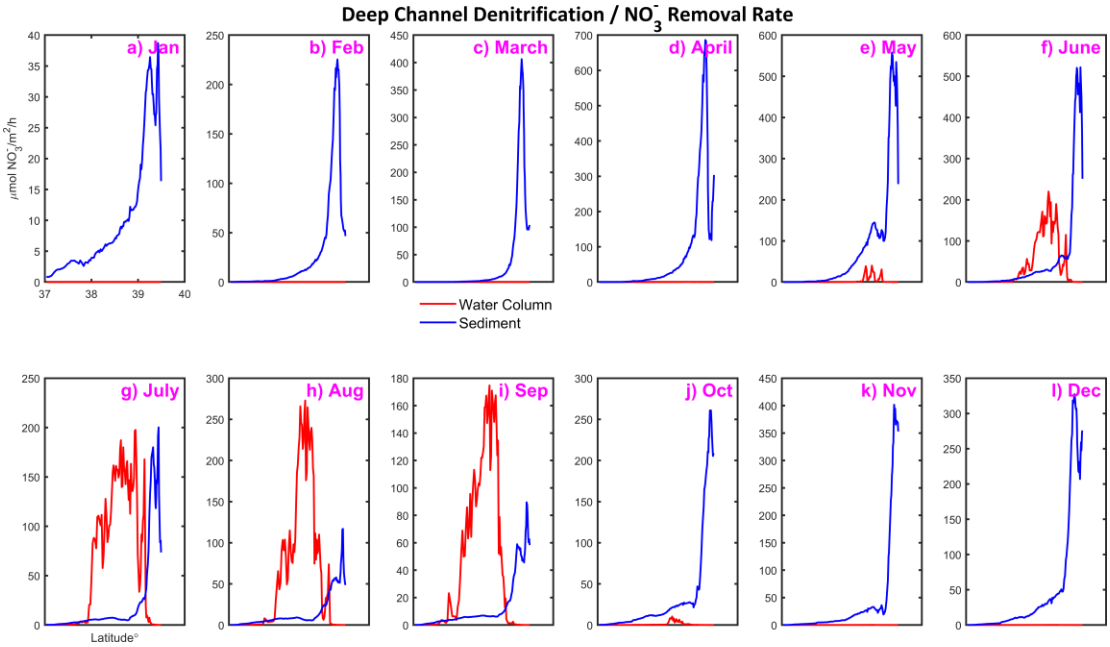

Figure 4.13: Along channel spatial and monthly variation of model-estimated denitrification rate in 2001. The red lines and blue lines represent water column (vertically integrated) and sediment contribution, respectively.

Table 4-1 Descriptions of model runs

Model ID	Description
A	Base run, with high bottom background oxygen consumption rate (62.5 mmol/m^2/day) during summertime,90% anaerobic respiration when full oxygen level in the upper water column,90% reduction in sinking speed in the bottom layer, low oxygen half saturation coefficient (0.01mmol oxygen /m^3).
B	Low bottom background oxygen consumption rate (31.25 oxygen mmol/m^2/day) during summertime with high oxygen half saturation coefficient (26.5 mmol oxygen /m^3).
C	No Ditoro: 14% anaerobic respiration when full oxygen level in the upper water column.
D	99% reduction n sinking speed in the bottom layer.
E	Wind rotates by 180° during May-Aug in 2001.

Table 4-2 Modified Biogeochemical Parameters different from Gross Primary Production (Chapter 3,GPP).

Description	Symbol	GPP	2001	2002	Units
phytoplankton growth rate at 0 °C	μ_0	1.45	1.0	1.45	d^{-1}
Half-saturation concentration for uptake of NO_3	k_{NO3}	2	0.5	2	mmol N m^{-3}
Half-saturation concentration for uptake of NH_4	k_{NH4}	2	0.5	2	mmol N m^{-3}
Half-saturation concentration of phytoplankton ingestion	k_{phy}	15	10	1	(mmol N m^{-3})^2
Zooplankton maximum growth rate	g_{max}	1.3	1.3	1.5	(mmol N m^{-3}) d^{-1}
Half-saturation concentration for denitrification	K_{DNF}	10	10	1	mmol N m^{-3}

Table 4-3 Denitrification Budget for year 2001. (unit 10^9 gram Nitrogen/year)

Model ID	Sediment	Water Column	Total	Water column Percentage %
A	35.79	3.13	38.92	8.04
B	33.47	12.85	46.32	27.74
C	44.87	2.83	47.7	5.93
D	10.95	7.05	18.00	39.17
E	36.14	2.28	38.42	5.93

References

Babbin, A.R., A. Jayakumar, and B.B. Ward. 2016. Organic Matter Loading Modifies the Microbial Community Responsible for Nitrogen Loss in Estuarine Sediments. *Microbial Ecology* 71: 555-565. doi: 10.1007/s00248-015-0693-5

Babbin, A.R., and B.B. Ward. 2013. Controls on Nitrogen Loss Processes in Chesapeake Bay Sediments. *Environmental Science & Technology* 47: 4189-4196. doi: 10.1021/es304842r

Beaulieu, J.J., J.L. Tank, S.K. Hamilton, W.M. Wollheim, R.O. Hall, P.J. Mulholland, B.J. Peterson, L.R. Ashkenas, L.W. Cooper, C.N. Dahm, W.K. Dodds, N.B. Grimm, S.L. Johnson, W.H. McDowell, G.C. Poole, H.M. Valett, C.P. Arango, M.J. Bernot, A.J. Burgin, C.L. Crenshaw, A.M. Helton, L.T. Johnson, J.M. Brien, J.D. Potter, R.W. Sheibley, D.J. Sobota, and S.M. Thomas. 2011. Nitrous oxide emission from denitrification in stream and river networks.

Proceedings of the National Academy of Sciences 108: 214. doi: 10.1073/pnas.1011464108

Bianucci, L., K. Fennel, and K.L. Denman. 2012. Role of sediment denitrification in water column oxygen dynamics: comparison of the North American East and West Coasts. *Biogeosciences* 9: 2673-2682. doi: 10.5194/bg-9-2673-2012

Bonaglia, S., F.J.A. Nascimento, M. Bartoli, I. Klawonn, and V. Bruchert. 2014. Meiofauna increases bacterial denitrification in marine sediments. *Nature Communications* 5. doi: 10.1038/ncomms6133

Bouwman, A.F., A.H.W. Beusen, and G. Billen. 2009. Human alteration of the global nitrogen and phosphorus soil balances for the period 1970-2050. *Global Biogeochemical Cycles* 23. doi: 10.1029/2009GB003576

Boynton, W., J. Garber, R. Summers, and W. Kemp. 1995. Inputs, transformations, and transport of nitrogen and phosphorus in Chesapeake Bay and selected tributaries. *Estuaries and Coasts* 18: 285-314. doi: 10.2307/1352640

Bulow, S.E., J.J. Rich, H.S. Naik, A.K. Pratihary, and B.B. Ward. 2010. Denitrification exceeds anammox as a nitrogen loss pathway in the Arabian Sea oxygen minimum zone. *Deep-Sea Research Part I-Oceanographic Research Papers* 57: 384-393. doi: 10.1016/j.dsr.2009.10.014

Chang, B.X., A.H. Devol, and S.R. Emerson. 2010. Denitrification and the nitrogen gas excess in the eastern tropical South Pacific oxygen deficient zone. *Deep-Sea Research Part I-Oceanographic Research Papers* 57: 1092-1101. doi: 10.1016/j.dsr.2010.05.009

Christensen, J.P., J.W. Murray, A.H. Devol, and L.A. Codispoti. 1987. Denitrification in continental shelf sediments has major impact on the oceanic nitrogen budget. *Global Biogeochemical Cycles* 1: 97-116. doi: 10.1029/GB001i002p00097

Cornwell, J.C., W.M. Kemp, and T.M. Kana. 1999. Denitrification in coastal ecosystems: methods, environmental controls, and ecosystem level controls, a review. *Aquatic Ecology* 33: 41-54. doi: 10.1023/A:1009921414151

Cornwell, J.C., M.S. Owens, W.R. Boynton, and L.A. Harris. 2016. Sediment-Water Nitrogen Exchange along the Potomac River Estuarine Salinity Gradient. *Journal of Coastal Research*: 776-787. doi: 10.2112/jcoastres-d-15-00159.1

Cowan, J.L.W., and W.R. Boynton. 1996. Sediment-water oxygen and nutrient exchanges along the longitudinal axis of Chesapeake Bay: Seasonal patterns, controlling factors and ecological significance. *Estuaries* 19: 562-580. doi: 10.2307/1352518

Dalsgaard, T., D.E. Canfield, J. Petersen, B. Thamdrup, and J. Acuna-Gonzalez. 2003. N-2 production by the anammox reaction in the anoxic water column of Golfo Dulce, Costa Rica. *Nature* 422: 606-608. doi: 10.1038/nature01526

Dalsgaard, T., and B. Thamdrup. 2002. Factors controlling anaerobic ammonium oxidation with nitrite in marine sediments. *Applied and Environmental Microbiology* 68: 3802-3808. doi: 10.1128/aem.68.8.3802-3808.2002

Deek, A., K. Dahnke, J. van Beusekom, S. Meyer, M. Voss, and K. Emeis. 2013. N-2 fluxes in sediments of the Elbe Estuary and adjacent coastal zones. *Marine Ecology Progress Series* 493: 9-21. doi: 10.3354/meps10514

DeVries, T., C. Deutsch, F. Primeau, B. Chang, and A. Devol. 2012. Global rates of water-column denitrification derived from nitrogen gas measurements. *Nature Geoscience* 5: 547-550. doi: 10.1038/ngeo1515

Di Toro, D.M. 2001. *Sediment flux modeling*. New York: Wiley-Interscience.

Dodds, W.K., W.W. Bouska, J.L. Eitzmann, T.J. Pilger, K.L. Pitts, A.J. Riley, J.T. Schloesser, and D.J. Thornbrugh. 2009. Eutrophication of US Freshwaters: Analysis of Potential Economic Damages. *Environmental Science & Technology* 43: 12-19. doi: 10.1021/es801217q

Fear, J.M., S.P. Thompson, T.E. Gallo, and H.W. Paerl. 2005. Denitrification rates measured along a salinity gradient in the eutrophic Neuse River Estuary, North Carolina, USA. *Estuaries* 28: 608-619. doi: 10.1007/bf02696071

Feng, Y., M.A.M. Friedrichs, J. Wilkin, H.Q. Tian, Q.C. Yang, E.E. Hofmann, J.D. Wiggert, and R.R. Hood. 2015. Chesapeake Bay nitrogen fluxes derived from a land-estuarine ocean biogeochemical modeling system: Model description, evaluation, and nitrogen budgets. *Journal of Geophysical Research-Biogeosciences* 120: 1666-1695. doi: 10.1002/2015jg002931

Fennel, K., D. Brady, D. Di Toro, R.W. Fulweiler, W.S. Gardner, A. Giblin, M.J. McCarthy, A. Rao, S. Seitzinger, M. Thouvenot-Korppoo, and C. Tobias. 2009. Modeling denitrification in aquatic sediments. *Biogeochemistry* 93: 159-178. doi: 10.1007/s10533-008-9270-z

Fennel, K., and J.M. Testa. 2019. Biogeochemical Controls on Coastal Hypoxia. In *Annual Review of Marine Science, Vol 11*, ed. C.A. Carlson and S.J. Giovannoni, 105-130. doi: 10.1146/annurev-marine-010318-095138

Fennel, K., J. Wilkin, J. Levin, J. Moisan, J. O'Reilly, and D. Haidvogel. 2006. Nitrogen cycling in the Middle Atlantic Bight: Results from a three-dimensional model and implications for the North Atlantic nitrogen budget. *Global Biogeochemical Cycles* 20. doi: 10.1029/2005GB002456

Fuchsman, C.A., A.H. Devol, J.K. Saunders, C. McKay, and G. Rocap. 2017. Niche Partitioning of the N Cycling Microbial Community of an Offshore Oxygen Deficient Zone. *Frontiers in Microbiology* 8: 18. doi: 10.3389/fmicb.2017.02384

Fuchsman, C.A., B. Paul, J.T. Staley, E.V. Yakushev, and J.W. Murray. 2019. Detection of Transient Denitrification During a High Organic Matter Event in the Black Sea. *Global Biogeochemical Cycles* 33: 143-162. doi: 10.1029/2018gb006032

Grosse, F., K. Fennel, and A. Laurent. 2019. Quantifying the Relative Importance of Riverine and Open-Ocean Nitrogen Sources for Hypoxia Formation in the Northern Gulf of Mexico. *Journal of Geophysical Research-Oceans* 124: 5451-5467. doi: 10.1029/2019jc015230

Hagy, J.D., W.R. Boynton, and D.A. Jasinski. 2005. Modelling phytoplankton deposition to Chesapeake Bay sediments during winter-spring: interannual variability in relation to river flow. *Estuarine, Coastal and Shelf Science* 62: 25-40. doi: 10.1016/j.ecss.2004.08.004

Horak, R.E.A., W. Ruef, B.B. Ward, and A.H. Devol. 2016. Expansion of denitrification and anoxia in the eastern tropical North Pacific from 1972 to

2012. *Geophysical Research Letters* 43: 5252-5260. doi: 10.1002/2016gl068871

Ji, Q., C. Frey, X. Sun, M. Jackson, Y.S. Lee, A. Jayakumar, J.C. Cornwell, and B.B. Ward. 2018. Nitrogen and oxygen availabilities control water column nitrous oxide production during seasonal anoxia in the Chesapeake Bay. *Biogeosciences* 15: 6127-6138. doi: 10.5194/bg-15-6127-2018

Kana, T.M., J.C. Cornwell, and L.J. Zhong. 2006. Determination of denitrification in the Chesapeake Bay from measurements of N-2 accumulation in bottom water. *Estuaries and Coasts* 29: 222-231. doi: 10.1007/bf02781991

Kemp, W.M., W.R. Boynton, J.E. Adolf, D.F. Boesch, W.C. Boicourt, G. Brush, J.C. Cornwell, T.R. Fisher, P.M. Glibert, J.D. Hagy, L.W. Harding, E.D. Houde, D.G. Kimmel, W.D. Miller, R.I.E. Newell, M.R. Roman, E.M. Smith, and J.C. Stevenson. 2005. Eutrophication of Chesapeake Bay: historical trends and ecological interactions. *Marine Ecology Progress Series* 303: 1-29. doi: 10.3354/Meps303001

Kemp, W.M., P. Sampou, J. Caffrey, M. Mayer, K. Henriksen, and W.R. Boynton. 1990. Ammonium recycling versus denitrification in Chesapeake Bay sediments. *Limnology and Oceanography* 35: 1545-1563. doi: 10.4319/lo.1990.35.7.1545

Kemp, W.M., J.M. Testa, D.J. Conley, D. Gilbert, and J.D. Hagy. 2009. Temporal responses of coastal hypoxia to nutrient loading and physical controls. *Biogeosciences* 6: 2985-3008. doi: 10.5194/bg-6-2985-2009

Lam, P., G. Lavik, M.M. Jensen, J. van de Vossenberg, M. Schmid, D. Woebken, G. Dimitri, R. Amann, M.S.M. Jetten, and M.M.M. Kuypers. 2009. Revising the nitrogen cycle in the Peruvian oxygen minimum zone. *Proceedings of the National Academy of Sciences of the United States of America* 106: 4752-4757. doi: 10.1073/pnas.0812444106

Laperriere, S.M., N.J. Nidzieko, R.J. Fox, A.W. Fisher, and A.E. Santoro. 2018. Observations of Variable Ammonia Oxidation and Nitrous Oxide Flux in a Eutrophic Estuary. *Estuaries and Coasts*. doi: 10.1007/s12237-018-0441-4

Laperriere, S.M., N.J. Nidzieko, R.J. Fox, A.W. Fisher, and A.E. Santoro. 2019. Observations of Variable Ammonia Oxidation and Nitrous Oxide Flux in a Eutrophic Estuary. *Estuaries and Coasts* 42: 33-44. doi: 10.1007/s12237-018-0441-4

Li, Y., and M. Li. 2011. Effects of winds on stratification and circulation in a partially mixed estuary. *Journal of Geophysical Research* 116. doi: 10.1029/2010jc006893

Li, Y., and M. Li. 2012. Wind-driven lateral circulation in a stratified estuary and its effects on the along-channel flow. *Journal of Geophysical Research: Oceans* 117. doi: 10.1029/2011jc007829

Li, Y., M. Li, and W.M. Kemp. 2015. A Budget Analysis of Bottom-Water Dissolved Oxygen in Chesapeake Bay. *Estuaries and Coasts*. doi: 10.1007/s12237-014-9928-9

Luettich, R.A., L.D. Wright, R. Signell, C. Friedrichs, M. Friedrichs, J. Harding, K. Fennel, E. Howlett, S. Graves, E. Smith, G. Crane, and R. Baltes. 2013. Introduction to special section on The U.S. IOOS Coastal and Ocean

Modeling Testbed. *Journal of Geophysical Research: Oceans* 118: 6319-6328. doi: 10.1002/2013jc008939

Ma, L., H. Lin, X.B. Xie, M.H. Dai, and Y. Zhang. 2019. Major role of ammonia-oxidizing bacteria in N2O production in the Pearl River estuary. *Biogeosciences* 16: 4765-4781. doi: 10.5194/bg-16-4765-2019

Mueller, N.D., L. Lassaletta, B.C. Runck, G. Billen, J. Garnier, and J.S. Gerber. 2017. Declining spatial efficiency of global cropland nitrogen allocation. *Global Biogeochemical Cycles* 31: 245-257. doi: 10.1002/2016GB005515

Rich, J.J., O.R. Dale, B. Song, and B.B. Ward. 2008. Anaerobic ammonium oxidation (Anammox) in Chesapeake Bay sediments. *Microbial Ecology* 55: 311-320. doi: 10.1007/s00248-007-9277-3

Russ, E., and C. Palinkas. 2020. Evolving sediment dynamics due to anthropogenic processes in upper Chesapeake Bay. *Estuarine Coastal and Shelf Science* 235: 12. doi: 10.1016/j.ecss.2020.106596

Sanford, L.P., W. Panageotou, and J.P. Halka. 1991. Tidal resuspension of sediments in northern Chesapeake Bay. *Marine Geology* 97: 87-103. doi: 10.1016/0025-3227(91)90020-5

Scully, M.E. 2013. Physical controls on hypoxia in Chesapeake Bay: A numerical modeling study. *Journal of Geophysical Research: Oceans* 118: 1239-1256. doi: 10.1002/jgrc.20138

Scully, M.E. 2016. The contribution of physical processes to inter-annual variations of hypoxia in Chesapeake Bay: A 30-yr modeling study. *Limnology and Oceanography* 61: 2243-2260. doi: 10.1002/lno.10372

Seitzinger, S., J.A. Harrison, J.K. Bohlke, A.F. Bouwman, R. Lowrance, B. Peterson, C. Tobias, and G. Van Drecht. 2006. Denitrification across landscapes and waterscapes: A synthesis. *Ecological Applications* 16: 2064-2090. doi: 10.1890/1051-0761(2006)016[2064:dalawa]2.0.co;2

Seitzinger, S.P. 1988. Denitrification in freshwater and coastal marine ecosystems: Ecological and geochemical significance. *Limnology and Oceanography* 33: 702-724. doi: 10.4319/lo.1988.33.4part2.0702

Seitzinger, S.P., and A.E. Giblin. 1996. Estimating denitrification in North Atlantic continental shelf sediments. *Biogeochemistry* 35: 235-260. doi: 10.1007/BF02179829

Shen, J., B. Hong, and A.Y. Kuo. 2013. Using timescales to interpret dissolved oxygen distributions in the bottom waters of Chesapeake Bay. *Limnology and Oceanography* 58: 2237-2248. doi: 10.4319/lo.2013.58.6.2237

Shen, X., E.A. Toorman, B.J. Lee, and M. Fettweis. 2018. Biophysical flocculation of suspended particulate matters in Belgian coastal zones. *Journal of Hydrology* 567: 238-252. doi: 10.1016/j.jhydrol.2018.10.028

Shen, X.T., E.A. Toorman, B.J. Lee, and M. Fettweis. 2019. An Approach to Modeling Biofilm Growth During the Flocculation of Suspended Cohesive Sediments. *Journal of Geophysical Research-Oceans* 124: 4098-4116. doi: 10.1029/2018jc014493

Smith, V.H. 2003. Eutrophication of freshwater and coastal marine ecosystems - A global problem. *Environmental Science and Pollution Research* 10: 126-139. doi: 10.1065/espr2002.12.142

Testa, J.M., D.C. Brady, D.M. Di Toro, W.R. Boynton, J.C. Cornwell, and W.M. Kemp. 2013. Sediment flux modeling: Simulating nitrogen, phosphorus, and silica cycles. *Estuarine, Coastal and Shelf Science* 131: 245-263. doi: 10.1016/j.ecss.2013.06.014

Testa, J.M., and W.M. Kemp. 2012. Hypoxia-induced shifts in nitrogen and phosphorus cycling in Chesapeake Bay. *Limnology and Oceanography* 57: 835-850. doi: 10.4319/lo.2012.57.3.0835

Testa, J.M., and W.M. Kemp. 2014. Spatial and temporal patterns in winter-spring oxygen depletion in Chesapeake Bay bottom waters. *Estuaries and Coasts* 37: 1432-1448. doi: 10.1007/s12237-014-9775-8

Testa, J.M., W.M. Kemp, and W.R. Boynton. 2018a. Season-specific trends and linkages of nitrogen and oxygen cycles in Chesapeake Bay. *Limnology and Oceanography* 63: 2045-2064. doi: 10.1002/lno.10823

Testa, J.M., R.R. Murphy, D.C. Brady, and W.M. Kemp. 2018b. Nutrient- and Climate-Induced Shifts in the Phenology of Linked Biogeochemical Cycles in a Temperate Estuary. *Frontiers in Marine Science* 5. doi: 10.3389/fmars.2018.00114

Thamdrup, B., and T. Dalsgaard. 2002. Production of N-2 through anaerobic ammonium oxidation coupled to nitrate reduction in marine sediments. *Applied and Environmental Microbiology* 68: 1312-1318. doi: 10.1128/aem.68.3.1312-1318.2002

Ward, B.B., A.H. Devol, J.J. Rich, B.X. Chang, S.E. Bulow, H. Naik, A. Pratihary, and A. Jayakumar. 2009. Denitrification as the dominant nitrogen loss process in the Arabian Sea. *Nature* 461: 78-U77. doi: 10.1038/nature08276

Weston, N.B., A.E. Giblin, G.T. Banta, C.S. Hopkinson, and J. Tucker. 2010. The Effects of Varying Salinity on Ammonium Exchange in Estuarine Sediments of the Parker River, Massachusetts. *Estuaries and Coasts* 33: 985-1003. doi: 10.1007/s12237-010-9282-5

Willmott, C.J. 1981. On the validation of models. *Physical Geography* 2: 184-194. doi: 10.1080/02723646.1981.10642213

Xu, J., and R.R. Hood. 2006. Modeling biogeochemical cycles in Chesapeake Bay with a coupled physical–biological model. *Estuarine, Coastal and Shelf Science* 69: 19-46. doi: 10.1016/j.ecss.2006.03.021

Yang, S., N. Gruber, M.C. Long, and M. Vogt. 2017. ENSO-Driven Variability of Denitrification and Suboxia in the Eastern Tropical Pacific Ocean. *Global Biogeochemical Cycles* 31: 1470-1487. doi: 10.1002/2016gb005596

Yu, L.Q., K. Fennel, and A. Laurent. 2015. A modeling study of physical controls on hypoxia generation in the northern Gulf of Mexico. *Journal of Geophysical Research-Oceans* 120: 5019-5039. doi: 10.1002/2014jc010634

Zhang, X. 2017. Biogeochemistry: A plan for efficient use of nitrogen fertilizers. *Nature* 543: 322-323. doi: 10.1038/543322a

Zumft, W.G. 1997. Cell biology and molecular basis of denitrification. *Microbiology and Molecular Biology Reviews* 61: 533-+. doi: 10.1128/.61.4.533-616.1997

Chapter 5: Conclusion and Future Research

Conclusion

In my dissertation, a coupled physical-biogeochemical model was validated and used to simulate biogeochemical variability in Chesapeake Bay and also understand the fundamental physical and biogeochemical processes that drive this variability. My research efforts have focused fundamental biogeochemical processes which similar biogeochemical numerical model publications in the same region have not fully addressed (Da et al. 2018; Feng et al. 2015; Shen et al. 2019; Testa et al. 2014). The model was reparameterized for each chapter of my thesis to focus on specific biogeochemical process. Although there are some clear deficiencies in the model, I argue that my research has resulted in some important new research findings:

1. For the particulate organic nitrogen (PON) transport chapter, the model was shown to have good skill in reproducing the spatial and temporal variability of chlorophyll and other biogeochemical constituents in Chesapeake Bay. Given this skill I concluded that the model is sufficient to examine PON production, transport, and transformation in Chesapeake Bay. From my analysis I conclude that the bottom accumulation of organic matter is due to sinking from the upper water column, as well as the lateral transport. The deep channel is also exporting mass to the western shore and there is also convergence on the western shore. The mechanism behind these transport patters is consistent with the theory from Scully et al. (2009). Wind plays a role in changing the magnitude of the mass transport, but it does not change

the bottom background transport pattern. This suggests that at the seasonal scale in the Chesapeake Bay, the freshwater discharge and tidal forcing are the dominant drivers for the bottom lateral organic matter transport direction. The upper bay deep channel is dominated by upwelling, consistent with classic estuarine circulation. The downward sinking fluxes of PON are substantially balanced by upward vertical advection in the same region.

2. For the gross primary production (GPP) and biomass chapter, I used a 3-dimensional coupled physical-biological model to simulate seasonal and spatial patterns in phytoplankton biomass (chlorophyll) and primary production in Chesapeake Bay, USA. I showed that the model can capture the seasonal variability of both chlorophyll and primary production and that it can reproduce the observed spring maximum in depth-integrated chlorophyll and summer maximum in depth-integrated primary production that has been reported in many observational studies, but has not been previously modeled. The key to reproducing these patterns is simulating seasonal changes phytoplankton growth rate, i.e., the model must generate growth rates during summer that are three times higher than they are during spring. These results also highlight the idea that increased phytoplankton growth rate during summer is an important factor that drives high primary production during summer. Furthermore, these seasonal changes in phytoplankton growth rate explain how primary production can be several times higher in summer compared to spring when euphotic zone averaged chlorophyll is roughly the same. The model is also capable of reproducing the biomass accumulation on

the bottom in spring that is observed in the CBP data, but not observed in satellite chlorophyll estimates that only detect near surface concentrations. The summertime high primary production (and growth rated) is the result of the combined effects of high temperature, light availability, and nutrient supplements in the form of NH_4^+ that is provided through both the transport and mixing processes (new nitrogen) and euphotic zone recycling (old nitrogen). My control volume budget analysis reveals substantial nutrient inputs in the form of NH_4^+. The F-ratio calculated from the model simulations was as large as 60%. This finding was also consistent with previous nutrient cycling and budget research in the Chesapeake Bay and it provides an explanation for the conundrum revealed in previous studies that nutrients remineralized from bottom detritus can only support part of the summer primary production. The explanation emerging from this study is that the remaining nutrients are supplied through euphotic zone recycling (old nitrogen). For future study, an important goal will be to fully simulate high summer primary production rates (that are underestimated in our simulations) while still maintaining reasonable model skill simulating chlorophyll concentrations.

3. For the denitrification chapter, I used the same coupled physical-biogeochemical model to simulate benthic and water column denitrification variability in Chesapeake Bay. I validated the model using observed O_2, NO_3^- and NH_4^+ concentrations combined with sparse measurements of sediment denitrification and estimates of water column denitrification derived from

measurement of N_2O production. The model-estimated Bay wide denitrification rate is consistent with previously derived estimates (Boynton et al. 1995; Feng et al. 2015). The model predicts that sediment denitrification rates are highest in late spring after the spring bloom when organic matter fluxes to the bottom are high. These results are also consistent with previous modeling studies (Feng et al. 2015; Testa et al. 2013) and observations (Boynton et al. 1995; Kana et al. 2006). During the summer, sediment denitrification is shut down due to NO_3^- depletion even though anoxic conditions should facilitate the anaerobic respiration. In contrast, rates of water column denitrification are highest in early summertime when the deep water starts to go anoxic. This denitrification happens in the transition zone between oxygenated waters near the surface and oxygen depleted waters at depth where NO_3^- is supplied by nitrification. That model predicts that water column denitrification is about 13% of that compared with the sediment denitrification, which is consistent with the idea that water column denitrification rates in Chesapeake Bay are small (Boynton et al. 1995). The relative amounts of water column and sediment denitrification predicted by the model are dependent on oxygen concentrations, nitrate availability and anaerobic respiration efficiency. The results from our research clearly illustrate the importance of the role of water column denitrification in Chesapeake Bay. It is shown that, without the water column denitrification, the summertime primary productivity is significantly elevated in the middle to upper Bay region, but the effect is not pronounced in the lower Bay. These

patterns are consistent with the two-layer estuarine circulation patterns, i.e., without the water column denitrification, NH_4^+ concentrations increase in the deep channel where they are transported northward/upstream and mixed to the euphotic zone, providing extra nutrients to the relatively low nutrient surface water, which, in turn, results in enhanced primary production in the upper mesohaline Chesapeake Bay. Finally, an examination of the sensitivity of the model-predicted denitrification rates to key model parameters reveals that the relative amounts of water column and sediment denitrification are sensitive to the assumed percentage of aerobic and anaerobic respiration in the sediments under a fully oxic overlying water column. In addition, the relative amounts of sediment and water denitrification that are predicted by the model are also sensitive to the O_2 half-saturation coefficient for water column denitrification. Efforts to better constrain these parameters should be undertaken. More in situ measurements of sediment and water column denitrification are also needed to better constrain the model.

Future Research

My overarching motivation for investigating nutrient cycling in Chesapeake Bay is to obtain a better understanding of the chronic oxygen depletion in the bottom water that occurs during summer. I have undertaken substantial efforts to get my model to simulate dissolved oxygen with strong model skill. One important conclusion that I have drawn from these efforts is that it is very difficult to parameterize my model to provide good model skill for both chlorophyll (particulate organic nitrogen) and oxygen in three dimensions, seasonally along the estuarine salinity gradient. This in

turn, has impeded my efforts to provide give a full assessment on the relative roles of physical process and biogeochemical processes in controlling oxygen draw down in the main stem of the Chesapeake Bay. This has led me to conclude that the coastal nitrogen cycle model (Fennel et al. 2006) that provides the foundation for my model has some significant limitations for its application in a partially mixed estuary like Chesapeake Bay. For example, complex sediment biogeochemical processes, including sediment burial, resuspension and biogeochemical transformation, are very important for simulating seasonal variations in the sediment oxygen demand (Moriarty et al. 2017; Moriarty et al. 2018), but these processes are grossly oversimplified in my model. Similarly, my model includes only one phytoplankton state variable whereas, in Chesapeake Bay, there are dramatic seasonal changes in phytoplankton community composition. A model with at least two kinds of phytoplankton is therefore desirable for application in Chesapeake Bay (Testa et al. 2014). Finally, for denitrification, more in-site measurements of both bottom and water column denitrification are desperately needed to validate model simulations and better understand the spatial and temporal variability of sediment and water column denitrification in Chesapeake Bay.

References

Boynton, W., J. Garber, R. Summers, and W. Kemp. 1995. Inputs, transformations, and transport of nitrogen and phosphorus in Chesapeake Bay and selected tributaries. *Estuaries and Coasts* 18: 285-314. doi: 10.2307/1352640

Da, F., M.A.M. Friedrichs, and P. St-Laurent. 2018. Impacts of Atmospheric Nitrogen Deposition and Coastal Nitrogen Fluxes on Oxygen Concentrations in Chesapeake Bay. *Journal of Geophysical Research-Oceans* 123: 5004-5025. doi: 10.1029/2018jc014009

Feng, Y., M.A.M. Friedrichs, J. Wilkin, H.Q. Tian, Q.C. Yang, E.E. Hofmann, J.D. Wiggert, and R.R. Hood. 2015. Chesapeake Bay nitrogen fluxes derived from

a land-estuarine ocean biogeochemical modeling system: Model description, evaluation, and nitrogen budgets. *Journal of Geophysical Research-Biogeosciences* 120: 1666-1695. doi: 10.1002/2015jg002931

Fennel, K., J. Wilkin, J. Levin, J. Moisan, J. O'Reilly, and D. Haidvogel. 2006. Nitrogen cycling in the Middle Atlantic Bight: Results from a three-dimensional model and implications for the North Atlantic nitrogen budget. *Global Biogeochemical Cycles* 20. doi: 10.1029/2005GB002456

Kana, T.M., J.C. Cornwell, and L.J. Zhong. 2006. Determination of denitrification in the Chesapeake Bay from measurements of N-2 accumulation in bottom water. *Estuaries and Coasts* 29: 222-231. doi: 10.1007/bf02781991

Moriarty, J.M., C.K. Harris, K. Fennel, M.A.M. Friedrichs, K.H. Xu, and C. Rabouille. 2017. The roles of resuspension, diffusion and biogeochemical processes on oxygen dynamics offshore of the Rhone River, France: A numerical modeling study. *Biogeosciences* 14: 1919-1946. doi: 10.5194/bg-14-1919-2017

Moriarty, J.M., C.K. Harris, M.A.M. Friedrichs, K. Fennel, and K.H. Xu. 2018. Impact of Seabed Resuspension on Oxygen and Nitrogen Dynamics in the Northern Gulf of Mexico: A Numerical Modeling Study. *Journal of Geophysical Research-Oceans* 123: 7237-7263. doi: 10.1029/2018jc013950

Scully, M.E., W.R. Geyer, and J.A. Lerczak. 2009. The influence of lateral advection on the residual estuarine circulation: a numerical modeling study of the Hudson River estuary. *Journal of Physical Oceanography* 39: 107-124. doi: 10.1175/2008jpo3952.1

Shen, C.Q., J.M. Testa, M. Li, W.J. Cai, G.G. Waldbusser, W.F. Ni, W.M. Kemp, J. Cornwell, B.S. Chen, J. Brodeur, and J.Z. Su. 2019. Controls on Carbonate System Dynamics in a Coastal Plain Estuary: A Modeling Study. *Journal of Geophysical Research-Biogeosciences* 124: 61-78. doi: 10.1029/2018jg004802

Testa, J.M., D.C. Brady, D.M. Di Toro, W.R. Boynton, J.C. Cornwell, and W.M. Kemp. 2013. Sediment flux modeling: Simulating nitrogen, phosphorus, and silica cycles. *Estuarine, Coastal and Shelf Science* 131: 245-263. doi: 10.1016/j.ecss.2013.06.014

Testa, J.M., Y. Li, Y.J. Lee, M. Li, D.C. Brady, D.M. Di Toro, W.M. Kemp, and J.J. Fitzpatrick. 2014. Quantifying the effects of nutrient loading on dissolved O2 cycling and hypoxia in Chesapeake Bay using a coupled hydrodynamic–biogeochemical model. *Journal of Marine Systems* 139: 139-158. doi: 10.1016/j.jmarsys.2014.05.018

Appendices

Table 0-1 Parameter for biological model used in this study. Units are following Feng et al. (2015) unless specified.

Symbol	Parameter	Value	Unit
μ_0	phytoplankton growth rate at 0 C	1.45	d^{-1}
k_{NO_3}	half-saturation concentration for uptake of NO_3^-	2.0	mmol N m^{-3}
k_{NH_4}	half-saturation concentration for uptake of NH_4^+	2.0	mmol N m^{-3}
α	initial slope of the P-I curve	0.125	mol C $gChl^{-1}$ $(W\ m^{-2})^{-1}$ d^{-1}
γ	phytoplankton exudation fraction	0.001	dimensionless
g_{max}	maximum grazing rate	1.3	$(mmol\ N\ m^{-3})^{-1}$ d^{-1}
k_P	half-saturation concentration of phytoplankton ingestion	15	$(mmol\ N\ m^{-3})^2$
m_P	phytoplankton mortality	0.0125	$(mmol\ N/m^3)^{-1}$ d^{-1}
δ	phytoplankton mortality fraction to DON	0.75	dimensionless
τ	aggregation parameter	0.003	$(mmol\ N\ m^{-3})^{-1}$ d^{-1}
Θ_{max}	maximum chlorophyll to phytoplankton ratio	Spring:18.7 Summer: 50	mg Chl mgC^{-1}
β	assimilation efficiency	0.99	dimensionless

l_{BM}	excretion rate due to basal metabolism	0.01	d^{-1}
l_E	maximum rate of assimilation related excretion	0.01	d^{-1}
m_Z	zooplankton mortality	0.125	$(mmol\ N/m^3)^{-1}\ d^{-1}$
r_S	remineralization rate of small detritus	0.5	d^{-1}
r_D	remineralization rate of large detritus	0.2	d^{-1}
n_{max}	maximum nitrification rate	0.05	d^{-1}
k_I	light intensity at which the inhibition of nitrification is half-saturated	0.1	$W\ m^{-2}$
I_{NTR}	threshold for light-inhibition of nitrification	0.0095	$W\ m^{-2}$
w_P	sinking velocity of phytoplankton	Spring: 3.0 Summer: 1.0	d^{-1}
w_S	sinking velocity of small detritus	0.1	d^{-1}
w_L	sinking velocity of larger particles	3.0	d^{-1}
K_{BNO_3}	half-saturation concentration of bottom nitrate level for denitrification	10	$mmol\ N\ m^{-3}$
K_{BO_2}	half-saturation concentration of bottom oxygen level for denitrification	10	$mmol\ oxygen\ m^{-3}$

Table 0-2 State variable biogeochemical source/ sink terms, similar as same as (Feng et al. 2015) unless specified

Variable (Symbol)	Processes ← From which pool; → To which pool.	Time rate of change in each term
Phytoplankton (P)	Change per unit time =	$\partial \mathrm{P}/\,\partial \mathrm{t} =$
	+Primary production ($\leftarrow[NH_4^+]$+ $[NO_3]$)	$+\mu_0 \mathrm{L_I}\left(\mathrm{L_{NO_3}} + \mathrm{L_{NH_4}}\right)\mathrm{P}$
	-Exudation ($\rightarrow$[DON])	$-\gamma\mu_0 \mathrm{L_I}(\mathrm{L_{NO_3}}+\mathrm{L_{NH_4}})\mathrm{P}$
	-Grazing ($\rightarrow$Z)	$-\mathrm{gZ}$
	-Mortality ($\rightarrow D_S$)	$-\mathrm{m_P P}$
	-Aggregation ($\rightarrow D_L$)	$-\tau(\mathrm{D_S} + \mathrm{P})\mathrm{P}$
	-Sinking	$-w_P\,\partial \mathrm{P}/\,\partial \mathrm{z}$
Chlorophyll ([Chl])	Change per unit time =	$\partial[\mathrm{Chl}]/\,\partial \mathrm{t} =$
	+ Primary production ($[NH_4^+]$+ $[NO_3]\rightarrow$ P)	$\rho_{\mathrm{Chl}}\mu_0 \mathrm{L_I}\left(\mathrm{L_{NO_3}} + \mathrm{L_{NH_4}}\right)[\mathrm{Chl}]$
	-Exudation (P$\rightarrow$[DON])	$-\gamma\rho_{\mathrm{Chl}}\mu_0 \mathrm{L_I}\left(\mathrm{L_{NO_3}} + \mathrm{L_{NH_4}}\right)[\mathrm{Chl}]$
	-Grazing	$-\mathrm{gZ}\frac{\mathrm{Chl}}{\mathrm{P}}$
	-Mortality (P $\rightarrow D_S$)	$-\mathrm{m_P}[\mathrm{Chl}]$
	-Aggregation (P $\rightarrow D_L$)	$-\tau(\mathrm{D_S} + \mathrm{P})[\mathrm{Chl}]$
	- Sinking	$-\mathrm{w_P}\,\partial[\mathrm{Chl}]/\,\partial \mathrm{z}$
Zooplankton (Z)	Change per unit time =	$\partial \mathrm{Z}/\,\partial \mathrm{t} =$
	+Grazing assimilation ($\leftarrow$ P)	$+\beta \mathrm{gZ}$
	- Excretion ($\rightarrow[NH_4^+]$)	$-(\mathrm{l_{BM}} + \mathrm{l_E}\beta\frac{\mathrm{P}^2}{\mathrm{K_P}+\mathrm{P}^2})\mathrm{Z}$
	- Mortality (($\rightarrow D_L$)	$-\mathrm{m_z Z}^2$
Small Detritus (D_S)	Change per unit time =	$\partial \mathrm{D_S}/\,\partial \mathrm{t} =$
	+Grazing assimilation ($\leftarrow$ P)	$+(1-\beta)\mathrm{gZ}$
	+ Mortality Solubilization ($\leftarrow$ P)	$+(1-\delta)\mathrm{m_P P}$
	- Aggregation ($\rightarrow D_L$)	$-\tau(\mathrm{D_S} + \mathrm{P})\mathrm{D_S}$

	- Remineralization (→[NH_4^+])	$-r_S \exp\,[0.086(\mathrm{T}-30)]D_S$
	- Sinking	$-\mathrm{w_P}\,\partial \mathrm{D_S}/\,\partial \mathrm{z}$
Large Detritus (D_L)	Change per unit time =	$\partial \mathrm{D_L}/\,\partial \mathrm{t} =$
	+ Aggregation (←D_S + P)	$+\tau(\mathrm{D_S}+\mathrm{P})^2$
	+ Mortality (←Z)	$+\mathrm{m_z Z^2}$
	- Remineralization (→[NH_4])	$-r_D \exp\,[0.086(\mathrm{T}-30)]D_L$
	- Sinking	$-w_S\,\partial D_L/\,\partial \mathrm{z}$
Dissolved Organic Nitrogen [DON]	Change per unit time =	$\partial[\mathrm{DON}]/\,\partial \mathrm{t} =$
	+ Exudation (← P)	$+\gamma \mathrm{L_I}(\mathrm{L_{NO_3}}+\mathrm{L_{NH_4}})\mathrm{P}$
	+ Mortality Solubilization (← P)	$+\delta \mathrm{m_P P}$
	- Remineralization (→ [NH_4^+])	$-r_{DON} \exp[0.086(\mathrm{T}-30)]\,[DON]$
Ammonium [NH_4]	Change per unit time =	$\partial[NH_4]/\partial t =$
	- Uptake (→ P)	$-\mu_0 \mathrm{L_I L_{NH_4} P}$
	- Nitrification (→[NO_3])	$+\mathrm{n} f_{NTR}[\mathrm{NH_4}]$
	+ Excretion (←Z)	$+(\mathrm{l_{BM}}+\mathrm{l_E}\beta\frac{\mathrm{P}^2}{\mathrm{K_P}+\mathrm{P}^2})\mathrm{Z}$
	+ Remineralization (←D_S + D_L)	$+\eta_{O_2:NO_3} \exp[0.086(\mathrm{T}-30)](\mathrm{r_S D_S}+\mathrm{r_D D_D})$
	+ Remineralization (← [DON])	$+\eta_{O_2:NO_3} \exp\,[0.086(\mathrm{T}-30)]\mathrm{r_{DON}}[\mathrm{DON}]$
Nitrate [NO_3]	Change per unit time =	$\partial[\mathrm{NO3}]/\,\partial \mathrm{t}=$
	- Uptake (→ P)	$-\mu_0 \mathrm{L_I L_{NO_3} P}$
	- Water column denitrification (→ N_2)	$-min[f_{NTR}, f_{WC}](\exp[0.086(\mathrm{T}-30)](\mathrm{r_S D_S}+\mathrm{r_D D_D}+\mathrm{r_{DON}}[\mathrm{DON}])$
	+ Nitrification (←[NH_4^+])	$+\mathrm{n} f_{NTR}[\mathrm{NH_4}]$
Oxygen [O_2]	Change per unit time =	$\partial[O_2]/\partial t =$
	+ Air-sea flux at surface	$+\upsilon\frac{K_{O_2}}{\Delta z}([O_2]_{sat}-[O_2])$
	+ Primary production	$\mu_0 \mathrm{L_I}(\eta_{O_2:NO_3}\mathrm{L_{NO_3}}+\eta_{O_2:NH_4}\mathrm{L_{NH_4}})\mathrm{P}$

	([NH_4^+] + [NO_3] → P)	
	- Nitrification ([NH_4^+] → [NO_3])	$-2\mathrm{n} f_{NTR}[\mathrm{NH_4}]$
	- Excretion (Z → [NH_4^+])	$-\eta_{O_2:NH_4}(l_{BM} + l_E\beta\frac{P^2}{K_P+P^2})\mathrm{Z}$
	- Remineralization (D_S → [NH_4^+])	$-\eta_{O_2:NH_4} r_S \exp\,[0.086(\mathrm{T}-30)] D_S$
	- Remineralization (D_L → [NH_4^+])	$-\eta_{O_2:NH_4} r_L \exp\,[0.086(\mathrm{T}-30)] D_L$
	- Remineralization ([DON] → [NH_4^+])	$-\eta_{O_2:NH_4}\, r_{DON} \exp[0.086(\mathrm{T}-30)]\,[DON]$

Table 0-3 Biogeochemical source/ sink terms at the bottom (sediment) Boundary

Variable (Symbol)	Processes ← From which pool; → To which pool.	Time rate of change in each term
Ammonium [NH_4^+]	Change per unit time =	$\partial NH_4/\partial t\,|_{z=H} =$
	+ Remineralization (←D_S + D_L+P)	$+\frac{\mathrm{cff1}}{16}(16-\frac{0.8}{400}\times[O_2])$
Nitrate [NO_3]	Change per unit time =	$\partial NO_3/\partial t\,|_{z=H}$
	- denitrification (→ N_2)	$-\frac{\mathrm{cff1}}{16}(84.8-\frac{5.04}{400}\times[O_2])fb_{NO3}$
Oxygen [O_2]	Change per unit time =	$\partial O_2/\partial t\,|_{z=H}$
	- Remineralization (D_S +D_L +P→ [NH_4^+])	$\frac{\mathrm{cff1}\times 6.9}{400}\times[O_2]$
Inorganic suspended solid [ISS])	Change per unit time =	$\partial ISS/\partial t\,|_{z=H}$
	+Resuspended inorganic matter	$=\xi(\tau-\tau_c)$

Table 0-4 Definitions of functions used in state variables equations.

Symbol	Description	Equation
Cff1	Flux organic matter reach to the bottom	$w_p P \mid_{z=H} + w_{D_s} D_S \mid_{z=H} + w_{D_L} D_L \mid_{z=H}$
ϕ_1	Burial efficiency	$\min(0.45; 0.092 F_{BC}^{0.5797})$

Feng, Y., M.A.M. Friedrichs, J. Wilkin, H.Q. Tian, Q.C. Yang, E.E. Hofmann, J.D. Wiggert, and R.R. Hood. 2015. Chesapeake Bay nitrogen fluxes derived from a land-estuarine ocean biogeochemical modeling system: Model description, evaluation, and nitrogen budgets. *Journal of Geophysical Research-Biogeosciences* 120: 1666-1695. doi: 10.1002/2015jg002931

Bibliography

Adolf, J.E., C.L. Yeager, W.D. Miller, M.E. Mallonee, and L.W. Harding. 2006. Environmental forcing of phytoplankton floral composition, biomass, and primary productivity in Chesapeake Bay, USA. *Estuarine Coastal and Shelf Science* 67: 108-122. doi: 10.1016/j.ecss.2005.11.030

Boesch, D., E. Burreson, W. Dennison, E. Houde, M. Kemp, V. Kennedy, R. Newell, K. Paynter, R. Orth, and R. Ulanowicz. 2001. Factors in the Decline of Coastal Ecosystems. *Science* 293: 1589. doi: 10.1126/science.293.5535.1589c

Boynton, W., J. Garber, R. Summers, and W. Kemp. 1995. Inputs, transformations, and transport of nitrogen and phosphorus in Chesapeake Bay and selected tributaries. *Estuaries and Coasts* 18: 285-314. doi: 10.2307/1352640

Bradley, P.B., M.P. Sanderson, M.E. Frischer, J. Brofft, M.G. Booth, L.J. Kerkhof, and D.A. Bronk. 2010. Inorganic and organic nitrogen uptake by phytoplankton and heterotrophic bacteria in the stratified Mid-Atlantic Bight. *Estuarine, Coastal and Shelf Science* 88: 429-441. doi: 10.1016/j.ecss.2010.02.001

Breitburg, D., L.A. Levin, A. Oschlies, M. Grégoire, F.P. Chavez, D.J. Conley, V. Garçon, D. Gilbert, D. Gutiérrez, K. Isensee, G.S. Jacinto, K.E. Limburg, I. Montes, S.W.A. Naqvi, G.C. Pitcher, N.N. Rabalais, M.R. Roman, K.A. Rose, B.A. Seibel, M. Telszewski, M. Yasuhara, and J. Zhang. 2018. Declining oxygen in the global ocean and coastal waters. *Science* 359. doi: 10.1126/science.aam7240

Brown, C.W., R.R. Hood, W. Long, J. Jacobs, D.L. Ramers, C. Wazniak, J.D. Wiggert, R. Wood, and J. Xu. 2013. Ecological forecasting in Chesapeake Bay: Using a mechanistic–empirical modeling approach. *Journal of Marine Systems* 125: 113-125. doi: 10.1016/j.jmarsys.2012.12.007

Cerco, C.F., and M.R. Noel. 2004. Process-based primary production modeling in Chesapeake Bay. *Marine Ecology Progress Series* 282: 45-58. doi: 10.3354/meps282045

Chen, S.-N., and L.P. Sanford. 2009. Lateral circulation driven by boundary mixing and the associated transport of sediments in idealized partially mixed estuaries. *Continental Shelf Research* 29: 101-118. doi: 10.1016/j.csr.2008.01.001

Cowan, J.L.W., and W.R. Boynton. 1996. Sediment-water oxygen and nutrient exchanges along the longitudinal axis of Chesapeake Bay: Seasonal patterns, controlling factors and ecological significance. *Estuaries* 19: 562-580. doi: 10.2307/1352518

Da, F., M.A.M. Friedrichs, and P. St-Laurent. 2018. Impacts of Atmospheric Nitrogen Deposition and Coastal Nitrogen Fluxes on Oxygen Concentrations in Chesapeake Bay. *Journal of Geophysical Research-Oceans* 123: 5004-5025. doi: 10.1029/2018jc014009

Deegan, L.A., D.S. Johnson, R.S. Warren, B.J. Peterson, J.W. Fleeger, S. Fagherazzi, and W.M. Wollheim. 2012. Coastal eutrophication as a driver of salt marsh loss. *Nature* 490: 388. doi: 10.1038/nature11533

Diaz, R.J., and R. Rosenberg. 2008. Spreading dead zones and consequences for marine ecosystems. *Science* 321: 926-929. doi: 10.1126/science.1156401

Du, J.B., and J. Shen. 2016. Water residence time in Chesapeake Bay for 1980-2012. *Journal of Marine Systems* 164: 101-111. doi: 10.1016/j.jmarsys.2016.08.011

Du, J.B., and J. Shen. 2017. Transport of riverine material from multiple rivers in the Chesapeake Bay: Important control of estuarine circulation on the material distribution. *Journal of Geophysical Research-Biogeosciences* 122: 2998-3013. doi: 10.1002/2016jg003707

Feng, Y., M.A.M. Friedrichs, J. Wilkin, H.Q. Tian, Q.C. Yang, E.E. Hofmann, J.D. Wiggert, and R.R. Hood. 2015. Chesapeake Bay nitrogen fluxes derived from a land-estuarine ocean biogeochemical modeling system: Model description, evaluation, and nitrogen budgets. *Journal of Geophysical Research-Biogeosciences* 120: 1666-1695. doi: 10.1002/2015jg002931

Fennel, K., J. Wilkin, J. Levin, J. Moisan, J. O'Reilly, and D. Haidvogel. 2006. Nitrogen cycling in the Middle Atlantic Bight: Results from a three-dimensional model and implications for the North Atlantic nitrogen budget. *Global Biogeochemical Cycles* 20. doi: 10.1029/2005GB002456

Fernandez-Urruzola, I., N. Osma, M. Gomez, F. Pollehne, L. Postel, and T.T. Packard. 2016. Modeling downward particulate organic nitrogen flux from zooplankton ammonium regeneration in the northern Benguela. *Progress in Oceanography* 149: 121-133. doi: 10.1016/j.pocean.2016.10.010

Geyer, W.R., and P. MacCready. 2014. The Estuarine Circulation. *Annual Review of Fluid Mechanics* 46: 175-197. doi: 10.1146/annurev-fluid-010313-141302

Hagy, J.D., W.R. Boynton, and D.A. Jasinski. 2005. Modelling phytoplankton deposition to Chesapeake Bay sediments during winter-spring: interannual variability in relation to river flow. *Estuarine, Coastal and Shelf Science* 62: 25-40. doi: 10.1016/j.ecss.2004.08.004

Hofmann, E., J.N. Druon, K. Fennel, M. Friedrichs, D. Haidvogel, C. Lee, A. Mannino, C. McClain, R. Najjar, J. O'Reilly, D. Pollard, M. Previdi, S. Seitzinger, J. Siewert, S. Signorini, J. Wilkin, and U.S. Team. 2008. Eastern US continental shelf carbon budget: integrating models, data assimilation, and analysis. *Oceanography* 21: 86-104. doi: 10.5670/oceanog.2008.70

Howarth, R., F. Chan, D.J. Conley, J. Garnier, S.C. Doney, R. Marino, and G. Billen. 2011. Coupled biogeochemical cycles: eutrophication and hypoxia in temperate estuaries and coastal marine ecosystems. *Frontiers in Ecology and the Environment* 9: 18-26. doi: 10.1890/100008

Irby, I.D., M.A.M. Friedrichs, C.T. Friedrichs, A.J. Bever, R.R. Hood, L.W.J. Lanerolle, M. Li, L. Linker, M.E. Scully, K. Sellner, J. Shen, J. Testa, H. Wang, P. Wang, and M. Xia. 2016. Challenges associated with modeling low-oxygen waters in Chesapeake Bay: a multiple model comparison. *Biogeosciences* 13: 2011-2028. doi: 10.5194/bg-13-2011-2016

Jolliff, J.K., J.C. Kindle, I. Shulman, B. Penta, M.A.M. Friedrichs, R. Helber, and R.A. Arnone. 2009. Summary diagrams for coupled hydrodynamic-ecosystem model skill assessment. *Journal of Marine Systems* 76: 64-82. doi: 10.1016/j.jmarsys.2008.05.014

Kemp, W.M., W.R. Boynton, J.E. Adolf, D.F. Boesch, W.C. Boicourt, G. Brush, J.C. Cornwell, T.R. Fisher, P.M. Glibert, J.D. Hagy, L.W. Harding, E.D. Houde, D.G. Kimmel, W.D. Miller, R.I.E. Newell, M.R. Roman, E.M. Smith, and J.C. Stevenson. 2005. Eutrophication of Chesapeake Bay: historical trends and ecological interactions. *Marine Ecology Progress Series* 303: 1-29. doi: 10.3354/Meps303001

Kemp, W.M., P.A. Sampou, J. Garber, J. Tuttle, and W.R. Boynton. 1992. Seasonal depletion of oxygen from bottom waters of Chesapeake Bay: Roles of benthic and planktonic respiration and physical exchange processes. *Marine Ecology Progress Series* 85: 137-152. doi: 10.3354/meps085137

Kemp, W.M., E.M. Smith, M. Marvin-DiPasquale, and W.R. Boynton. 1997. Organic carbon balance and net ecosystem metabolism in Chesapeake Bay. *Marine Ecology Progress Series* 150: 229-248. doi: 10.3354/meps150229

Kemp, W.M., J.M. Testa, D.J. Conley, D. Gilbert, and J.D. Hagy. 2009. Temporal responses of coastal hypoxia to nutrient loading and physical controls. *Biogeosciences* 6: 2985-3008. doi: 10.5194/bg-6-2985-2009

Lee, Y.J., W.R. Boynton, M. Li, and Y. Li. 2013. Role of late winter–spring wind influencing summer hypoxia in Chesapeake Bay. *Estuaries and Coasts* 36: 683-696. doi: 10.1007/s12237-013-9592-5

Li, M., L.J. Zhong, and L.W. Harding. 2009. Sensitivity of plankton biomass and productivity to variations in physical forcing and biological parameters in Chesapeake Bay. *Journal of Marine Research* 67: 667-700. doi: 10.1357/002224009791218878

Li, Y., and M. Li. 2011. Effects of winds on stratification and circulation in a partially mixed estuary. *Journal of Geophysical Research-Oceans* 116. doi: 10.1029/2010jc006893

Li, Y., and M. Li. 2012. Wind-driven lateral circulation in a stratified estuary and its effects on the along-channel flow. *Journal of Geophysical Research-Oceans* 117. doi: 10.1029/2011jc007829

Malone, T., L. Crocker, S. Pike, and B. Wendler. 1988. Influences of river flow on the dynamics of phytoplankton production in a partially stratified estuary. *Marine Ecology Progress Series*: 235-249. doi: 10.3354/meps048235

Malone, T.C., W.M. Kemp, H.W. Ducklow, W.R. Boynton, J.H. Tuttle, and R.B. Jonas. 1986. Lateral variation in the production and fate of phytoplankton in a partially stratified estuary *Marine Ecology Progress Series* 32: 149-160. doi: 10.3354/meps032149

Marshall, H.G., and K.K. Nesius. 1996. Phytoplankton composition in relation to primary production in Chesapeake Bay. *Marine Biology* 125: 611-617. doi: 10.1007/BF00353272

Murphy, R.R., W.M. Kemp, and W.P. Ball. 2011. Long-Term Trends in Chesapeake Bay Seasonal Hypoxia, Stratification, and Nutrient Loading. *Estuaries and Coasts* 34: 1293-1309. doi: 10.1007/s12237-011-9413-7

Olabarrieta, M., W.R. Geyer, G. Coco, C.T. Friedrichs, and Z.D. Cao. 2018. Effects of Density-Driven Flows on the Long-Term Morphodynamic Evolution of Funnel-Shaped Estuaries. *Journal Of Geophysical Research-Earth Surface* 123: 2901-2924. doi: 10.1029/2017jf004527

Paerl, H.W., and J.T. Scott. 2010. Throwing Fuel on the Fire: Synergistic Effects of Excessive Nitrogen Inputs and Global Warming on Harmful Algal Blooms. *Environmental Science & Technology* 44: 7756-7758. doi: 10.1021/es102665e

Pan, J.Y., Y.Z. Gu, and D.X. Wang. 2014. Observations and numerical modeling of the Pearl River plume in summer season. *Journal of Geophysical Research-Oceans* 119: 2480-2500. doi: 10.1002/2013jc009042

Rabalais, N.N., R.E. Turner, R.J. Diaz, and D. Justic. 2009. Global change and eutrophication of coastal waters. *Ices Journal of Marine Science* 66: 1528-1537. doi: 10.1093/icesjms/fsp047

Ralston, D.K., W.R. Geyer, J.A. Lerczak, and M. Scully. 2010. Turbulent mixing in a strongly forced salt wedge estuary. *Journal of Geophysical Research* 115. doi: 10.1029/2009jc006061

Scully, M.E. 2010a. The importance of climate variability to wind-driven modulation of hypoxia in Chesapeake Bay. *Journal of Physical Oceanography* 40: 1435-1440. doi: 10.1175/2010jpo4321.1

Scully, M.E. 2010b. Wind modulation of dissolved oxygen in Chesapeake Bay. *Estuaries and Coasts* 33: 1164-1175. doi: 10.1007/s12237-010-9319-9

Scully, M.E. 2013. Physical controls on hypoxia in Chesapeake Bay: A numerical modeling study. *Journal of Geophysical Research: Oceans* 118: 1239-1256. doi: 10.1002/jgrc.20138

Scully, M.E. 2016a. The contribution of physical processes to inter-annual variations of hypoxia in Chesapeake Bay: A 30-yr modeling study. *Limnology and Oceanography* 61: 2243-2260. doi: 10.1002/lno.10372

Scully, M.E. 2016b. Mixing of dissolved oxygen in Chesapeake Bay driven by the interaction between wind-driven circulation and estuarine bathymetry. *Journal of Geophysical Research-Oceans* 121: 5639-5654. doi: 10.1002/2016jc011924

Scully, M.E., and C.T. Friedrichs. 2007. The importance of tidal and lateral asymmetries in stratification to residual circulation in partially mixed estuaries. *Journal of Physical Oceanography* 37: 1496-1511. doi: 10.1175/jpo3071.1

Scully, M.E., and W.R. Geyer. 2012. The role of advection, straining, and mixing on the tidal variability of estuarine stratification. *Journal of Physical Oceanography* 42: 855-868. doi: 10.1175/jpo-d-10-05010.1

Scully, M.E., W.R. Geyer, and J.A. Lerczak. 2009. The influence of lateral advection on the residual estuarine circulation: a numerical modeling study of the Hudson River estuary. *Journal of Physical Oceanography* 39: 107-124. doi: 10.1175/2008jpo3952.1

Shchepetkin, A.F., and J.C. McWilliams. 2005. The regional oceanic modeling system (ROMS): A split-explicit, free-surface, topography-following-coordinate oceanic model. *Ocean Modelling* 9: 347-404. doi: 10.1016/j.ocemod.2004.08.002

Shen, C., J.M. Testa, W. Ni, W.-J. Cai, M. Li, and W.M. Kemp. 2019. Ecosystem Metabolism and Carbon Balance in Chesapeake Bay: A 30-Year Analysis Using a Coupled Hydrodynamic-Biogeochemical Model. *Journal of Geophysical Research: Oceans* 124: 6141-6153. doi: 10.1029/2019jc015296

Shen, X., B.J. Lee, M. Fettweis, and E.A. Toorman. 2018a. A tri-modal flocculation model coupled with TELEMAC for estuarine muds both in the laboratory and in the field. *Water Research* 145: 473-486. doi: 10.1016/j.watres.2018.08.062

Shen, X., E.A. Toorman, B.J. Lee, and M. Fettweis. 2018b. Biophysical flocculation of suspended particulate matters in Belgian coastal zones. *Journal of Hydrology* 567: 238-252. doi: 10.1016/j.jhydrol.2018.10.028

Smetacek, V.S. 1985. Role of sinking in diatom life-history cycles: ecological, evolutionary and geological significance. *Marine Biology* 84: 239-251. doi: 10.1007/BF00392493

Smil, V. 2000. Phosphorus in the environment: Natural flows and human interferences. *Annual Review of Energy and the Environment* 25: 53-88. doi: 10.1146/annurev.energy.25.1.53

Taylor, K.E. 2001. Summarizing multiple aspects of model performance in a single diagram. *Journal of Geophysical Research-Atmospheres* 106: 7183-7192. doi: 10.1029/2000jd900719

Testa, J.M., and W.M. Kemp. 2012. Hypoxia-induced shifts in nitrogen and phosphorus cycling in Chesapeake Bay. *Limnology and Oceanography* 57: 835-850. doi: 10.4319/lo.2012.57.3.0835

Testa, J.M., and W.M. Kemp. 2014. Spatial and temporal patterns in winter-spring oxygen depletion in Chesapeake Bay bottom waters. *Estuaries and Coasts* 37: 1432-1448. doi: 10.1007/s12237-014-9775-8

Testa, J.M., Y. Li, Y.J. Lee, M. Li, D.C. Brady, D.M. Di Toro, W.M. Kemp, and J.J. Fitzpatrick. 2014. Quantifying the effects of nutrient loading on dissolved O2 cycling and hypoxia in Chesapeake Bay using a coupled hydrodynamic–biogeochemical model. *Journal of Marine Systems* 139: 139-158. doi: 10.1016/j.jmarsys.2014.05.018

Testa, J.M., R.R. Murphy, D.C. Brady, and W.M. Kemp. 2018. Nutrient- and Climate-Induced Shifts in the Phenology of Linked Biogeochemical Cycles in a Temperate Estuary. *Frontiers in Marine Science* 5. doi: 10.3389/fmars.2018.00114

Wang, J., H.S. Hong, Y.W. Jiang, F. Chai, and X.H. Yan. 2013. Summer nitrogenous nutrient transport and its fate in the Taiwan Strait: A coupled physical-biological modeling approach. *Journal of Geophysical Research-Oceans* 118: 4184-4200. doi: 10.1002/jgrc.20300

Wang, P., H. Wang, and L. Linker. 2015. Relative Importance of Nutrient Load and Wind on Regulating Interannual Summer Hypoxia in the Chesapeake Bay. *Estuaries and Coasts* 38: 1048-1061. doi: 10.1007/s12237-014-9867-5

Wei, X., M. Kumar, and H.M. Schuttelaars. 2017. Three-Dimensional Salt Dynamics in Well-Mixed Estuaries: Influence of Estuarine Convergence, Coriolis, and Bathymetry. *Journal of Physical Oceanography* 47: 1843-1871. doi: 10.1175/JPO-D-16-0247.1

Wiggert, J.D., R.R. Hood, and C.W. Brown. 2017. Modeling Hypoxia and Its Ecological Consequences in Chesapeake Bay. In *Modeling Coastal Hypoxia*, ed. D. Justic, K. Rose, R. Hetland and K. Fennel, 119-147. Cham: Springer. doi: 10.1007/978-3-319-54571-4_6

Willmott, C.J. 1981. On the validation of models. *Physical Geography* 2: 184-194. doi: 10.1080/02723646.1981.10642213

Xie, X., and M. Li. 2018. Effects of wind straining on estuarine circulation: A combined observational and modeling study. *Journal of Geophysical Research: Oceans* 123: 2363-2380. doi: 10.1002/2017JC013470

Xie, X., M. Li, and W.C. Boicourt. 2017. Baroclinic effects on wind-driven lateral circulation in Chesapeake Bay. *Journal of Physical Oceanography* 47: 433-445. doi: 10.1175/JPO-D-15-0233.1

Xu, J., and R.R. Hood. 2006. Modeling biogeochemical cycles in Chesapeake Bay with a coupled physical–biological model. *Estuarine, Coastal and Shelf Science* 69: 19-46. doi: 10.1016/j.ecss.2006.03.021

Xu, J., R.R. Hood, and S.-Y. Chao. 2005. A simple empirical optical model for simulating light attenuation variability in a partially mixed estuary. *Estuaries* 28: 572-580. doi: 10.1007/BF02696068

Xu, J.T., W. Long, J.D. Wiggert, L.W.J. Lanerolle, C.W. Brown, R. Murtugudde, and R.R. Hood. 2012. Climate forcing and salinity variability in Chesapeake Bay, USA. *Estuaries and Coasts* 35: 237-261. doi: 10.1007/s12237-011-9423-5

Zhang, W., Y. Cao, Y.L. Zhu, J.H. Zheng, X.M. Ji, Y.W. Xu, Y. Wu, and A.J.F. Hoitink. 2018. Unravelling the causes of tidal asymmetry in deltas. *Journal of Hydrology* 564: 588-604. doi: 10.1016/j.jhydrol.2018.07.023

Zhang, X. 2017. Biogeochemistry: A plan for efficient use of nitrogen fertilizers. *Nature* 543: 322-323. doi: 10.1038/543322a

Zhou, Y., D. Scavia, and A.M. Michalak. 2014. Nutrient loading and meteorological conditions explain interannual variability of hypoxia in the Chesapeake Bay. *Limnology and Oceanography* 59: 373-384. doi: 10.4319/lo.2014.59.2.0373